INTERMITTENT DYNAMICS OF AN EXTERNAL-CAVITY SEMICONDUCTOR LASER

A Dissertation
Presented to
The Academic Faculty

By

Daeyoung Choi

In Partial Fulfillment
of the Requirements for the Degree
Doctor of Philosophy in the
School of Electrical and Computer Engineering

Georgia Institute of Technology

August 2018

INTERMITTENT DYNAMICS OF AN EXTERNAL-CAVITY SEMICONDUCTOR LASER

Approved by:

Dr. David Citrin, Advisor
School of Electrical and Computer Engineering
Georgia Institute of Technology

Dr. Alexandre Locquet, Co-advisor
School of Electrical and Computer Engineering
Georgia Institute of Technology

Dr. Douglas Williams
School of Electrical and Computer Engineering
Georgia Institute of Technology

Dr. Robert Butera
School of Electrical and Computer Engineering
Georgia Institute of Technology

Dr. Paul Douglas Yoder
School of Electrical and Computer Engineering
Georgia Institute of Technology

Dr. Kurt Wiesenfeld
School of Physics
Georgia Institute of Technology

Date Approved: June 14, 2018

When God said “Let there be light”, he surely must have meant perfectly coherent light.

Charles Townes

ACKNOWLEDGEMENTS

I would like to express my sincere gratitude to my advisors, Dr. David Citrin and Dr. Alexandre Locquet, for granting me the opportunity to work with them. Their insights and advices are like the lighthouse in the mist, guiding me in the right direction along this tough PhD journey. Although I am a quite slow-learner, thanks to their strong patience, I eventually learned a lot of things from them not only about scientific approaches but also about how to face with life struggles.

I extend my sincere gratitude to my PhD colleagues in the lab; Bobby Kim helped me to settle in the lab without any problems when I first came to France for research. He also taught me about basic principles of experimental techniques and laser dynamics. Ted Chang, from the Physics department, worked with me too. His different views towards laser physics and experimentalism helped me make up for the weakness of my research ideas. I also appreciate the traditional gifts he gave to me whenever he came back from vacations in Taiwan. l am very proud of working with them. I owe special thanks to Michael J Wishon who spent most of time with me working in the lab and had fun talks many times. Creative ideas he suggested when I stuck in difficult problems was like the blessed rain following a drought. He proved that a good teammate is invaluable.

I am also grateful to all the people that I met in the Atlanta campus; a group of friends named Hypen-Nines. Their humorous minds filled with high level of intelligence always made me laugh out loud, and sometimes, gave me second-thoughts related to some controversial topics. Also, I thank friends that I played soccer together as a team and won the championship in the Georgia Tech Intramurals. I never felt bored during my staying in Atlanta thanks to them.

I have to add my appreciation towards my best friends, as also known as Hobbits. They are rather short men but their sincerity towards life is as tall as giants. My Hobbits inspired me to study abroad when I was in undergraduate. Definitely, they played a big

role in changing my life. Obviously, I cannot forget all my nerdy friends that have spent all my 20s together. We were grown up playing computer games and watching Japanese animations together. During my vacations, they gladly visited me and travelled together around Europe. I will never forget such a great moment, talking about funny stories in our life while traveling beautiful places together.

Last but not least, I deeply appreciate that my parents always support me with all their love and cheers. They are like a giant tree for me; they have become the shade where I could take a rest when I was exhausted in my life. I always feel sorry whenever I think about my parents as they are getting older and their health conditions are not as good as they used to be. Now, it is time for me to become their shelter in return.

TABLE OF CONTENTS

LIST OF TABLES

LIST OF FIGURES

SUMMARY

The main objective in this thesis is to investigate experimentally nonlinear dynamical behaviors of an external-cavity semiconductor laser (ECSL) when it is subjected to time-delayed optical feedback with various operating parameters. To begin with, we demonstrate experimental studies of fundamental nonlinear dynamics by using semiconductor laser systems. Systematic information concerning the dynamical regimes and the bifurcations between them will be introduced by bifurcation diagrams (BDs), which are obtained by fixing all but one parameter and then mapping out the extremal variables from the ECSL dynamics as a parameter varies. BDs provide a global picture of the dynamical system and enables systematic investigations of the rich variety of dynamical behaviors observed in ECSLs. While obtaining several experimental BDs, we find that there are intermittent phenomena between dynamical regimes. When an ECSL is operated at low injection current slightly above threshold, we can observe intermittency between stationary operation and low frequency fluctuations. We find that some of those fluctuations in intermittency lead to extreme events, which is one of common dynamical phenomena found in nature and various dynamics systems. In addition, we investigate multistate intermittency, and intermittency between period-doubled dynamics and fully developed coherence collapse when the ECSL is operated at higher injection current. Interestingly, intermittent dynamics in the ECSL are in much slower time scales given the fact that the ECSL dynamics are in sub-nano time scales. Thus, we investigate statistically characteristics of these intermittencies and compare with other types of intermittency observed in different dynamical systems. Last but not least, given the circumstance that ECSLs exhibit the continuous wave operation without interrupted by intermittent or irregular dynamics, we suggest a simple and compact ECSL system that is possible to detect displacement of the remote target with a few tens-of-nanometers resolution.

CHAPTER 1
GENERAL INTRODUCTION

1.1 Dynamics of External-cavity Semiconductor Lasers

The study of nonlinear dynamics in lasers was initiated by Haken in 1975 [1] when he established the mathematical model of laser dynamics from the Maxwell-Bloch equations. Since then, much attention has been paid to the nonlinear dynamics of lasers as it has been supported by many experiments in optics with the advent of high-speed computers and refined experimental techniques. Laser systems retain inherent instabilities which were experimentally verified with gas lasers [2] and solid state lasers [3]. The observation of instabilities was also made in semiconductor lasers (or laser diodes), which has accelerated research on nonlinear laser dynamics [4, 5, 6, 7]. The reason SLs are particularly considered is because they are suitable and efficient source of coherent light in various technical applications due to their compact size, low cost and high efficiency.

There are several ways to induce instability of semiconductor lasers (SLs); optical injection [8], current modulation [9], and external optical feedback [10]. In general, SLs with time-delayed optical feedback, as known as external cavity semiconductor lasers (ECSLs) are widely used to study model-systems that undergo high-dimensional nonlinear dynamics. The external cavity is formed with a distant reflecting mirror that enables the emitted light to be re-injected into the laser cavity. Solitary SLs (without feedback) have two degrees of freedom. Hence, they exhibit light generated by the coupling of the electrical field and carrier numbers, resulting in only monotonous dynamical behavior by its nature. The round trip from the external cavity introduces a time delay to the dynamics and adds an infinite number of degrees of freedom to solitary SLs.

The dynamics of ECSLs are known to be complex with difficulty of controlling but have

been widely investigated in the perspective of rich dynamical behaviors because ESLs can give an insight into essential questions in nonlinear dynamics fields by conducting practical experiments and have a high potential for many applications based on the optical feedback that can generate either stabilized or high-dimensional chaotic emissions. Some applications based on nonlinear dynamics of ECSLs achieve their high performances after suppressing feedback induced instabilities. Meanwhile, in some cases, some applications in modern technology even aims for utilization of feedback induced instabilities. Recently, the intriguing properties of high-dimensional chaotic dynamics have attracted much attention since they offer potential for realization of novel applications that utilize chaotic signals; secure communications [11, 12, 13], light detection and ranging (LiDAR) [14], optoelectronic oscillator [15, 16], random-number generation (RNG) [17, 18], compressive sensing [19], and reservoir computing [20, 21]. A thorough understanding of a complex ECSL system will help to understand nonlinear dynamics and enhance those applications.

There were no theoretical models that could accurately describe the origins of the dynamical operation of ECSLs until 1980. Eventually, Lang and Kobayashi (LK) [3] presented differential equations that show the dynamical changes in the carrier density of the SL due to optical feedback lead to a modification of the refractive index, which in turn alters the resonant frequency of the laser. They also demonstrated valuable information that could describe some of the dynamical behavior of lasers. Thus, when numerical interpretations are needed, we mostly rely on the LK models to discuss our results in thesis.

The characteristics of different dynamical regimes in ECSLs essentially depend on different parameters; pump current, optical feedback, and the length of the external cavity. To better describe the transition from one dynamical regime to another by varying a parameter in ECSLs, one can exploit a bifurcation diagram.

1.2 Chaos and Bifurcation

Li and Yorke [22] used the word chaos for the first time. Chaos means non-periodic oscillatory state from the nonlinear nature of the deterministic physical systems. Basically, a dynamic system can be neither static nor periodic in order to be classified as a chaotic system. Chaos is found in a wide variety of systems including lasers, chemical reactions, fluid dynamics, weather and earthquakes. Afterwards, Lorenz [23] introduced deterministic chaos with the evolution of a simple model of the atmosphere in 1963 with the idea of "a slight change in the initial position of a system could lead to huge differences", suggested by Henri poincaré [24]. Theory of deterministic chaos has marked a breakthrough in the understanding of nonlinear systems and initiated nonlinear dynamics and chaos to grow vigorously in various scientific fields.

In the beginning, poor computational power for implementing mathematical concepts made it very difficult to analyze and explain chaotic dynamics. Thanks to high-speed computing systems and cutting-edge experimental devices, experiments to confirm and support theoretical ideas on nonlinear dynamics has been feasible today. Among various dynamical systems used for controlling the nonlinearity, lasers have often been utilized in experiments because they have unstable dynamics under certain conditions and the light is one of main sources in telecommunications. Especially, SLs are regarded as an ideal testbed for fundamental nonlinearity since they possess inherent instabilities caused by spontaneous emission.

Before a dynamical system exhibiting chaos, transitions are made between different dynamic behaviors (regimes) as also known as *route to chaos*. Universal routes to chaos have been observed in various systems; the quaisperiodic route [25], the period-doubling route [26], intermittency [27], and crisis [28].

By dictionary definition, bifurcation means "a forking or division into two: the point at which a forking occurs". In the context of nonlinear dynamics, a bifurcation is the

point where a sudden qualitative or topological change in its behavior in a system. The bifurcation theory was firstly introduced by Henri Poincaré in 1885 [29]. A bifurcation occurs, in general, when a small smooth transition is operated for the parameter values (the bifurcation parameters) in a system and several forms of bifurcations are categorized according to how stability is lost [8, 30].

A bifurcation diagram (BD) can be obtained by varying a controllable parameter, which enables us to understand substantial systematic information. The detailed dynamical transitions of various regimes can be conveniently summarized in BDs. Hence, investigation of BDs provides new vantage point from which to view ECSLs. In this thesis, we focus on drawing BDs with various operating parameters (injection current, external-cavity length, feedback strength, feedback phase) to disclose a global picture of the ECSL dynamics. Furthermore, based on the results of BDs, we will present stationary state, multistability, intermittency between different dynamical states, and various routes to chaos.

More importantly, our experimental BDs will be compared with simulated BDs by the LK model, which will affirm the validation of experimentally obtained BDs. The excellent agreement between experiment and simulation BDs within the boundary of the parameters will be used to explain the observed experimental phenomena with phase-space trajectories.

1.3 Extreme Events

From many experimental BDs that we have obtained, we consistently observe that several intermittent behaviors occur under different conditions. When the ECSL is operated at low injection current (slightly above threshold current) with moderate feedback level, it displays a chaotic behavior, as known as low-frequency fluctuations (LFFs). Under this feedback condition, intermittency between stationary oscillations *i.e.*, continuous wave (CW) and LFF may occur when injection current is increased from the point that the ECSL starts to emit. The optical intensity of an ECSL shows very abrupt changes since LFFs have a larger trajectories in phase space while CW stays in one of stable solutions in the ECSL.

We have investigated how to analyze intermittency between CW and LFF in the context of extensive work in other areas: hydrodynamics, oceanography, economics, meteorology, acoustics, and optics, to name a few. By definition, the word *extreme* simply means that something is far-away from the ordinary or average and exceeds the boundary. As scientists were able to collect a huge amount of data from nature and different nonlinear systems, certain criteria have been established to define extreme events among many events. The scientific definition of "extreme events" will be introduced in chapter 4.

In a SL system, Bonatto *et al*. [31] showed extreme events from an optically injected SL that rare giant pulses could be observed in a purely deterministic dynamical system. Perrone *et al*. [32] further showed numerically that a weak modulation of the pump current could be used to control the frequency of these giant pulses. Reinoso *et al*. [33] demonstrated that these giant pulses could be predicted with large anticipation time and originated in a crisis process. As those research topics implies, main topics in the extreme events field is to find deterministic mechanism of extreme events in various dynamical systems and anticipate extreme events before it happens, and even, to control it if possible. Indeed, extreme events exist in real, and sometimes might be detrimental to human-beings.

Based on the theory of extreme events, we analyze statistically how those irregular behaviors change as a function of parameters (injection current, feedback level, external cavity) and what dynamical mechanisms are involved in such irregular behaviors in an ECSL. The results of these studies will be used to consolidate our subsequent research; we will investigate how to maintain stable ECSLs by avoiding conditions that cause irregular dynamical behaviors.

1.4 Intermittency

Intermittency is characterized by the erratic alternation between regular and irregular dynamics [34]. Intermittency has recently become of great interest to many scientists because it is often observed in nature and various dynamical systems. As we have seen intermittent

dynamical behaviors in the route to chaos through the bifurcation diagrams (BDs) with different conditions, we intend to investigate inherent intermittent behaviors in order to fully understand the ECSL.

It is known that intermittency appears in nonlinear systems when a bifurcation parameter approaches a critical value corresponding to a bifurcation point or a crisis. Of course, different types of bifurcations lead to different intermittent behaviors; various types of intermittency have been continually revealed and analyzed. We will introduce different types of intermittencies and discuss what kinds of intermittencies are observed in the ECSL in chapter 5.

In order to define the characteristics of intermittency, critical exponents are widely used because it is believed, although not yet proven, that they are universal properties and do not depend on the details of the physical system. In general, critical exponents are of the form $\tau \sim (P - P_c)^{-K}$ where τ is the average duration of stable phase, P is the controlling parameter, P_c is the critical parameter, and K is the critical exponent. Critical exponents can be obtained from phase transitions via the power-law relation. During a phase transition of a given medium, certain properties change as a result of the change of some external condition. In statistics, a power-law means a functional relationship between two quantities where a relative change in one quantity leads to a proportional change in the other quantity. Hence, as critical exponents is associated with the variation of certain physical properties (the dimension and the range of the interaction) of the system near its phase transition point, it is tied to the type of bifurcation around which intermittency occurs and we can figure out the behavior of physical quantities near continuous phase transitions through the power-law relation, *i.e.*, systematized coefficient between dynamics regimes.

Intermittency has been observed and explored in various types of lasers including Nd-YAG [35], fiber [36, 37, 38, 39], optically pumped ring lasers [40, 41], and semiconductor lasers [42, 43, 44]. In particular, when an ECSL is biased slightly above the threshold current J_{th}, intermittency between continuous-wave operation and low-frequency fluctuations

(LFFs) may be observed. For this intermittency, we will discuss and interpret based on the theory of extreme events.

When the ECSL is operated at high injection current, we observe much complex intermittent dynamics due to generalized multistability of the ECSL. In particular, different transitional dynamics are involved after the ECSL displays the first instability; often it is called Hopf bifurcation. Consequently, different routes to chaos are demonstrated in the ECSL due to sensitivity to the initial states. Interestingly, as the feedback level is increased to the moderate feedback level, the ECSL exhibits the similar sequence of dynamical regimes, involving periodicity, intermittency, subharmonics, period-doubling, and fully-developed coherence collapse (CC). We will show experimentally that two regimes of intermittency can be observed on the route to chaos of a semiconductor laser subjected to optical feedback from a long external cavity, as the feedback level is increased.

1.5 The Dynamics of Terminal Voltage of External-cavity Semiconductor Lasers

The dynamics of an ECSL has been studied for various applications by sampling the photo-detected optical output. For compact and simple applications, terminal voltage V_{LD} across a laser junction can be preferred since a laser system does not necessitate photo-detectors. However, only few applications using V_{LD} of a LD have been discussed [45, 46].

In order to properly understand the dynamics of V_{LD} when the feedback is applied on ECSL, we investigate various dynamics regimes including abrupt transitions between dynamical state. It is known that instantaneous change in optical feedback leads to the significant changes in the carrier density N because the quasi-Fermi level difference across the *p-i-n* active-medium changes proportional to change in N. We focus on the dynamical regimes as well as bifurcations, which are indeed evidenced in the dc component V_{dc} of V_{LD} along with the photo-detected optical output. We will explain the dynamics of V_{dc} and optical intensity based on the Lang and Kobayashi (LK) model and see experimentally if the V_{LD} and the optically detected signal are in agreement with the LK model.

Moreover, we experimentally investigate the emission frequency and V_{LD} of an external-cavity semiconductor laser under weak optical feedback when the length of the external cavity varies on the sub-wavelength scale. This phase change influences the properties of an ECSL such as laser emission frequency, linewidth, and threshold gain. Self-mixing interferometry (SMI) is of a great interest for metrological applications since the changes in the properties of a SL convey information about the remote target. Also, SMI allows one to perform high-accuracy measurement with a simple and compact configuration compared to conventional Michelson and Mach-Zehnder interferometry.

Self-mixing is universally observed in various types of lasers and has been exploited for imaging [47, 48, 49] and measuring absolute distance [50, 51, 52, 53, 54], displacement [55, 56, 57, 58, 59], and velocity [60, 61]. Recently, it was revealed that relaxation oscillations of a LD can be used for displacement sensing [62]. Still, there is a lack of experimental studies on the laser emission frequency when the phase delay changes in an ECSL.

We investigate how the laser emission frequency varies as the mirror moves towards (away from) the laser diode and undergoes discontinuities with a period of half of the optical wavelength. V_{LD} can provide an alternative to a photodiode for ultracompact optical-feedback interferometry as it is highly correlated with the variations of the emission frequency when feedback phase is varied. We find that optimal conditions for nano-displacement sensing can be achieved when the external-cavity length is sufficiently short in which external cavity modes are suppressed with low optical feedback level.

1.6 Scope of the Study and Thesis Outline

The thesis will be presented as follows,

In chapter 2, we will provide fundamental properties of semiconductor lasers, followed by discussion on the dynamics of semiconductor lasers when they are subjected to optical feedback. We will also introduce the Lang and Kobayashi (LK) equations since they are

well-known to present physical insights into the experimentally observed dynamics.

In chapter 3, with regard to fundamental properties, we will demonstrate several bifurcation diagrams (BDs) obtained by tracking the intensity time series of the output light as the feedback strength is varied from zero to large values. These BDs with different conditions will enable us to understand a global picture of laser dynamics.

In chapter 4, we have obtained experimental BDs of an ECSL operated at just above threshold current and subjected to optical feedback. We will interpret intermittent behaviors between CW and LFFs with regards to extreme events and present how the parameters (injection current, feedback level, external-cavity length) of ECSL influence the frequency of extreme events in the ECSL dynamics.

In chapter 5, the behaviors of ECSL dynamics at high injection current are is largely different from the case of low injection current. As soon as intermittency between CW and LFF is not observed, two different types of intermittencies are involved in the route to chaos; one is multistate intermittency, the other is intermittency between period-doubled dynamics and coherence collapse. We will present the statistical properties of these intermittencies.

In chapter 6, after a thorough understanding of the dynamical behavior of the ECSL from chapter 2 to 5, we understand the the external feedback level affects not only the electrical field, but also the carrier density in the active region of the semiconductor laser. Therefore, we show that measuring the laser terminal voltage is the simple alternative way of measuring the optical intensity of an ECSL via photodiode(s). We will also discuss a laser self-mixing interferometry with terminal voltage.

Finally in chapter 7, we will summarize the main results of the thesis and presents some perspectives and possible directions to investigate ECSLs.

CHAPTER 2
THEORETICAL BACKGROUND OF SEMICONDUCTOR LASERS WITH OPTICAL FEEDBACK

Lasers are utilized in many aspects of life; high-speed telecommunication, drilling, cutting, alignment, guidance, surgery, holography, reading bar codes, and recording and playing compact discs, just to name a few. Especially, semiconductor lasers or laser diodes are more often used because they are cheap and compact-size thanks to development in semiconductor manufacturing technologies. As high potentials of semiconductor lasers are expected for more applications, studies of laser dynamics under various conditions has become of great interest. Particularly, it is very crucial to understand the dynamics of lasers when they are affected by optical feedback. Due to high sensitivity to optical feedback, technical applications using semiconductor lasers (for example, DVD/Blu-ray data storage/readout systems and optical fiber-based telecommunication devices) need to deal with this issue as they are sometimes accompanied by unintentional reflections from a system's components, which can easily destabilize a laser and result in complex emission dynamics.

In this chapter, we will first describe general characteristics of semiconductor lasers and discuss the dynamics of semiconductor lasers when they are subjected to optical feedback, also known as external cavity lasers (ECLs). The well-know theoretical model, Lang and Kobayashi equations, will also be presented.

2.1 General description of semiconductor lasers

A laser is defined as a device that generates light by amplification of stimulated emission of radiation. In order to explain how a laser to exhibit a beam of coherent light or electromagnetic radiation, two electronic energy states are used for simplicity. Electrons are generally stable in their ground state E_1 and some of them are spontaneously pumped to be

in the excited state E_2, *i.e.*, higher energy level. Since the excited electrons are unstable, they spontaneously decay to the ground state by emitting the absorbed energy into photons. This radiation is called *spontaneous emission*. However, when we continue to pump electrons to be in their excited states, maintaining photon emissions, *population inversion* can be observed as the population of excited electrons is greater than the population of electrons in the ground state. Hence, some electrons at a certain high-energy level ($E_2 - E_1 = h\nu$), will return to the ground state by emitting identical photons. Namely, the photons generated by stimulated emission have the same wavelength, phase and direction as the incoming photons. This results in coherent amplification of the incident light while the photons from spontaneous emission are incoherent as emitted in random directions without phase relation. To briefly summarize, the basic operational principles of lasers are; 1) energy is pumped into the medium to stimulate the emission of light, 2) the population inversion takes place in the laser gain medium, and 3) the laser cavity is formed between the rear mirror and the front one. The rear mirror is highly reflective while the front one is partially reflective, which enables photons to be amplified through the stimulated emission process and some of photons leave the cavity through the partially reflective mirror.

Although there are many different types of lasers, A p-n junction, forming the gain medium, is often used to describe the concept of a semiconductor laser because of it simple structure as shown in Fig. 2.1. The depletion layer is formed between semiconductor materials with different doping where some electrons in the n region will go through the junction and recombine with the holes in the p region. When external voltage (*i.e.* energy) is applied, the p-n junction enables current to flow in one direction and then, the electrons and the holes recombine and release energy as photons. Two cleaved end facets in the depletion layer form an optical oscillator that comprises an externally pumped active medium and a resonant cavity. Spontaneous emission noise may initiate an oscillation process and photons propagating in the cavity can be amplified due to the two reflective facets. In other words, feedback and amplification mechanism are realized in the cavity by selecting

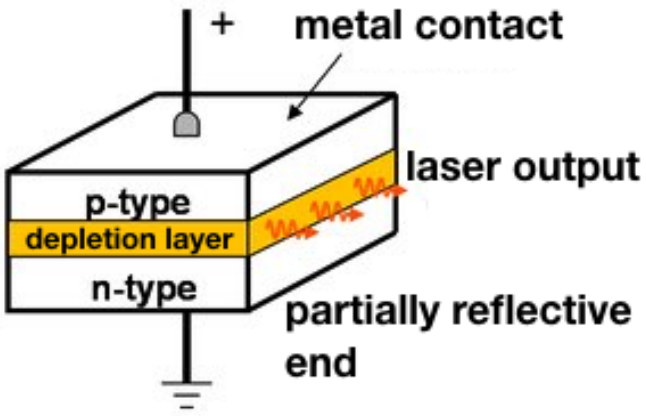

Figure 2.1: Scheme of a p-n junction semiconductor laser.

the modes of the electromagnetic field and amplifying part of the coherent light which is emitted through one of (partially reflective) end facets.

Recently, there are more ways to excite different types of atoms as the development in semiconductor fabrications is achieved. Hetero-junction architecture consisted of multiple quantum wells formed by different types of semiconductor materials is more often used than p-n junction because better confinement of electrons, holes, and more photons are possible. Semiconductor lasers are characterized by different types of cavities; the Fabry-Pèrot laser has a resonant cavity with two cleaved end facets; the distributed Bragg reflector (DBR) has multiple layers of alternating materials with different refractive index, or by periodic variation of some characteristic of a dielectric waveguide; the distributed feedback (DFB) whose the active medium is periodically structured as a diffraction grating. Note that a vertical cavity surface-emitting laser (VCSEL), as the name implies, light propagates in the direction perpendicular to the active region although we only consider edge-emitting lasers in this thesis.

Semiconductor lasers convert electrical energy into optical output and its relation can be expressed by light *vs.* current as shown in Fig. 2.2. This *L-I* curve is one of fundamentals to understand the characteristics of a laser as one can figure out a laser's efficiency and

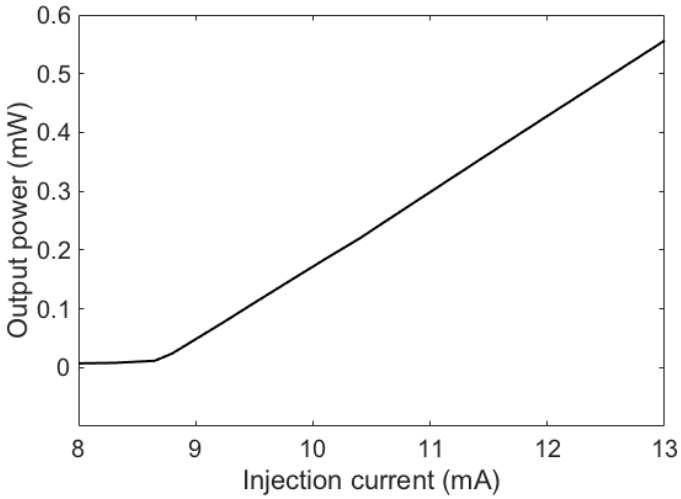

Figure 2.2: Output power vs. injection current of a laser diode. Typical characteristics of a single longitudinal-mode edge-emitting InGaAsP multi-quantum-well DFB laser used in our experiments.

threshold current J_{th}. In particular, J_{th} is the critical value that the laser diode can starts lasing at which the net gain overcomes all losses such as the transmission losses at the laser facets, the internal losses due to photon absorption inside the cavity without generation of carrier, and the loss due to light scattering. When low injection current (below J_{th}) is applied to a laser diode, the number of electron-hole pairs supplied by the injection current is small and spontaneous emission dominates in the active depletion layer. Beyond transparency *i.e.* the rates of stimulated emission and photon absorption are equal, population inversion is achieved.

When J_{th} is reached (for example, 8.8 mA at $25°$C in Fig. 2.2), the laser starts to emit stimulated light, and then the output power linearly increases as a function of injection current. This is because the number of electron-hole pairs remains stick to its threshold value and, at the same time, most of the excess electron-hole pairs are recombined via stimulated emission within the selected cavity modes.

In addition, temperature is one of important factors that contributes to $L - I$ curve. Temperature changes not only a laser's gain spectrum but the refractive index of the active medium. More current is required when a laser is operated at higher temperature conditions

[63]. We keep a laser diode stay at room temperature (25°C) in our experiments.

Arecchi *et al* [64] showed that lasers can be categorized in three (A, B, and C) classes with respect to three differential equations for the dynamical variables, the electrical field $E(t)$, the polarization $P(t)$, and population inversion $N(t)$ by using the semi-classical Maxwell-Bloch equations.

$$\frac{dE}{dt} = -(i\omega_E + \gamma_E)E(t) - i_g P(t), \tag{2.1}$$

$$\frac{dP}{dt} = -(i\omega_P + \gamma_P)P(t) + gE(t)N(t). \tag{2.2}$$

$$\frac{dN}{dt} = J - \gamma_N N(t) - i_g[E(t)^* P(t) - E(t)P(t)^*]. \tag{2.3}$$

The Eqs. (2.1-3) explain characteristics of lasers such as the resonance frequency of the laser resonator ω_E, and the optical transition ω_P and lasers' specific decay rates, which stems from the properties of the light-matter interaction in the laser cavity. Note that the decay rate of the optical field in the laser resonator γ_E, often considered as cavity decay rate; the decay rate of the polarization γ_P; the decay rate of the inversion γ_N; and the bias current of the semiconductor laser J. These parameters are associated with the characteristics of the light-matter interaction in the laser cavity and lead to three different laser categories for which the appropriate model equations exhibit different nonlinear dynamics. Of note, from the dynamics point of view, the Poincaré-Bendixon-Theorem [65] explains that systems with less than three degrees of freedom cannot exhibit chaotic behavior. Namely, at least, three degrees of freedom is required to allow a system to exhibit chaotic dynamics. Systems can have more degree of freedom via external modulations or noise.

In class A lasers, the polarization and population inversion decay on much faster than the electric field and the two quantities follow adiabatically the electric field. Consequently, Maxwell-Bloch equations can be reduced to one equation that represents the electric field

amplitude. Thus, it is safe to say that class A lasers are the most stable lasers with a high Q-factor compared to other class lasers. In class B lasers, (in fact, semiconductor lasers are classified as class-B) the polarization time constant is small enough compared to that of the other quantities, electric field and population inversion such that the polarization equation can be eliminated. In other words, semiconductor lasers are intrinsically stable lasers that can be fully described by two quantities: the slowly varying electric field and the carrier density (*i.e.*, population inversion). Lastly, class C lasers are described by the three decay rates from the Eqs. (2.1-3).

In semiconductor lasers, the interplay between the two quantities, electric field and the carrier density, produces the light-carrier density oscillation as is called the relaxation oscillation. This relaxation oscillation is an important characteristics of semiconductor lasers since it depends on the carriers which cannot instantaneously follow the photon decay rate, leading to the well-known *relaxation oscillation frequency* or f_{RO}. The two quantities, carriers and photons, periodically exchange the energy inside the laser cavity before damping and returning to the steady state. Semiconductor lasers display strongly damped relaxation oscillation with rather high relaxation oscillation frequencies. Therefore, semiconductor lasers cannot produce sustained oscillations by themselves. However, f_{RO} can easily be excited by a step function of the injection current or external perturbation such as external feedback or optical injection. Thus, the relaxation oscillation of the solitary laser plays a crucial role in the instability of semiconductor lasers especially when they are subject to time-delayed optical feedback. The population inversion can be simply replaced by electron concentration and the electric field, which are expressed with its slowly varying complex amplitude, i.e. the amplitude and the phase of the electric field. Thus, if we describe it with three equations, the two equations can be the electric field and electron concentration and the third is the phase equation. These equations will be discussed in more details in the next section.

A DFB laser is one of various types of semiconductor lasers and mainly investigated

in this thesis. Our experiments are conducted by using single longitudinal-mode edge-emitting InGaAsP multi-quantum-well DFB lasers since they are commercially mass-produced and used in many telecommunications. Single-mode operation is in general expected to observe from a DFB laser as it is fabricated by incorporating a periodic thickness variation in one of the cladding layers to form a part of the heterostructure. The feedback is distributed throughout the intra-cavity length by using a periodic index perturbation integrated in the laser structure. The laser usually oscillates at or near the maximum of the gain spectrum, which is the peak gain and typically described with a linear function of carrier density.

2.2 Semiconductor lasers with time-delayed optical feedback

Lasers are nonlinear systems and can display chaotic behavior on their output power are coupled together such that three nonlinear degrees of freedom are involved in the system [1]. The possible dynamics of semiconductor lasers are directly related to the variables such as carriers, photons, and their relaxation times. It was reported in the late 1970s that the emission properties of semiconductor lasers notably vary if the semiconductor laser is affected by external optical feedback from a distant reflector (*i.e.*, an external-cavity laser or ECL). Since then, semiconductor lasers with optical feedback have been intensively investigated and, as a result, sophisticated solutions have been suggested to utilize delayed feedback for stability of the optical output of semiconductor lasers and for narrowing the linewidth of the emitted light [5, 66, 67, 68].

Tkach and Chraplyvy [69] revealed different dynamical regimes in an ECL and they are essentially determined by the pumping current and the optical feedback conditions; the amount of light that reenters the active region of the semiconductor laser, the length of the external cavity and the feedback phase. In general, the degrees of freedom in lasers are confined in a few experimental variables, which allows clear distinction of dynamical states and makes it relatively easer to investigate various dynamical phenomena than other dynamical systems. Thus, with the help of these practical experimental systems, nonlinear

dynamics of an ECL can give us answers to the key questions of the field of nonlinear dynamics.

Here we introduce a couple of ways to add one more degree of freedom to a laser; 1) injected current modulation is relatively easier than other methods to create chaos in semiconductor lasers. Based on the modulation frequency of the injection current, different dynamics are observed such as period-doubling dynamics when the modulation frequency is higher than f_{RO} before entering chaos. 2) external optical feedback, as is the method mainly considered in this thesis, can perturbed a laser's cavity via a distant feedback reflector. Time-delayed optical feedback lead to infinite dimensional chaos. It can be simply implemented and used for several applications such as interferometry. 3) external optical injection can effectively control and produce stability (or instability) of a system. Since a system is separated by master and slave lasers, perturbing a system with an independent optical field is possible, which provides useful information about the laser cavity and gain medium. With this method, injection locking, frequency stability, and noise reduction are possible.

The emission properties of a semiconductor laser have been of huge interest when a fraction of the light, reflected back from the reflecting target, re-enters the laser cavity and modulates the laser emission from the nonlinear dynamics point of view. This is named as *external-cavity* semiconductor lasers (ECSLs). ECSLs have a high potential for many applications based on the optical feedback that can generate either stabilized or high-dimensional chaotic emission. Moreover, ECSLs can give an insight into essential questions to nonlinear dynamics fields by highlighting these practical systems generating various dynamics. Therefore, in recent year, the emission dynamics of such semiconductor laser systems has been intensively studied and various nonlinear dynamical phenomena, comprising high-dimensional chaotic intensity dynamics, has been identified.

Figure 2.3 displays schematic diagram of an ECSL. When a solitary semiconductor laser with facet reflectivity M_1 and M_2 is pumped by injection current I_{DC}, the light emitted

Figure 2.3: Scheme of a semiconductor laser subject to delayed optical feedback.

from the facet propagates towards an external mirror and is fed back into the semiconductor laser after a time delay. The length between the two facets L_{SL} denotes as the internal cavity. The conventional length of internal cavity is around 300μm. The external cavity L_{EC} is defined by the front facet of the semiconductor laser and the external mirror. The time delay in an ECSL is defined as $(2L_{EC})/c$ where c is the *in vacuo* speed of light. When the reflected light is fed back into the laser cavity and interacts coherently with the intra cavity electric field, threshold current of the laser is reduced; the more reduction is made with stronger feedback. The other influence of time-delay on an ECSL is that the coupling of photons and carrier numbers are affected by the time-delay such that high-dimensional complex dynamics are generated.

It might be expected in experiments that one could gain all information on properties of dynamics from accessible parameters and variables. Unfortunately, given the fact that ECSLs deal with the gain medium and phase complexities, some of parameters in the system are inaccessible to measure, and therefore not able to analyze them. From this perspective, a proper numerical model is necessary as it can provide us with concepts of the fundamental mechanism of an ECSL and compare with observations in the ECSL dynamics.

In 1980, Lang and Kobayashi (LK) proposed a numerical equations on a semiconductor laser, describing well that the dynamical changes in the electric field and carrier density of an ECSL with several physical parameters [3].

$$\frac{dE}{dt} = \frac{1+i\alpha}{2}\left(\mathcal{G} - \frac{1}{\tau_p}\right)E(t) + \frac{\kappa}{\tau_{\text{in}}}E(t-\tau)e^{-i\omega_o\tau} + F_E, \tag{2.4}$$

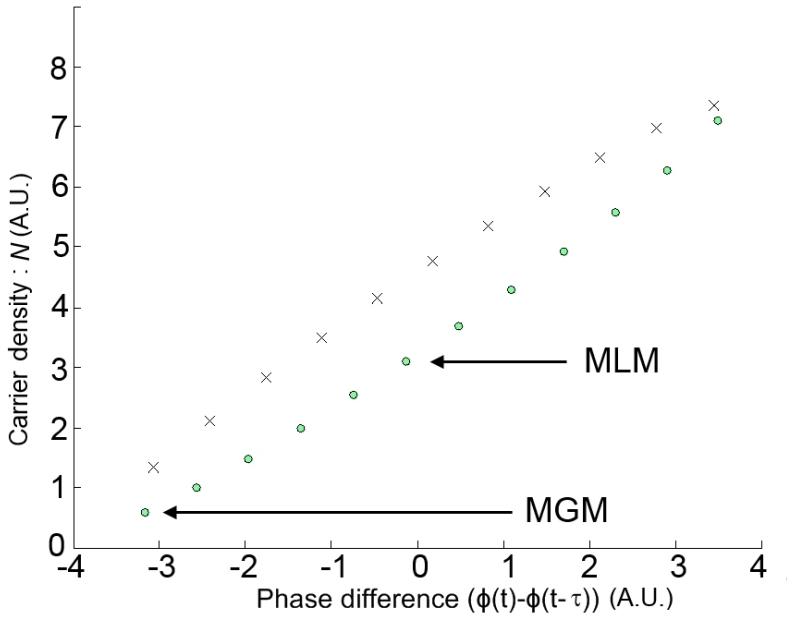

Figure 2.4: Ellipse structure of fixed points in the phase-difference-vs.-N plane for κ = 0.007 and τ= 1 ns. Circles represent ECMs; crosses represent antimodes. Adopted from Ref. [70].

$$\frac{dN}{dt} = pJ_{\text{th}} - \frac{N(t)}{\tau_s} - \mathcal{G}|E|^2. \tag{2.5}$$

with $\mathcal{G} = G[N(t) - N_o]$ being the optical gain where G is the gain coefficient, the complex electric-field amplitude $E(t)$, and the carrier density $N(t)$. N_o is the carrier density at transparency. In addition, τ_p is the photon lifetime, τ_s the carrier lifetime, τ_{in} the optical round-trip time within the laser cavity, α the linewidth-enhancement factor, p the pumping factor, and J_{th} the threshold current. The spontaneous-emission noise is a term $F_E = \sqrt{2\beta N}\xi$, where β is a spontaneous-emission noise factor and ξ is a complex Gaussian white noise of zero and auto-covariance function $C_x(t-t') = \langle \xi(t)\xi(t') \rangle = 2\xi(t-t')$. We numerically integrated Eqs. (1) and (2) with the following parameters: $G = 8.1 \times 10^{-13}$ m^{3}s^{-1}, $N_o = 1.1 \times 10^{24}$ m^{-3}, $\tau_p = 1$ ps, $\tau_s = 1$ ns, $\tau_{\text{in}} = 8$ ps, $\alpha = 3$, and $\omega_o\tau = 0$. The external cavity in the LK model is described by the three parameters: theoretical feedback strength κ (proportional to experimental feedback strength), delay time τ (proportional to L), and the feedback phase $\omega_o\tau$, with the solitary laser angular frequency ω_o.

The first term on the rhs of the Eq. 2.4 is the solitary emission of a laser and the second term is about the external-cavity feedback parameters. The phase change in the external cavity is represented by $\Phi = \omega_0\tau/(2\pi)$ where ω_0 is the optical frequency of the solitary laser. The LK model does not consider noise effects which, under certain conditions, might play important roles in the dynamics because of the high sensitivity of semiconductor lasers even to small perturbations. Thus, sometimes it is necessary to insert the noise factor with F_E. In addition, nonlinear gain saturation effects are not considered and spatial and thermal effects are neglected. Surprisingly, even with these simplifications, The LK equations show some excellent and qualitative agreements with experimental observations from ECSLs and provides ideas of fundamental mechanism regarding the dynamical instabilities and emission properties of ECLs. The steady-state solutions of the LK model are based on interference between the intra-cavity field and the external-cavity feedback. The steady solutions are known as *external cavity modes* (ECMs), which are modes located in the constructive interference while anti-modes in the destructive interference. Solutions of ECMs are shown in Fig. 2.4. Two specific ECMs are displayed; the minimum linewidth mode (MLM) and the maximum gain mode (MGM). The MGM is the ECM with the lowest frequency (high-gain), and is typically stable [5, 71]. The MLM is the ECM most proximate in frequency to the solitary laser mode ω_0. In the general, trajectories in the space [Fig. 2.4] can be delineated parametrically in the time-dependent case such that it is possible to extract the detailed evolution of all dynamical variables of the system. The electric field intensity can be extracted from the phase-space trajectory and used to construct a theoretical BD, so as to compare with experimental BD. More discussion on ECMs will be extensively covered in the following chapter because the detailed analytics of ECL dynamics can be manifested with the combination of dynamical regimes and ECMs.

With the help of the LK model, several solutions for stabilizing lasers and for narrowing the linewidth of the emitted light were suggested [66, 67]. Various nonlinear dynamical phenomena as well as high-dimensional chaotic dynamics have been identified [72, 73].

The characteristics of different dynamical regimes in an ECL essentially depend on different parameters; pump current, optical feedback, and the length of the external cavity. To better describe the transition from one dynamical regime to another by varying a parameter in ECLs, one can exploit a bifurcation diagram.

CHAPTER 3
BIFURCATION DIAGRAMS OF AN EXTERNAL-CAVITY SEMICONDUCTOR LASER

3.1 Theoretical framework

We have discussed in chapter 2 that ECSLs exploit an external mirror to provide time-delayed optical feedback into the laser diode and their dynamical behaviors varies with the operating and design parameters. In particular, time-delayed feedback in ECSLs induces high-dimensional and highly multistable dynamics, which allows for chaotic behavior [74, 75]. More broadly, the dynamics of ECSLs has been extensively studied [5, 6, 17, 76, 77]. Despite numerous studies of ECSLs, there is still a lack of experimental investigations on ECSLs that illustrate detailed knowledge of the various dynamical regimes with various operating parameters, such as the feedback strength, the injection current, and the external cavity length. As a function of a parameter, ECSLs experiences a bifurcation between dynamical transitions at a certain value of the parameter. As methodology, visualized bifurcation diagrams (BDs) are largely used to obtain meaningful information concerning the detailed dynamical regimes and transitions between them. BDs can be obtained by fixing all but one parameter, and then mapping out the extremal values of measured dynamical variables as a function of a parameter. BDs provide clear and systematic experimental evidence of the way in which instabilities of various nature develop in an ECSL.

Several theoretical and numerical works have studied in detail the BDs of ECSLs as a function of the feedback strength [78, 79, 80]. However, only few experimentalists investigated changes of dynamical behaviors based on intensity time series or the optical/RF spectra through different operating parameters. Tkach and Chraplyvy [69] classified the five different regimes in the ECSL based on different external feedback strength; In regime

I, the laser linewidth is broadened or narrowed, depending on the phase of the optical feedback; Regime II: low-frequency mode hopping occurs between external cavity modes; Regime III: stable single-mode operation with a narrower linewidth reduction and the mode hopping is suppressed; Regime IV: unstable operation with coherence collapse, the relaxation oscillations become undamped and the linewidth are largely broadened; Regime V: stable operation with significant linewidth reduction and the laser emits on a single mode with a narrow linewidth. Of note, in the moderate feedback (regime IV), and long external-cavity case, the dynamical regimes of an ECSL, as injection current is increased, are noisy continuous emission, low-frequency fluctuations (LFFs), and coherence collapse (CC).

This chapter is based on the following publications:

- Byungchil Kim, A. Locquet, Nianqiang Li, Daeyoung Choi, and D. S. Citrin, "Bifurcation-Cascade Diagrams of an External-Cavity Semiconductor Laser: Experiment and Theory", IEEE Journal of Quantum Electronics, Vol. 50, No. 12, Dec (2014).

- Byungchil Kim, A. Locquet, Daeyoung Choi, and D. S. Citrin. "Experimental route to chaos of an external-cavity semiconductor laser" Physical Review A, 061802 (2015).

- A. Locquet, Byungchil Kim, Daeyoung Choi, Nianqiang Li, and D. S. Citrin. "Initial-state dependence of the route to chaos of an external-cavity laser", Physical Review A 95, 023801 (2017).

We further investigate the dynamical regimes of ECSLs through BDs based on a continuous change of a parameter. Controlling external cavity L, injection current J, and feedback strength η enable an ECSL to exhibit various dynamical behaviors and finally enter chaos regime, which is called route to chaos. A quasi-periodic route [81] is one of well-known routes to chaos in which a stable external-cavity mode (ECM) is replaced by a periodic oscillation at a frequency close to the relaxation-oscillation frequency f_{RO} of a solitary LD, then quasi-periodicity, involving a second frequency close to $1/\tau$, and chaos are observed.

A period-doubling route to chaos has also been observed [82]. In this case, a cascade of period-doubling bifurcations creates oscillations at frequencies close to sub-multiples of f_{RO}. When the conditions are such that several ECMs are destabilized simultaneously, generalized multistability drives several attractors or attractor ruins to coexist in phase space [5, 83].

Theoretical BDs of an ECSL as a function of the feedback strength have been presented [74, 75]. One remarkable example is the switching between a low-frequency-fluctuations (LFF) state and a state of stable emission (continuous wave or CW) observed in [44, 71, 84]. Experimental BDs have been obtained for other kinds of lasers such as optically injected solid-state lasers [85], Q-switched gas lasers [86, 87], and bifurcations transitions have been identified in lasers subjected to optical injection [88, 89]. In our recent paper [90], we overcame the experimental difficulties and presented the existence of BDs for ECSLs. We managed to control feedback strength η in minuscule steps by means of a motorized rotation stage in high-stability conditions which allows for very good horizontal resolution of the BDs. We also added a more systematic infomation, in light of experimental BDs, on the influence of operational parameters (current, length, feedback level, feedback phase) and conditions (forward and reverse BDs, influence of noise) on the ECSL dynamics, which will be discussed in this chapter.

We conduct various experiments extensively and compare with theoretical studies based on the Lang and Kobayashi (LK) model [3]. The LK equations have successfully predicted some dynamical trends as a function of various parameters [74, 75]. Thus, we make use of the LK model to elucidate the dynamics of an ECSL observed experimentally. Comparison between experiment and simulation will validate observed phenomena within the considered boundary of the parameters range, including the influence of J and L.

In addition, we discuss BDs obtained by different conditions (injection current, feedback strength, external-cavity length). Firstly, injection current plays a crucial role in the route to chaos. When an ECSL enters chaotic regimes, low and high injection current leads

to the two different types of chaotic behaviors, low frequency fluctuations (LFFs) and fully-developed coherence collapse (CC), respectively. Also, external-cavity length L is chosen such that the external-cavity free-spectral range of the light (f_τ= c/2L) is lower than the frequency of the relaxation oscillations of the solitary laser f_{RO}. By using the LK model, we compare experimental and numerical BDs and investigate how the trajectories of an ECSL are developed in phase space as a function of a parameter. In addition, we further scrutinize the BDs with different L and η at low and high injection current to see how they have impacts on the instability of an ECSL on the route to chaos. Lastly, we present that the different initial conditions result in different types of Hopf bifurcation via the innovative way of changing initial conditions in experiments.

3.2 Experimental setup

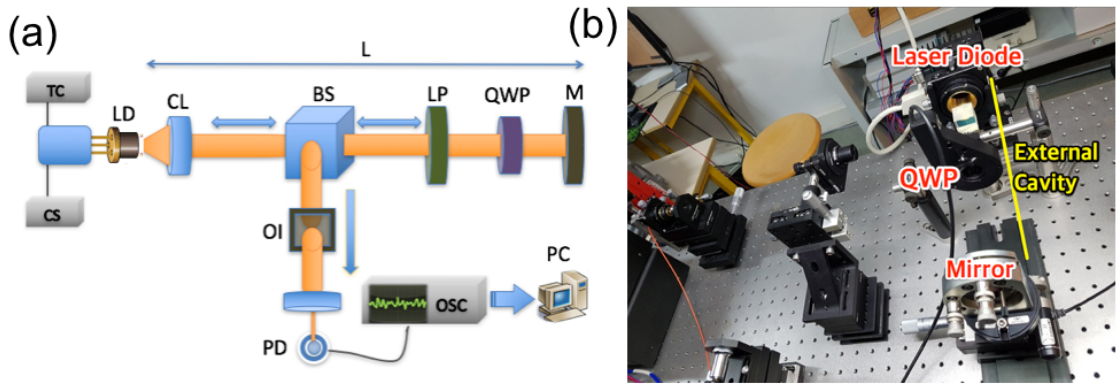

Figure 3.1: (a) Experimental schematics, (b) a setup of (a) in the lab. LD: laser diode, BS: beam splitter, L: external-cavity length. TC: temperature controller, CS: current supply, CL: collimation lens, LP: linear polarizer, QWP: quarter-wave plate, M: mirror, OI: optical isolator, PD: photo detector, OSC: oscilloscope, and PC: personal computer.

The experimental setup is shown in Fig. 3.1. Light from the laser diode (LD) is split into two free-space optical paths via a beam splitter (BS). One optical path is used for feedback into the LD and the other is for coupling and/or observing the dynamics of the intensity detected at the photodiode. The SL used in our experiments is an intrinsically single-longitudinal mode InGaAsP DFB laser that oscillates at wavelength 1550 nm. The

free-running threshold current (J_{th}) is 9.27 mA. A real-time oscilloscope with 12 GHz bandwidth is employed to capture the time series of the optical-intensity time series. In addition, we measure the RF spectrum of the optical intensity with a spectrum analyzer with a 23 GHz bandwidth. The optical spectrum is measured with a high resolution optical spectrum analyzer (BOSA200) with 10 MHz optical resolution. L is variously chosen to be 15, 30, or 65 cm which corresponds to external-cavity round time τ = 1, 2, or 4.3 ns, respectively.

It is essential to have highly stabilized temperature (temperature stability / 24 hours $<$ 0.002 $^\circ$ C) and current J (drift / 24 hours $<$ 100 μA) to ensure reproducibility. In addition, η is controlled in small steps by slowly changing the angle of the quarter-wave plate (QWP) in the external cavity by means of a motorized rotation stage. This allows for very good horizontal resolution of the BDs; indeed, the rotation velocity is 0.01 degree/minute and the resolution of the angle of QWP is 1/100 degree, leading to a 4500 possible different values of the feedback in a BD. The maximum feedback attainable in our experiment, corresponding to η = 0.8, is reached when the QWP is such that the polarization is not subjected to any rotation. Then, approximately 20% of the optical power is fed back onto the collimating lens.

3.3 Experimental bifurcation diagrams

3.3.1 Experimental bifurcation diagram at low injection current

An example of an experimental BD is shown in Fig. 3.2 for J = 10.54 mA with L = 15 cm, corresponding to a frequency spacing between ECMs of $\sim$1 GHz. The BD is obtained by taking the local extrema of the intensity time series from the high-bandwidth oscilloscope used in the experiment as a function of η. A probability density function of the extrema of the intensity time series is obtained and plotted with a color map, in which density is high in white (blue in the color figure) but low in black regions. The first experimental report of a cascade of bifurcations is due to Hohl and Gavrielides [76]. Here we observe a

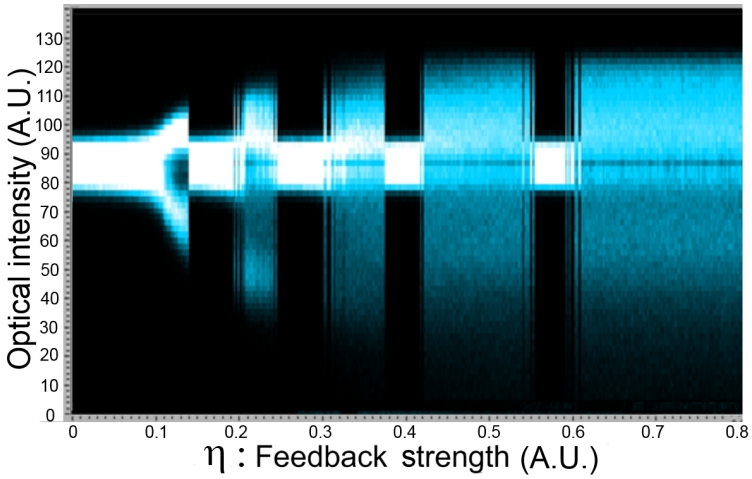

Figure 3.2: Experimental BD for J=10.54 mA and L=15 cm.

bifurcation cascade between stable and unstable regions.

At the low current, the photo-detected optical intensity is weak and cannot always be distinguishable from the system noise. The thinner regions in the optical intensity is the stable regions, not necessarily continuous wave (CW) behavior but contain regimes where instabilities around a single ECM are observed. The wider regions in the optical intensity are referred to unstable regions, typically corresponding to regimes in which trajectories wander around several ECMs due to chaotic itinerancy and thus clearly higher intensity than noise.

In order to analyze the effect of J, we obtain the experimental bifurcation cascades for J = 11.84 mA, 12.70 mA, 14.67 mA, and 16.01 mA [Fig. 3.3]. Commonly, we observe alternating stable and unstable regions, but no longer a systematically cascade involving the successive MGMs when η is increased. When J is increased, the BD exhibit larger regions of undisturbed chaotic behavior. For larger J, the stable regions, though limited in number, persist for a larger range of feedback levels than is the case for low J.

We consistently see the presence of alternating stable and unstable regions for all values of the current between J_{th} and $\sim 1.6 J_{\text{th}}$, which means that experimental cascades of BDs are relatively robust. Meanwhile, when $J > \sim 1.6 J_{\text{th}}$, we no longer observe any stable region in the range of BD. We therefore conclude that the laser we used never lies on or in the

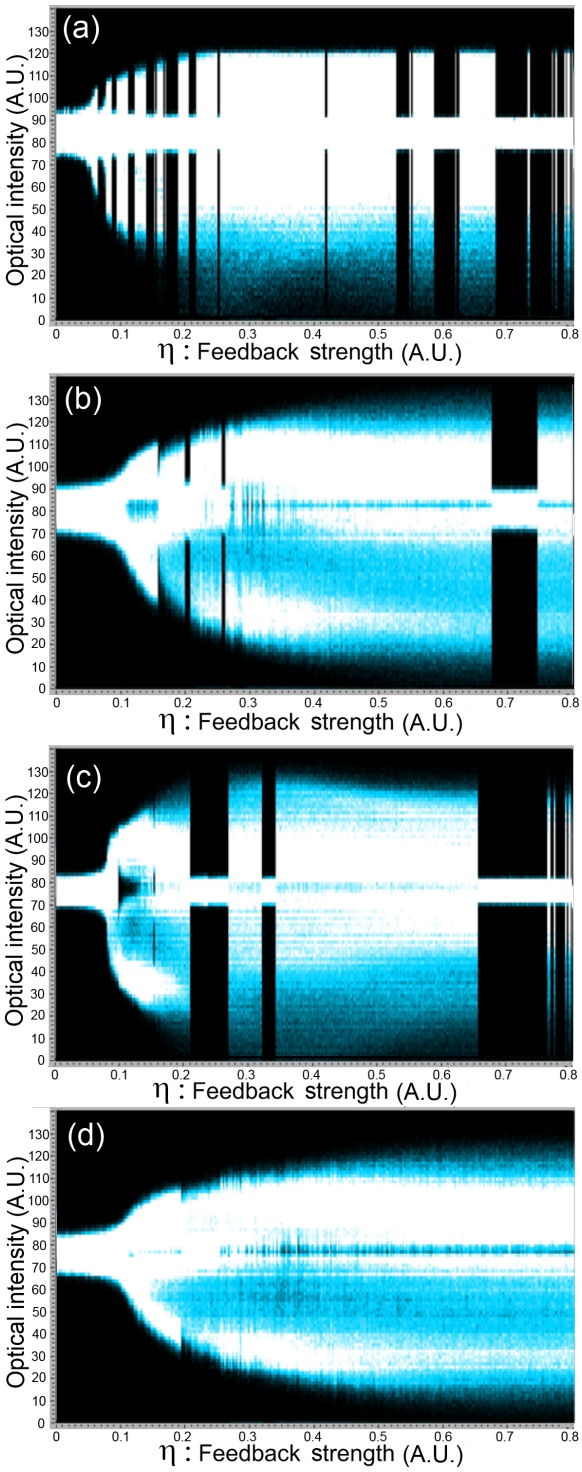

Figure 3.3: Experimental BDs for L = 30 cm with (a) J = 11.84 mA, (b) 12.70 mA, (c) 14.67 mA, and (d) 16.01 mA.

vicinity of a single ECM and its dynamics necessarily involves attractor ruins of several ECMs. The analysis of the time series, RF, and optical spectra [90] also reveals that the dynamical behavior in the first few unstable regions of the cascade is typically low frequency fluctuations (LFF) for currents up to $1.2J_{\text{th}}$, while larger feedback and current levels lead to fully-developed coherence collapse (CC).

In the unstable regions for low η, we systematically identify LFF, and in particular its typical random power dropouts. In contrast, for higher η, we do not observe LFF but a regime of fully developed CC. We systematically identify LFF until η $\sim$0.18 is reached while for larger J, we do not observe LFF.

The dependence of the BD on L is shown in Fig. 3.4. The experiment is conducted for four different external-cavity lengths L = 10, 30, 50, and 65 cm, at J = 11 mA. For a small L, significantly longer stable regions where the laser-output power dwells on a single ECM is seen before moving into the subsequent unstable regime, followed by the next ECM [Fig. 3.4(a)]. Thanks to the increased stability of short cavities, a well-resolved experimental Hopf bifurcation of the first ECM appears in the cascade. In Fig. 3.4(d), when L = 65 cm, we barely observe a cascade of bifurcations for small η. The laser-output power remains briefly on a single ECM, then moves into an unstable regime followed by the next stable ECM over a small range of η and we cannot observe any cascading behavior by further increasing η. This is because ECMs are closely located each other such that it becomes harder to stay in a single ECM.

A simulated BD of the optical intensity as a function of the theoretical feedback strength κ is utilized to interpret the influence of L and J on the BD. To further reflect our experiments where η is gradually ramped up, the initial state, for a given κ, is taken to be equal to the final state of the simulation corresponding to the previous, smaller value of κ. It is evident from the plot that alternating stable and unstable regions occur.

Figures 3.5(a) and (b) display the numerical BDs for different external cavity lengths (L = 15 cm and 65 cm). p is the numerical injection current relative to the threshold p_{th}. With

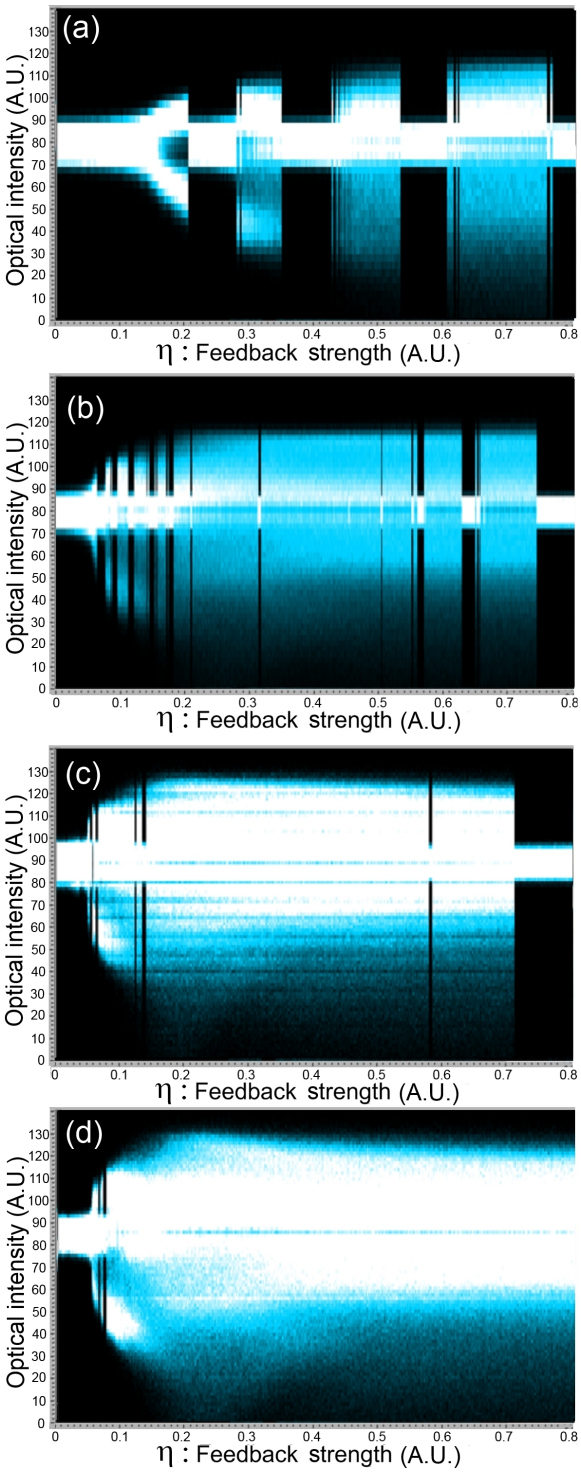

Figure 3.4: Experimental BDs for $J = 11$ mA with (a) $L = 10$ cm, (b) 30 cm, (c) 50 cm, and (d) 65 cm.

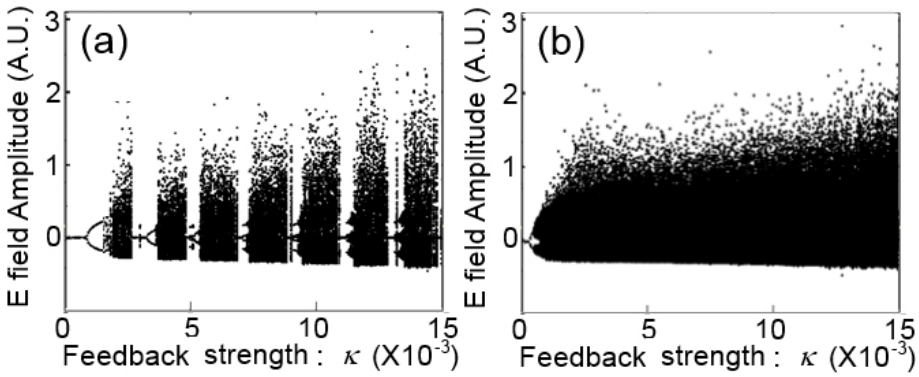

Figure 3.5: Numerical BD for (a) L = 15 cm and (b) L = 65 cm at $p = 1.03p_{th}$.

short L, we observe a cascade of bifurcations while and significantly longer stable regions before entering the subsequent unstable regime. And, as explained in [5], we observe the chaotic behavior that develops around a single ECM in the beginning, and then extends to several ECMs as neighboring attractors merge through a crisis (region φ of Fig. 3.6). This crisis leads to an abrupt change in the optical intensity. With respect to experimental BDs, the crisis corresponds to the onset of the moment when the amplitude of optical intensity jumps above the noise level.

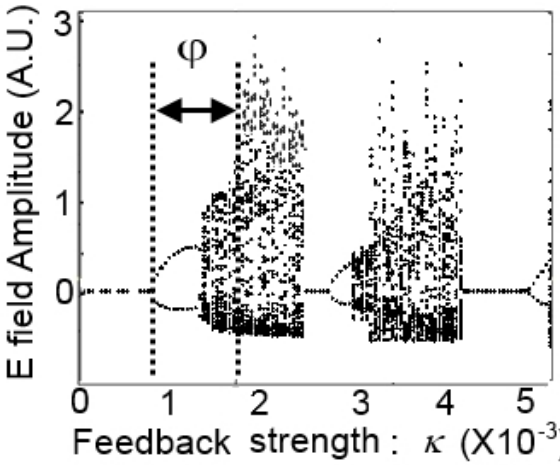

Figure 3.6: Numerical BD for $p = 1.03p_{th}$ and L = 15 cm ($0 \leq \kappa \leq 5.5\times10^{-3}$).

Meanwhile, when L is large, the spectral separation between ECMs is reduced (e.g., 1 GHz→15 cm, 500 MHz→30 cm, 233 MHz→65 cm) in the optical spectrum. Namely, each participating mode is closer in phase space and large-amplitude itinerancy between

several modes is easily observed. In the limit of a very long L, It was proved numerically that the laser is always unstable [91]. The numerical observation of the trajectories on the ellipse showed that the proximity to the ECMs interferes the development of independent stable attractors and thus prevents the existence of a cascade of stable and unstable regions, as confirmed in our experiments. In contrast, increasing distance between the ECMs for shorter L requires larger η needed before attractor merging, which is also observed in the experimental BDs of Fig. 3.4 as the longer stable regions.

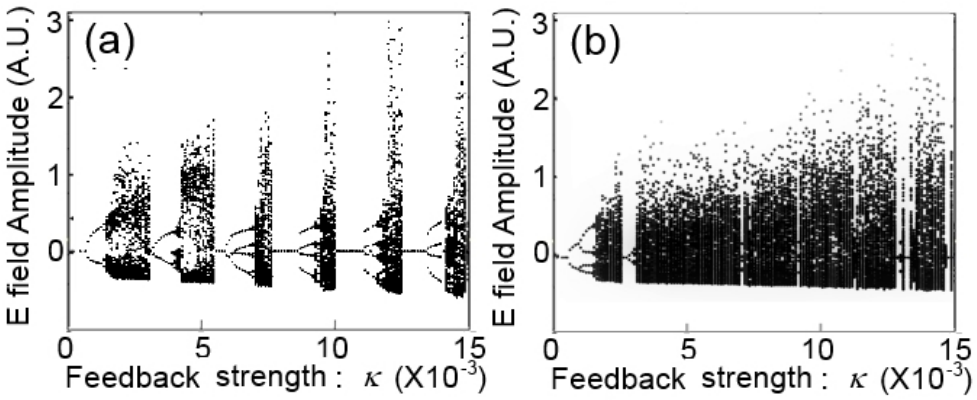

Figure 3.7: Numerical BD for (a) $p = 1.02p_{th}$ and (b) $p = 1.04p_{th}$ at L = 15 cm.

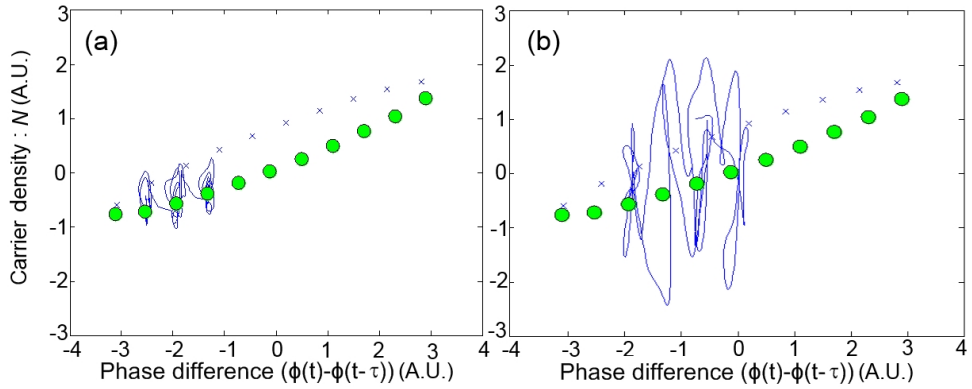

Figure 3.8: Trajectory in phase space with pumping currents (a) $p = 1.03p_{th}$ and (b) $p = 1.05p_{th}$ at τ = 2 ns and κ = 0.0025.

Figures 3.7(a) and (b) show simulated BDs for different normalized pumping currents (p = 1.02 and 1.04) and Fig. 3.8 presents the trajectory in phase space for identical parameters except for the current level p. These figures allow us to interpret the influence of J on

the BD. Larger J leads to larger changes in the optical intensity and thus to trajectories that explore a larger region of phase space. At low J, in the unstable regions (that is the LFF regime), a trajectory towards the MGM is observed. At larger J, in the unstable regions *i.e.*, fully-developed CC regime, chaotic itinerancy between ruins of ECMs is observed and there is no trajectory toward the MGM. This behavior explains the increased difficulty in reaching the MGM as J is increased. In particular, it explains why we observe numerically that at larger J, larger κ is needed to get out of an unstable region and reach the MGM. Otherwise, the MGM is not reached at all. We observe the perturbed aspect of the bifurcation cascades for larger J but some stable regions do not appear in the BD because the trajectory never settles in the MGM, and in this case, long uninterrupted regions of chaotic itinerancy are observed.

For the comparison to the experimental observation of the total absence of stable regions when the J is larger than $1.6J_{\text{th}}$, we calculate trajectories in phase space that above a certain feedback level, the ECSL dynamics show chaotic itinerancy among ECMs that are far away from the MGM, with no drift toward the MGM, such that the MGM is not accessible [74, 75].

Our experimental observations illustrate that long stable regions can be observed at larger J as being linked to the condition that larger κ is needed to destabilize the MGM when J is increased. In addition, the Eq. 21 in [81] gives an approximated value for κ at which Hopf instability sets in, which is in a good agreement with our observations. Moreover, for large values of J, two or more successive stable regions are linked with different, successively appearing ECMs. In the long stable regions, the slipping to the next ECM is observed from the ECSL dynamics without involving a phase of itinerancy around several ECMs.

To summarize, we have shown several aspects of the ECSL dynamics of ECSLs at low J, using BDs based on the optical intensity of a DFB laser subjected to optical feedback. We have also carried out theoretical calculations with the LK model. Despite its simpli-

fications, this model can successfully reproduce the bifurcation cascade at low J. The trajectory reaches the MGM occurs rarely for large *J* and larger κ is required to destabilize it. The behaviors of ECSL in the LK model are well-matched even with increasing L conditions in which attractor merging increases due to the increased proximity of ECMs in phase space.

3.3.2 Experimental bifurcation diagram at high injection current

We have seen that when injection current *J* is just above threshold J_{th}, spontaneous-emission noise obscures the details of the bifurcations, and thus reliable classification were not easily made. In this chapter, we obtain experimental BDs at relatively high injection current $(2-3)J_{th}$ in the long-cavity case. High *J* is important to suppress the relative importance of spontaneous-emission noise, bringing closer to the deterministic dynamics of the ECSL and identify the route to chaos, *i.e*, sequence of bifurcations leading to fully-developed coherence collapse (CC).

Figure 3.9(a) represents the experimental forward BD when I=22.08 mA with L=30 cm, resulting in f_{RO} $\sim$7.5 GHz and a spacing between ECMs of $\sim$500 MHz. As is done for the BDs for low J, this BD is obtained by taking the local extrema of $\mathcal{I}(t)$ as a function of η. Density is high in white but low in black regions. The terminal voltage of the LD V_{LD} is measured along with the BD in Fig. 3.9(b). V_{LD} is the time-averaged value of the LD terminal voltage and tracks the changes in the carrier density N [92, 93]. A reduction in N caused by the optical feedback, in turn, reduces the difference between quasi-Fermi levels in the p- and n-type quasi-neutral regions of the LD. The overall reduction in N in the active region leads to a reduction in V_{LD}. We thus use V_{LD} to determine the dynamical regime of the ECSL.

To investigate the ECSL dynamics, experimental RF spectra in linear scale (left column), optical spectra (right column), and $\mathcal{I}(t)$ (inset) at various feedback levels of the BD are illustrated in Fig. 3.10, for I=22.08 mA. Note that what is labeled to be 0 GHz in the

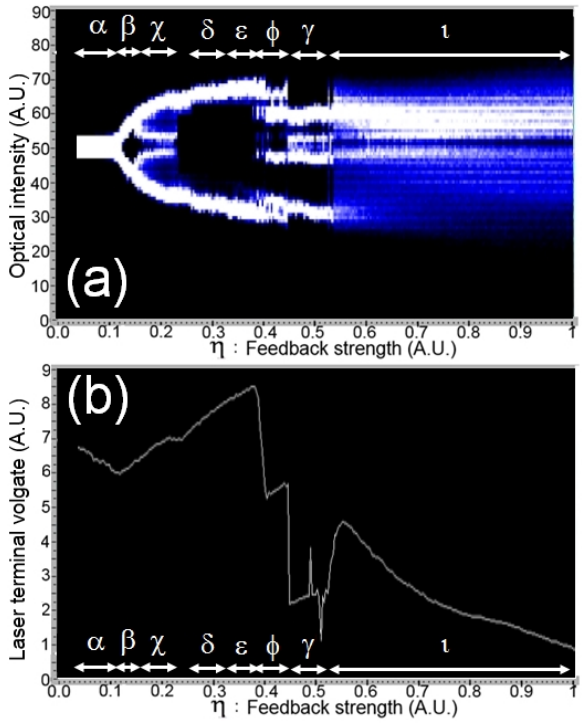

Figure 3.9: (a) Experimental forward BD for I = 22.08 mA and L = 30 cm and (b) corresponding V_{LD}.

optical spectrum actually corresponds to the frequency of the ECM (1) at 193.271 THz. We observe from Fig. 3.10 that the ECSL is initially in ECM (1). In the corresponding region α ($\eta \sim$0.05) of Figs. 3.9(a), (b) and 3.10(a1), (a2) only one fixed point (ECM 1) participates in the output, and the ECSL displays continuous wave (CW) behavior. From Fig. 3.9(b), V_{LD} decreases with increasing η, indicating a decrease in the carrier number and increase in power in this regime, which was predicted by the LK model [93].

As η is increased above 0.12, it can be clearly observed in the BD [inset of Fig. 3.10(b2)] that the ECSL undergoes a periodic oscillation. This oscillation is manifested with sidebands $\pm$ 8 GHz away from ECM 1, a frequency that also stands out in the RF spectrum [Fig. 3.10(b1)]. In this regime, V_{LD} is monotonically increasing in η [region β of Figs. 3.9(a), (b)]. This transition in the dynamics corresponds to a Hopf bifurcation leading to a limit cycle whose frequency is close to f_{RO}.

With increasing η, additional side bands around f_τ appear in the optical spectrum [Fig.

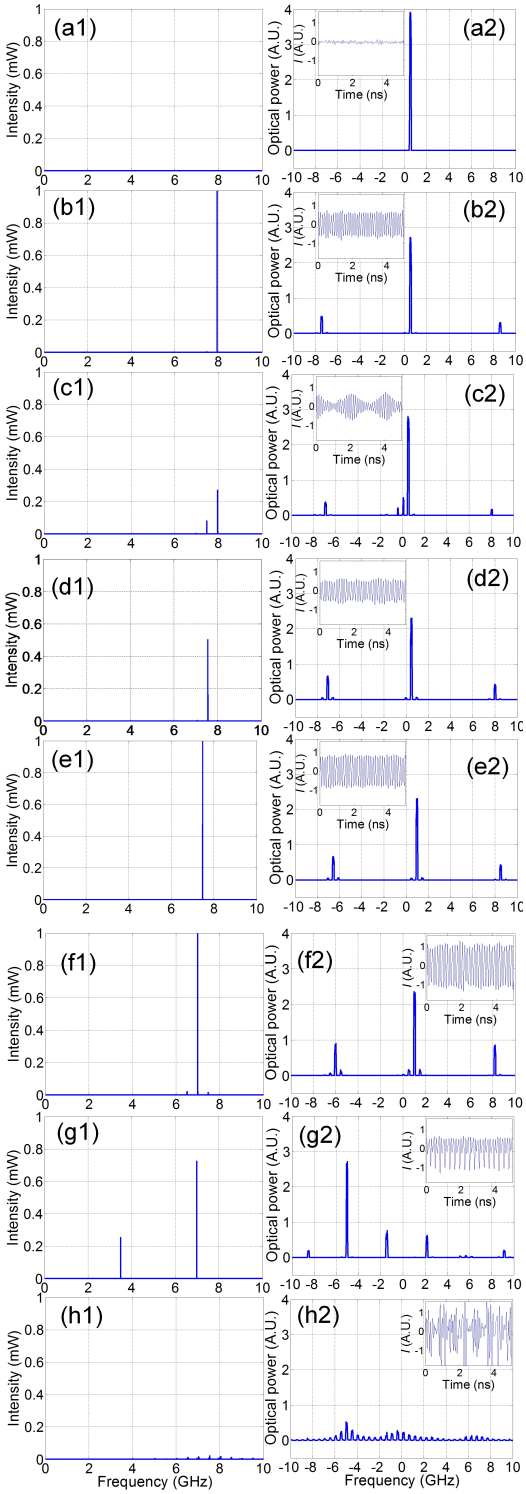

Figure 3.10: Experimental optical spectrum (first column) with an optical spectrum analyzer, associated $\mathcal{I}(t)$ (inset) and RF spectra of $\mathcal{I}(t)$ (second column) for (a1)(a2) η=0.05, (b1)(b2) 0.13, (c1)(c2) 0.2, (d1)(d2) 0.26, (e1)(e2) 0.28, (f1)(f2) 0.35, (g1)(g2) 0.5, and (h1)(h2) 0.8.

3.10(c2)], revealing a second frequency in the dynamics. This presence of the second frequency is confirmed by the RF spectrum [Fig. 3.10(c1)] and the corresponding time series of $I(t)$ reveals a quasi-periodic oscillation of the optical intensity [inset of [Fig. 3.10(c2)]. The undamped second frequency, close to f_{tau}, corresponds to a secondary Hopf bifurcation, which is associated with the development of a torus attractor in phase space as predicted by LK [6, 94]. Interestingly, both the limit cycle and the torus result from the destabilization of ECM (1).

For a further increase in η, another limit cycle appears. The optical spectrum shows [Fig. 3.10(d2)] that this cycle is still centered on ECM 1, and has now a frequency of approximately $\pm$7.5 GHz, as evidenced both by the RF [Fig. 3.10(d1)] and optical spectra [Fig. 3.10(d2)]. Pieroux *et al.* [95] have explained that multiple periodic solutions can occur in class-B lasers subjected to delayed feedback and that their interaction can lead to quasiperiodic solutions. As η is further increased, and region ϵ of Figs. 3.9(a) is reached, a small discontinuity in the BD, as well as a discontinuity in the slope of V_{LD} [Figs. 3.9(b)] are observed. From the optical spectrum [Figs. 3.10(e2)], this discontinuity is associated with the jumping from ECM 1 to 2. As evident in the time series [inset of Figs. 3.10(e2)], the ECSL continues to oscillate periodically, and both the optical and RF spectra [Fig. 3.10(e)] confirm that the frequency of the oscillations is still equal to 7.5 GHz. Hence, we can interpret that, combined with the previous observations, the trajectory moves in the positive-frequency direction and transits to another limit cycle, of the same frequency, on a different ECM. Increasing η even further, another limit cycle at $f_{\mathrm{RO}} \sim$7 GHz is observed [region ϕ of Figs. 3.9(a),(b) and 3.10(f1),(f2)]. The active ECM (2) does not change in the transition from region ε to ϕ of Fig. 3.9(a), indicating the existence of two different oscillation frequencies, 7.5 GHz and 7 GHz, again approximately separated by $\sim f_{\tau}$ on ECM 2.

A hitherto monotonic increase of V_{LD} is seen and V_{LD} is more increased than the initial condition (ECM 1) with $\eta \sim 0.02$. The trajectory moves toward shorter wavelength

[right half in the $\Delta\phi$-vs-N plane in Fig. 2.4]. The optical spectrum [Fig. 3.10(e2) and (f2)] also confirms that the dominant mode is ECM 2 at larger frequency. These observations are of a fundamental importance for understanding the route to chaos because of matching the numerical analysis based on LK model in ECSL. Our experimental results agree with Masoller and Abraham [5], who predicted that initially, for small feedback levels, the dominant peak is shifted by one or more multiples of the ECM frequency spacing towards positive frequency. They attributed this behavior to the fact that ECMs that are close to the MLM (e.g. ECM -1 and -2) but of lower frequency have very small basins of attraction compared to positive ECMs at low η for high J, while ECMs with large positive frequency shifts are highly unstable.

As η is further increased, two sudden drops in $V_{\rm LD}$ are observed. The one is around η =0.38, the other around 0.45. The values reached by $V_{\rm LD}$ are lower than the initial ECM (1) at η = 0.02. The trajectory has abruptly moved toward ECMs located at lower frequencies than the MLM [left in the $\Delta\phi$-vs-N plane in Fig. 2.4].

Figure 3.10(g) shows the behavior of the ECSL just after the second dropout (region ι of Figs. 3.9 (a),(b)). The optical spectrum shows that the ECM stays around ECM -10 [Fig. 3.10(g2)], while the RF spectrum highlights that the frequencies involved in the dynamics are $\sim$7 GHz and 3.5 GHz [Fig. 3.10(g1)]. This region corresponds to a period-doubled limit cycle oscillation around ECM (-10). Also, we interpret the previous region [γ of Figs. 3.9 (a),(b)] corresponds to a region intermittency is observed between regions ϕ and γ of Figs. 3.9 (a),(b). Non-stationary of ECSL behavior in this intermittency region will be further discussed in the following chapter.

Finally, when η becomes larger than $\sim$0.5, the trajectory wanders among several ECMs located at lower frequencies than the MLM. The optical intensity undergoes rapid chaotic fluctuations on the sub-ns time scale [Fig. 3.10(h2)] and the broad RF spectrum [Fig. 3.10(h1)] indicates the excitation of a continuous range of frequencies. This regime is widely termed as fully-developed coherence collapse (CC). This evolution of the laser dy-

namics around negatively shifted ECMs is typically predicted by the LK model including fully-developed CC.

To summarize, our results provide detailed experimental observations of the ECSL dynamics at high J through the bifurcation of a LD subjected to external optical feedback. Also we confirmed that our experimental BDs are compatible with some of the predictions of the LK model concerning the route to chaos for ECSLs.

3.3.3 Generalized multistabililty on the route to chaos with different initial conditions

As we have seen from experimental BDs with different operating parameters, ECSLs display a rich variety of dynamical behaviors due to the peculiarities of the delayed feedback and an infinite-dimensional dynamical system. The dimensionality of a dynamical system is important as it plays a key role in determining the types of phase-space trajectories that exist for a given set of system parameters. High-dimensional dynamical systems can exhibit generalized multistability in which several different attractors, at various stages of development, and each with a specific basin of attraction, coexist for a given set of parameters. It is known that hundreds of attractors or attractor ruins can coexist in the same region of phase space, known as generalized multistability, leading to a wealth of dynamical regimes of varying complexity [17, 74, 96, 97]. Previous work on generalized multistability has focused on intermittency between coexisting attractors [86, 98, 99] induced by noise or perhaps by the fact the apparently different coexisting attractors are actually parts of the same attractor weakly linked by a rarely visited region of phase space. Indirect evidence of multistability has been obtained experimentally in different lasers [70, 100, 101].

While coexistence of attractors and the associated multistability is expected based on theoretical considerations, in an experiment, as noted above, one might expect that the selection of initial conditions would have little effect on the BD, since it is reasonable to suppose that noise would cause the phase-space trajectory to converge rapidly toward the same attractor, regardless of initial conditions. In this chapter, we illustrate clear evidence

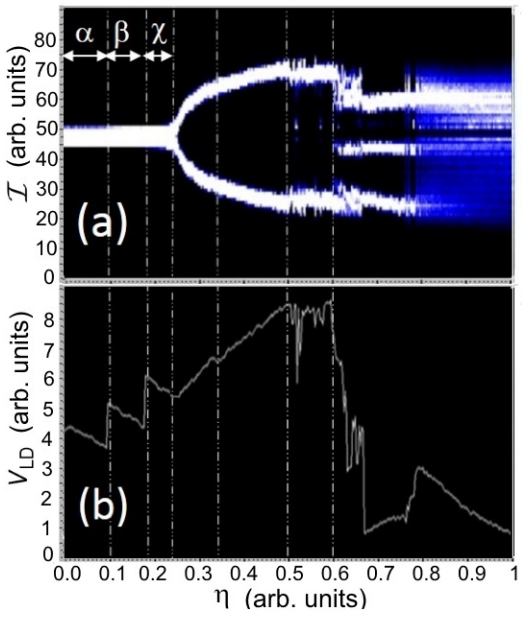

Figure 3.11: Reverse BDs. (a) Reverse BD, and (b) the corresponding $V_{\rm LD}$. $J = 22.59$ mA and $L = 30$ cm.

of generalized multistability based on observation of different BDs at high injection current, obtained by different initial states.

In numerical simulations, one simply chooses initial conditions and computes from there. In experiment, however, this can be quite challenging. We introduce a controlled method to select experimentally the initial ECM at low η where the ECSL otherwise operates continuous wave (CW) approximately like the solitary LD. The selection procedure is described as follows. Consider mapping out the forward BD starting with $\eta = 0$. In this case, the ECSL stays on the MLM; this is the initial state. Suppose we proceed ramping η up, and once the forward BD is obtained, map out the reverse BD starting from $\eta = 1$ and ramping it down. A typical example of the reverse BD is shown in Fig. 3.11(a) and the corresponding $V_{\rm LD}$ is shown in Fig. 3.11(b). It has been shown [92, 93] that $V_{\rm LD}$ tracks the changes in the time-averaged N. Two discontinuities in $V_{\rm LD}$ at $\eta = 0.1$ and 0.18 [Fig. 3.11(b)] in the horizontal band toward the left of the BD. These discontinuities reveal that different ECMs are participating in the light emission for regions α, β, and χ. As will be discussed later, the discontinuities in $V_{\rm LD}$ can be correlated with the changes in the optical

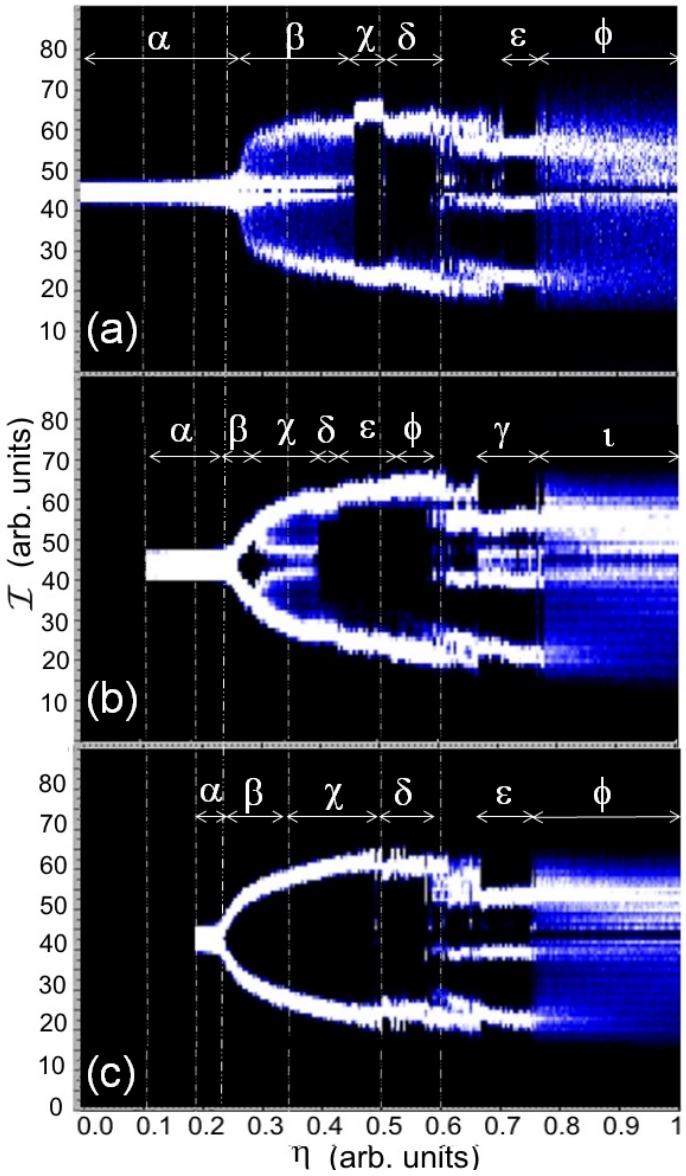

Figure 3.12: Forward BDs for several initial conditions. Initial mode (a) ECM 0, (b) ECM 1, and (c) ECM 2. J = 22.59 mA and L = 30 cm

spectrum. First, a shift is made from ECM 2 to 1, followed by a shift from ECM 1 to 0 as η is ramped from 0.24 down to 0. Fig. 3.13(a) corresponds to Fig. 3.11 α, Fig. 3.14(a) to Fig. 3.11 β, and Fig. 3.15(a) to Fig. 3.11 χ.

Having illustrated the ability to detect the relevant ECM dominating the emission at low η in Fig. 3.12 (a), (b), and (c), we show forward BDs beginning on different ECMs (0,1, and 2). The way we access different initial states is by ramping η down to a low value, for which the ECSL laser on the selected ECM, and then using this as the initial state from which we map out the forward BD as discussed in the previous BDs for high injection current. Although the lowest η reached in the three BDs is different, the three BDs overlap for η belonging to the interval [0.18,1]. In this interval, all the system parameters (including feedback phase) are identical except for the initial state of the ECSL at $\eta = 0.18$. As a result, the three BDs represent three different routes to fully developed CC of the same ECSL starting from three different initial states. The difference [see Fig. 3.12] among the three BDs starting from different ECMs is found to be significant in the sense that the route to chaos indeed depends on the initial state, as will be illustrated below.

Figure 3.12(a) shows the forward BD starting from ECM 0, and Fig. 3.13 shows the corresponding optical spectrum. It is clear from the optical spectrum that in region α of Figs. 3.12(a), only one ECM (ECM 0) of the solitary laser (MLM) participates to the dynamics. This stable mode is maintained in a CW regime over a large feedback interval ($\eta < 0.24$). When η is increased above that level, the optical spectrum [Fig. 3.13(b)] reveals that several ECMs (-3 to 3) start to participate in the emission. An analysis of the corresponding $\mathcal{I}(t)$ (not shown here), shows that the dynamical behavior is of a quasi-periodic nature. For a further increase in η (around 0.47), a discontinuity appears in the BD [region χ of Figs. 3.12(a)] that corresponds to an abrupt change of the dynamical behavior toward a limit-cycle oscillation. The optical spectrum [Fig. 3.13(c)] shows that the oscillation occurs around ECM 2, and the frequency of the oscillation 7.5 GHz as it corresponds to the distance between ECM 2 and its sidebands.

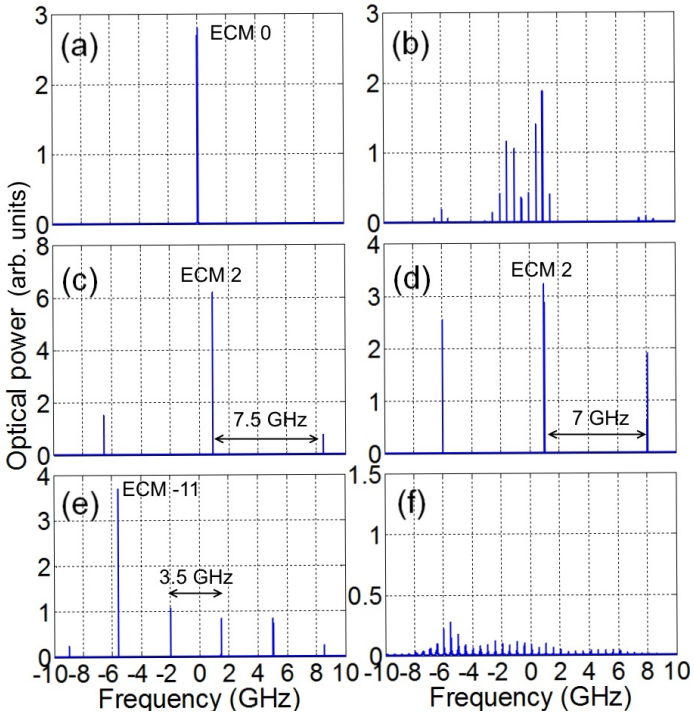

Figure 3.13: Optical spectra with the initial condition ECM 0. (a) $\eta = 0$, (b) 0.35, (c) 0.39, (d) 0.45, (e) 0.75, and (f) 0.9.

When η is increased to ~ 0.5, another limit cycle oscillating at $f_{\mathrm{RO}} \sim 7$ GHz is observed [region δ of Fig. 3.12(a)]. The optical spectrum of Fig. 3.13(d) further confirms that the oscillation is manifested as sidebands at around ± 7 GHz from ECM 2. Interestingly, the dominant mode (ECM 2) does not change in the transition from region χ to δ of Fig. 3.12(a), indicating two different frequencies at 7.5 GHz and 7 GHz on ECM 2. Previous works [6, 94] show that our observation of two limit cycles with different frequencies around the same ECM is compatible with the LK prediction.

For a further increase in η, at ~ 0.6, intermittency between the dynamical behaviors of regions δ and ϵ of Fig. 3.12(a) is seen. Of note, this intermittency is always observed before entering chaos regime in our experiments. Region ϵ, which corresponds to $\eta \gtrsim 0.74$, displays a periodic oscillation with a fundamental frequency of ~ 3.5 GHz and a harmonic at ~ 7 GHz, centered around ECM -11 [Fig. 3.13(e)]. The presence of the harmonics indicates that the 3.5 GHz limit cycle originates probably from a period-doubling bifurcation of

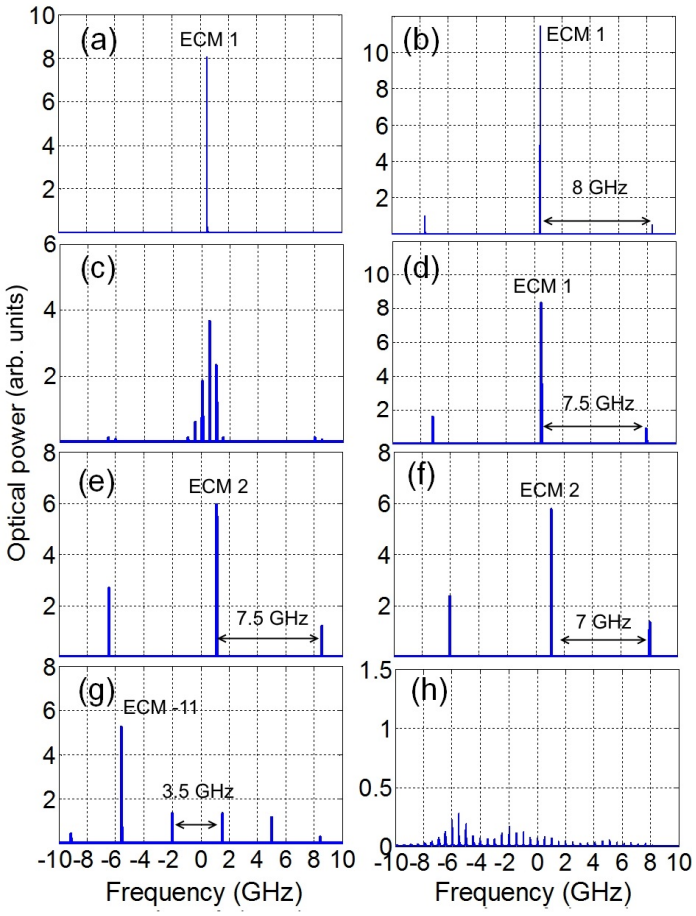

Figure 3.14: Optical spectra with the initial condition ECM 1. (a) $\eta = 0.15$, (b) 0.24, (c) 0.35, (d) 0.42, (e) 0.47, (f) 0.55, (g) 0.75, and (h) 0.9.

a 7GHz cycle that must have existed, at lower η, around ECM-11. If η is further increased, the limit-cycle oscillation disappears, giving rise to fully-developed CC, (region ϕ) which involves multiple ECMs negatively-shifted in frequency [Fig. 3.13 (f)].

Figure 3.12(b) shows the forward BD starting from ECM 1 and Fig. 3.14 shows the corresponding optical spectrum. As expected, the ECSL initially displays the CW behavior [Fig. 3.14(a)] (region α ($\eta \sim 0.22$) of Fig. 3.12(b)] because only one fixed point (ECM 1) is involved. As η is increased above 0.22, it is clearly seen in the BD that the ECSL undergoes a periodic oscillation. This oscillation is manifested as sidebands ± 8 GHz from ECM 1 [Fig. 3.14 (b)]. This transition in the dynamics corresponds to a Hopf bifurcation leading to a limit cycle with frequency close to f_{RO}, as predicted by LK [6, 7].

With further increasing η, additional sidebands near $\pm f_\tau$ appear in the optical spectrum [Fig. 3.14(c)], revealing the presence of a second frequency in the dynamics. The undamped second frequency close to f_τ corresponds to a second Hopf bifurcation and signals the development, in phase space, of a torus attractor. Note that both the limit cycle and the torus result from the destabilization of ECM 1 and are located around it in phase space [Figs. 3.14(b) and (c)].

Next, another limit cycle appears in the BD with increasing η. The optical spectrum shows [Fig. 3.14(d)] that this cycle is still centered on ECM 1, and has now a frequency of approximately ± 7.5 GHz. One notes that the dominant ECM 1 does not change in between Figs. 3.14(b) and (d), thus providing experimental evidence of the existence, at different η, around the same ECM, of two periodic solutions with different frequencies, 8 GHz and 7.5 GHz, whose separation is $\sim f_\tau$. As η is further increased, and region ϵ of Fig. 3.12(b) is reached, a small discontinuity is observed in the BD. The optical spectrum [Fig. 3.14(e)] reveals that this discontinuity corresponds to a shift from ECM 1 to 2. The ECSL still oscillates periodically, and the optical spectrum confirms that the frequency of the oscillations is still 7.5 GHz. Increasing η yet further, another limit cycle at $f_{\mathrm{RO}} \sim 7$ GHz is seen [region ϕ of Figs. 3.12(b)]. The active ECM 2 does not change in the transition from region ε to ϕ of Fig. 3.12(b), indicating again the existence of two different oscillation frequencies, 7.5 GHz and 7 GHz, again separated by $\sim f_\tau$ around a single ECM.

As η continues to increase further, the scenario is similar to the one observed for Fig. 3.12(a): the trajectory moves toward negatively-shifted ECMS: first, a period-doubled limit cycle around ECM -11 is observed (region γ) and then a regime of fully developed CC (region η). Figure 3.12(c) shows the forward BD starting from ECM 2 and Fig. 3.15 the corresponding optical spectrum. In the initial region α ($\eta \sim 0.22$) of Fig. 3.12(c), only one fixed point (ECM 2) participates in the output, and the ECSL displays a CW behavior [Fig. 3.15 (a)]. When η is increased above 0.22 and region β is reached, the ECSL undergoes a periodic oscillation [Fig. 3.15 (b)], manifested as sidebands ± 8 GHz from ECM 2. The

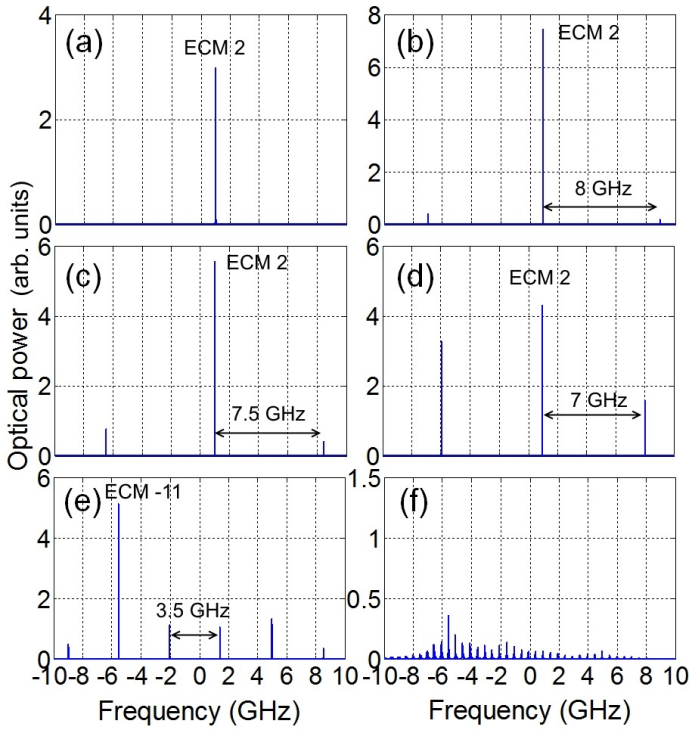

Figure 3.15: Optical spectra with the initial condition ECM 2. (a) $\eta = 0.2$, (b) 0.3, (c) 0.39, (d) 0.55, (e) 0.7, and (f) 0.9.

optical spectrum reveals the existence of two regions, χ and δ, corresponding to the appearance of two other limit cycles, of frequencies ± 7.5 GHz [Figs. 3.15 (c)] and ± 7 GHz [Figs. 3.15 (d)], still centered on ECM 2. It is noteworthy that the active ECM (2) does not change between Figs. 3.15(b),(c), and (d), thus providing evidence of the existence, at different η, of three periodic solutions with different frequencies, 8 GHz, 7.5 GHz and 7 GHz, whose separation is $\sim f_\tau$. The behavior of the BD is similar to that of the two previous cases for larger feedback regions.

To conclude, we show that the route to chaos exhibited by ECSLs has been largely impacted by different the initial states. In this aspect, we demonstrate experimentally in a direct and systematic way of generalized multistability in a high-dimensional delay system and, for the first time, that different routes to fully developed chaos are possible, depending on the selected initial state. Eventually, for $\eta \gtrsim 0.5$, the BDs become insensitive to the initial state selected; at these larger values of η, generalized multistability is no longer

evident. We note in particular that the qualitative behavior of the route to chaos changes considerably at small η. These observations can be interpreted by the fact that at moderately low η, various attractors have developed around several ECMs, but have not yet merged or only a few neighboring attractors have merged [102]. As a result, the initial state will be crucial in determining the dynamics experienced by the ECSL, confirming the predictions by Mork and Masoller [5, 81]. For larger η, most attractors have merged and, independent of the initial state of the BD, the trajectories end being attracted by a group of merged attractor ruins located around ECMs with a large negative frequency detuning, as is typical in a regime of fully developed coherence collapse.

3.4 Conclusion

A global experimental-based understanding of the various dynamical regimes is essential to gain a fundamental apprehension the dynamics of an ECSL. In this regard, we have examined several aspects of fundamental importance for the dynamics of ECSLs using BDs based on experimental time series of the optical intensity of a DFB laser subjected to optical feedback from a long cavity with optical/RF spectrum. We have shown the robust experimental results, combined with good matches with a deterministic model, within a large range of continuously varied parameters, supplies global evidence for the deterministic origin of ECSL dynamics.

At low J, in order to validate our interpretation of the experimental results, we have carried out theoretical calculations based on the well known LK model. Despite its simplifications, The LK model can successfully reproduce the bifurcation cascade as it is also observed experimentally. Indeed, LK predict that, at low *J*, the unstable regions correspond to the LFF regime, involving a drift toward the MGM. However, as J is further increased, the bifurcation cascades gradually disappear as the ECSL dynamics are hindered from heading to MGM. This is also the similar case for longer L case since closer proximity of ECMs in phase space prevent the ECL from staying in MGM.

On the other hand, at larger J, the route to fully-developed CC with no drift toward the MGM is observed instead of bifurcation cascades involving LFF behaviors. Starting from zero optical feedback, we have shown that Initial instabilities correspond to the first steps of a quasiperiodic route to chaos around a single ECM. The ECM loses stability via a Hopf bifurcation (sometimes it is called first-instability) to limit cycle behavior at a frequency close to those of relaxation oscillations, which undergoes a secondary Hopf bifurcation corresponding to the undamped second frequency, close to the delay frequency, and leading to quasi-periodic oscillations. As a result, the quasiperiodic route is seen via several interruptions by windows of periodicity, as well as by intermittent behavior. Also, we observed that limit cycles occur with different frequencies around the same ECM or two different neighboring ECMs when optical feedback strength is increased. Intermittent behaviors observed here will be thoroughly investigated in chapter 5.

Last but not least, we demonstrated experimentally how to initiate different initial conditions and showed that the different initial states lead to different routes to chaos. The qualitative behaviors of the route to chaos change noticeably at small η. However, after η is moderately increased ($\eta \gtrsim 0.5$), the BDs become insensitive to the initial state selected; at these larger values of η, generalized multistability is no longer evident. This generalized multistability at weak η can be interpreted as attractors have not yet merged or only a few neighboring attractors around several ECMs. Conversely, for the case of the BDs at larger η, the trajectories are attracted by a group of merged attractor ruins located around ECMs, resulting in fully developed CC.

CHAPTER 4

EXTREME EVENTS

4.1 Theoretical framework

We have seen numerically and experimentally that irregular dynamics behaviors such as switching between two dynamics is observed on the route to chaos. At low injection current, intermittency between continuous wave (CW) and low frequency fluctuations (LFFs) occurs. Thus, based on the perspective of extreme events, we statistically analyze the characteristics of intermittency between CW and LFF at low injection current when the ECSL is subjected to different optical feedback and external-cavity length. This chapter will be discussed based on the following publication:

- Daeyoung Choi, Michael J. Wishon, J. Barnoud, C. Y. Chang, Y. Bouazizi, A. Locquet, and D. S. Citrin."Low-frequency fluctuations in an external-cavity laser leading to extreme events", Physical Review E 93, 042216 (2016).

An extreme event (EE) is defined as a sudden surge of exceptional amplitude compared to the typical dynamics of a system. EEs were first reported in oceanography [103, 104] as very high amplitude waves, called rogue or freak waves, that appear unexpectedly, and that occur much more often than one would expect assuming a Gaussian or any other short-tailed distribution. EEs are not restricted to hydrodynamics; they have been observed in several other fields including economics [105], meteorology [106], acoustics [107], and optics [31, 32, 33, 108, 109, 110, 111, 112, 113, 114, 115].

EEs are determined by defining an EE threshold value EE_{th} for a given dynamical variable: features in a time series that exceed EE_{th} are deemed EEs. One common criteria for determining the threshold uses the standard deviation σ of the time series: any local maximum (or minimum) larger (or smaller) than the mean plus (or minus) 4 to 8 times σ is

considered an EE [103]. Another common criterion uses the abnormality index (AI) [104], which is the ratio between the height of the wave and the average wave height among one-third of the highest waves in a time series. Any wave for which AI> 2 is considered an EE. We explored EEs determined by the 4σ, 6σ, and AI criteria. We confirmed that regardless of criterion, the EE frequency exhibits the same trends with smooth transitions as a function of J and only the scales are different. We chose to focus on the $+6\sigma$ criterion as $EE_{\rm th}$ since it gave us good statistics without requiring extremely long experimental time series. Also, we only considered maxima in determining the EEs as extreme minima are far less frequent.

Bonatto *et al*. [31] showed that rare giant pulses could be observed in a purely deterministic dynamical system composed of a semiconductor slave laser optically injected by a semiconductor master laser. Ref. [33] demonstrated that these giant pulses could be predicted with large anticipation time and originated in a crisis-like process that creates a narrow "rogue wave door" in phase space. Perrone *et al*. [32] further showed numerically that a weak modulation of the pump current could be used to control the probability of occurrence of these giant pulses, or even suppress them. Laser diodes (LDs) subjected to optical feedback, ECSL are of great intrinsic interest and have also led to a large number of applications [17]. In the short-cavity case, numerical simulations show that in certain parameter ranges, associated with an expansion of an attractor in phase space, occasional EEs can be observed [110]. In the special case of optical feedback provided by an external phase-conjugating mirror, extreme intensity pulses with statistical properties similar to those of rogue waves have been observed [109] and reproduced numerically [114] with a rate equation model.

We observe experimentally the existence and frequency of EEs in the optical intensity $I(t)$ of a LD subjected to conventional, *i.e.* non phase-conjugating, time-delayed optical feedback. The experimental setup is the same as conducted for BDs in chapter 3. The external cavity length L corresponds to the time delay $\tau = 2L/c$. Depending on feedback

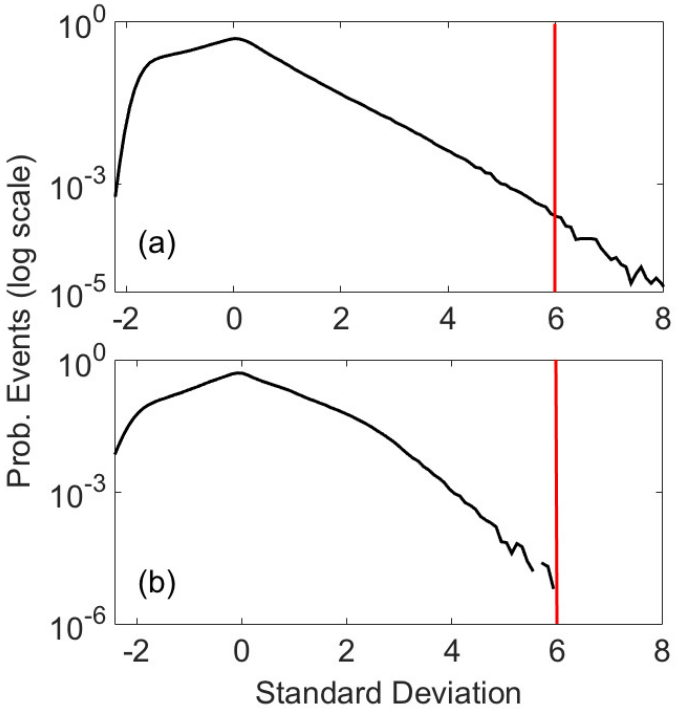

Figure 4.1: The standardized pdf in the LFF (a) and CC (b) regimes. The vertical (solid red) lines at 6 (in units of σ) indicate $EE_{\rm th}$. The standardized pdf in the LFF regime ($J = 9.8$ mA) has a long and exponential tail, which leads to a large EE frequency. In the CC regime ($J = 17.4$ mA), the pdf has a significantly shorter tail. $L = 55$ cm, $\eta = 0.6$.

strength η, injection current J, and external cavity length L, the ECSL exhibits various dynamical regimes [70, 116], the most relevant being low frequency fluctuation (LFF) and fully-developed coherence collapse (CC) [17]. Examples of time series of LFF and CC will be introduced below. We varied J from 8.0 to 18.0 mA by 0.1 mA increments, which allowed us to observe the transition from LFF to CC in detail, and record the corresponding optical intensity times series, each consisting of 3×10^6 samples.

4.2 Results and discussion

Of specific interest to this study is the transition between LFF and CC. LFF typically occurs near or slightly above $J_{\rm th}$ and exhibits a succession of intervals of average power build-ups interrupted by abrupt power dropouts at apparently randomly distributed times. The underlying instantaneous power is constituted by irregular intensity pulses whose duration

is in the several tens to a few hundreds of ps [117]. LFF can be easily identified by the presence of a slow dynamics (several tens or a few hundreds of MHz), corresponding to the alternation between build-ups and dropouts, that is evident from a low-pass filtered time series and the RF spectrum. CC typically happens at larger J and displays multi-GHz fluctuations of the optical intensity around its average value.

In Fig. 4.1, we plot examples of the standardized probability distribution function (pdf) of the intensity time series in LFF (a) and CC (b). The standardized pdf is defined as $[I(t) - \langle I \rangle]/\sigma$ with $\langle I \rangle$ the time-averaged intensity. Note that the vertical scale is logarithmic. We observe that in LFF, the standardized pdf exhibits a significantly long and exponential tail, leading to a large number of EEs. In CC, however, almost no features extend beyond EE_{th} set by 6σ; the tail is considerably suppressed by comparison, and the EE frequency negligible. We have also explored the transition between LFF and CC; as J increases and the laser leaves the LFF regime, the tail rapidly becomes shorter. Specifically, for $J = 9.8$ mA corresponding to LFF, the probability of observing an EE is 0.18 %, a value much larger than one would expect from a Gaussian distribution ($\sim 0.2 \times 10^{-6}$ %).

Examples of the raw and low-pass filtered $I(t)$ for increasing values of the injection current J are shown in Fig. 4.2. We have chosen a convenient cutoff frequency to visualize the dropouts easily; all quantitative analysis is carried out on the unfiltered time series. We observe that, for currents close to threshold, the ECSL first enters an intermittent regime, switching between continuous wave (CW) emission, associated with a high-gain mode [71] and transient LFF-like behavior [Fig. 4.2(a-b)]. As J is increased, the ECSL eventually reaches stable LFF behavior [Fig. 4.2(c-d)]. Next, the LFF character of the dynamics is lost as dropouts gradually disappear with increasing current, and the dynamics reaches the fully developed CC regime [Fig. 4.2(e-f)].

We now show that dropouts are associated with EEs. In Fig. 4.3, we observe that dropouts are followed by erratic pulses of increasing amplitude. The intensity of these pulses can exceed EE_{th} and be accounted for as EEs. We can thus infer that EEs are

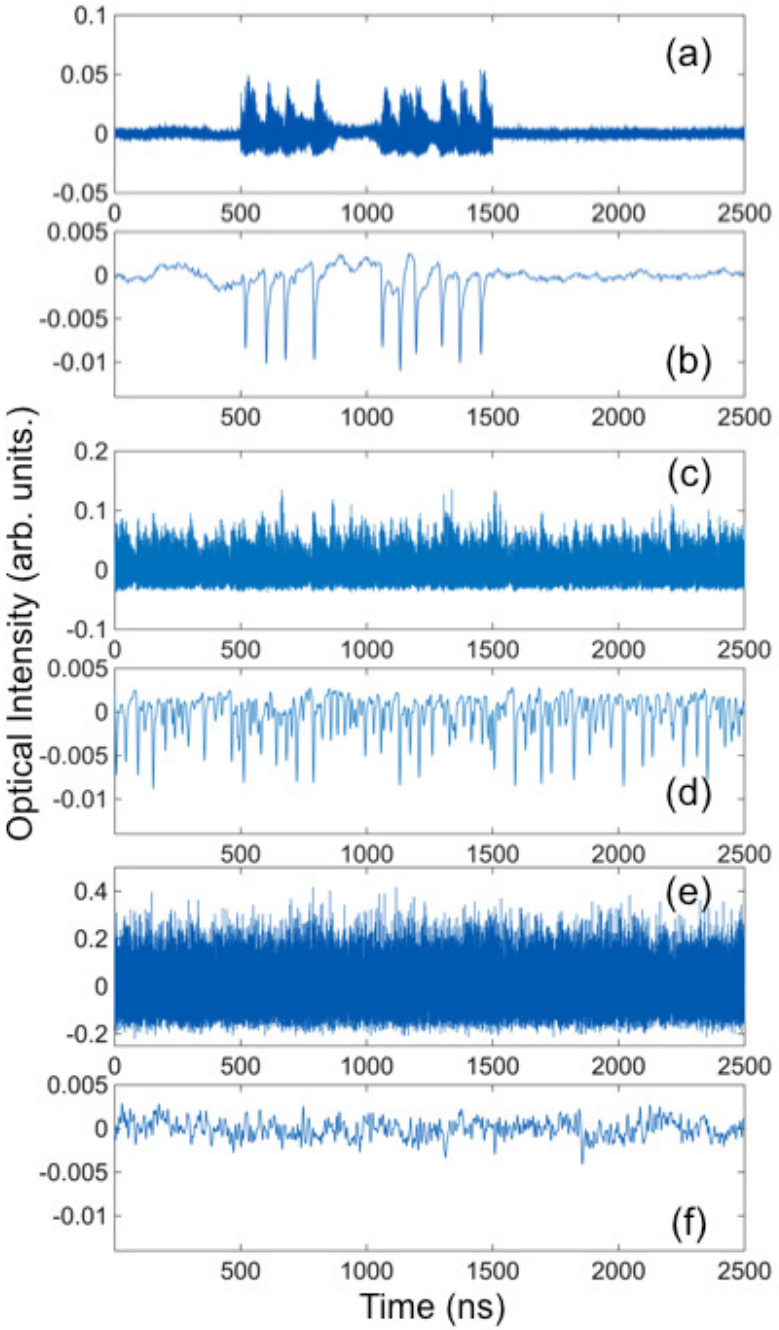

Figure 4.2: Examples of the time series $I(t)$ in each dynamical regime: (a, c, e) original time series, (b, d, f) time series low-pass filtered at 100 MHz. The ECSL starts in intermittency (a, b) and then enters the stable LFF (c, d) regime in which the intervals between dropouts decrease. The CC regime (e, f) is recognized by an absence of dropouts. Intermittency is measured at 9.1 mA, stable LFF at 9.8 mA, and CC at 17.0 mA. $L = 55$ cm, $\eta = 0.75$.

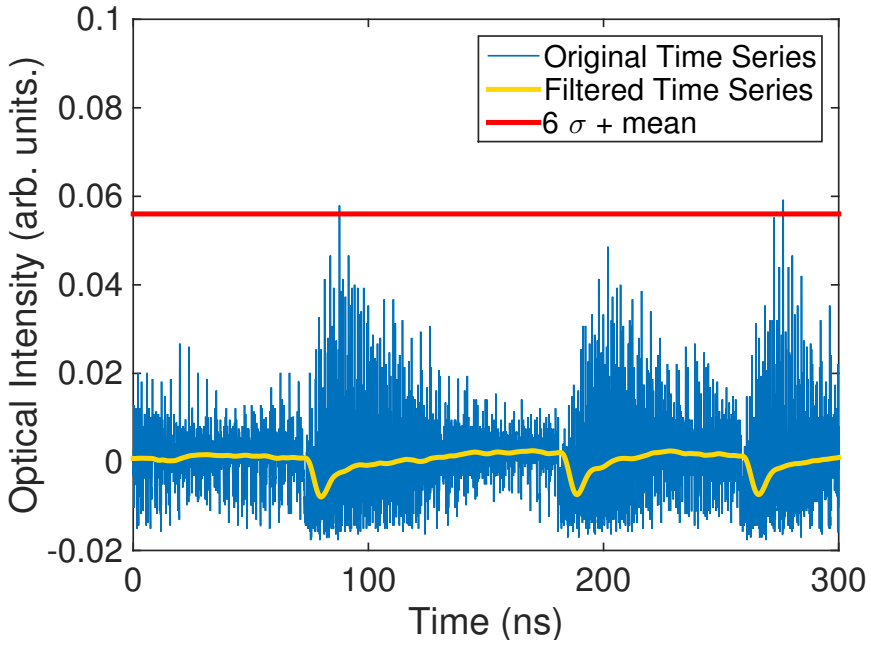

Figure 4.3: Large-amplitude ringing in $I(t)$ occurs immediately after dropouts. $J = 9.1$ mA, $L = 55$ cm and $\eta = 0.6$. The red horizontal line shows $EE_{\rm th}$.

linked to the so-called recovery process after dropouts [117, 118]. Note though that not all dropouts are followed by EEs.

Figure 4.4 depicts how EE frequency, i.e. the number of EEs per unit time, changes over the entire range of the measurement from 8 to 18 mA. After the ECSL starts lasing, the intermittent LFF-CW regime appears, in which the EE frequency increases steadily with J. It must be noted that in this regime, the calculation of the EEs is based on the LFF periods only. As J is further increased, stable LFF is reached, accompanied by the maximum in the EE frequency. For larger values of J, the ECSL exits the LFF regime and EE frequency is seen to steadily decrease. For $J > 18$ mA, EE frequency is negligible. We find that the increase of the EE frequency before stable LFF is reached is caused by a decrease in the average time between dropouts, in the LFF regime as was also observed in Ref. [119]. As the current is further increased, a transitional regime between LFF and CC [71] is observed, in which dropouts gradually disappear, leading to a progressive decrease in EE frequency. When the current exceeds 17 mA approximately, fully developed CC is observed and EE

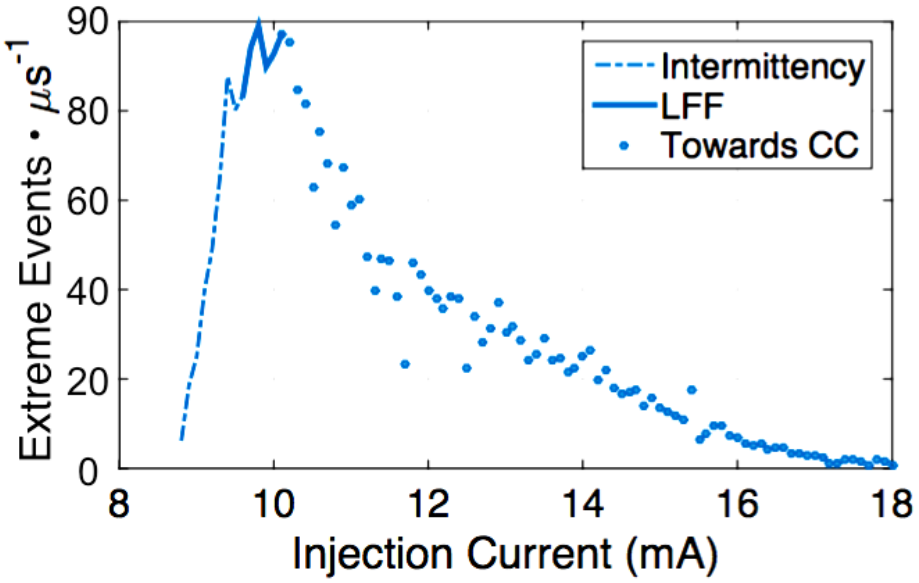

Figure 4.4: EE frequency as a function of J. EEs are most frequently observed in the LFF regime. As the ECSL leaves the stable LFF regime, EE frequency starts to decrease. L = 65 cm and η = 0.75.

frequency goes to zero. Finally, dropouts are no longer seen in CC resulting in a drastic reduction in EE frequency.

To better understand temporal correlations between EEs, we explored the autocorrelation function (ACF) of $I_{EE}(t)$ defined as $I_{EE}(t) = I(t)$ if $I(t) > EE_{\text{th}}$ or $I_{EE}(t) = EE_{\text{th}}$ if $I(t) \leq EE_{\text{th}}$ as shown in Fig. 4.5. Within the intermittency and LFF regimes, the ACF diplays a significant peak around the delay time τ and a peak around the average time in-between dropouts. We find that the peak around τ corresponds to the fact that, after a dropout, groups of a few consecutive EEs, approximately separated in time by τ, can sometimes be observed, similarly to what was reported in Ref. [109] for phase-conjugated feedback. It is interesting to notice that the ACF also exhibits a peak around 7τ, corresponding to the average time between dropouts, and thus confirming the link between the recovery process after a dropout and EEs. Finally, in the transitional regime towards CC, despite the fact that few EEs can still be observed, no clear peaks around the delay time or related to the time between dropouts, can be identified.

We computed the pdf of the difference between the logarithms of the times of occur-

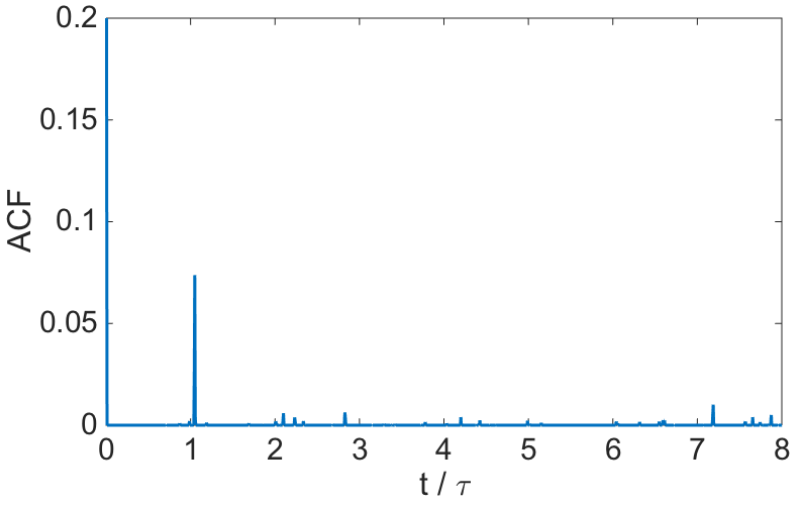

Figure 4.5: Normalized autocorrelation function of $I_{EE}(t)$, as defined in the text, in the LFF regime. τ is the delay time of an external cavity length. We observe a peak around the delay time τ ($t/\tau = 1$) as well as around 7τ corresponding to the average time separating consecutive dropouts. J = 10.1 mA, L = 65 cm and η = 0.75.

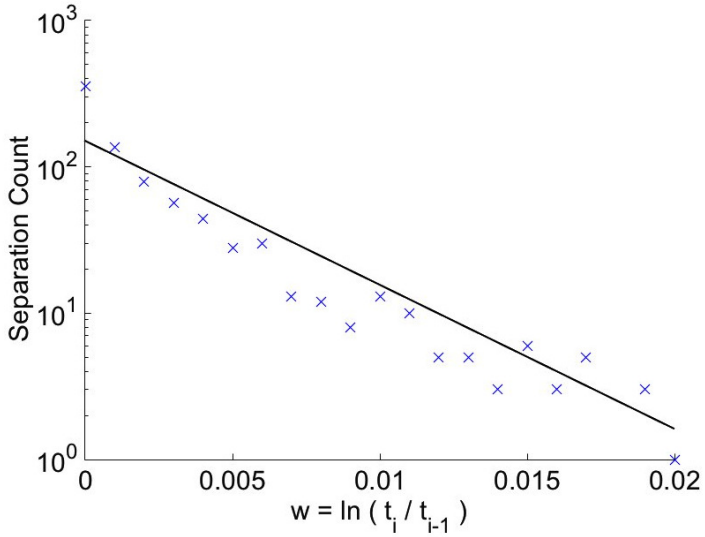

Figure 4.6: Statistics of waiting times between successive EEs in the LFF regime. The distribution has log-Poissonian characteristics. J = 9.9 mA, L = 65 cm and η = 0.75.

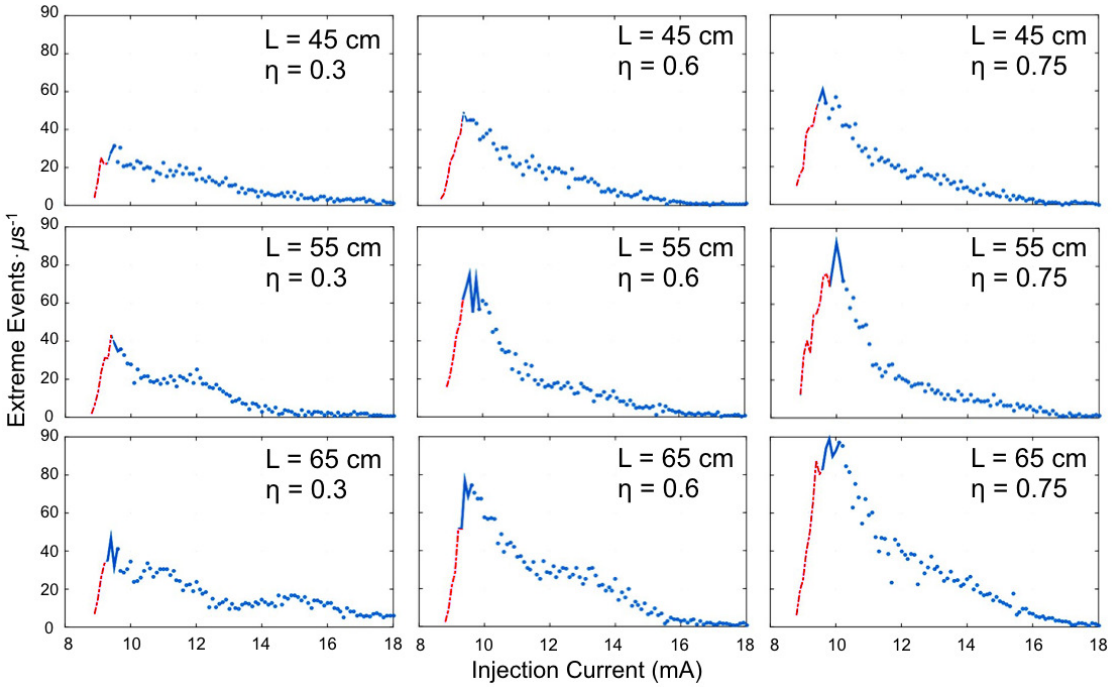

Figure 4.7: EE frequency for various values of L and η showing that the basic trends as a function of J are essentially robust to changes in these parameters. The maximum EE frequency is observed in all cases to occur in the LFF regime (blue solid line). As labeled in Fig. 4.4, the dashed line (red) and dots indicate the intermittency and CC regimes respectively.

rence of successive EEs, i.e. $w = ln(t_i) - ln(t_{i-1})$ where t_i is the time of occurrence of the EE. In the LFF regime, we find a log-Poissonian distribution as shown in Fig. 4.6. Similarly, a log-Poissonian was found in Refs. [109, 120].

We have further investigated the effect of changes in cavity length L and feedback strength η. Figure 4.7 illustrates the EE frequency as a function of J for various L and η. We observe consistently for $L = 45$, 55, and 65 cm, similar behavior at moderate $\eta = 0.3$, 0.6, and 0.75: (1) an increase in EE frequency during intermittency between CW and LFF, (2) a maximum around stable LFF, and (3) a gradual decrease toward CC. Trends associated with EE frequency are thus robust with respect to changes in L and η. In addition, it is noticeable from Fig. 4.7 that larger feedback levels lead to larger numbers of EEs. We find that this phenomenon is due to an increase of the pulse intensities with increasing feedback.

4.3 Conclusion

We have, for the first time, distinguished in a robust way the LFF and fully-developed CC regimes on the basis of extreme events. We have found that while a significant number of EEs are observed when LFF is stable or intermittent, no EEs can be observed in fully developed CC. We attribute this difference to the specific dynamics experienced by the ECSL in LFF, which involves an abrupt dropout followed by irregular multi-ps pulses, some of which can qualify as EEs. Interestingly, features similar to those identified numerically as being responsible for EEs in optically injected lasers and for ECSLs in the short cavity regime seem to be present in the LFF regimes: the existence of a crisis and of a "narrow door" in phase space. Indeed, according to the Lang and Kobaysashi model, LFF appears in a context of attractor-merging crises that lead to an expansion of the accessible phase space. Moreover, it is known [117] that it is only a portion of the trajectories that approach the maximum gain mode that end up being rejected along an unstable manifold, after going through a "wormhole" in phase space as mentioned in [118], leading thus to a dropout and successively to EEs. We can thus suspect that the existence of a crisis-induced phase space expansion associated with a narrow door for trajectories in phase space is a paradigm for EEs in purely deterministic dynamical systems.

CHAPTER 5
INTERMITTENCY

5.1 Theoretical framework

Intermittency has recently become of great interest to many scientists because it is often observed in various dynamical systems, and inevitably, one needs to investigate inherent intermittent behaviors in order to fully understand the systems. As we have seen intermittent dynamical behaviors in the route to chaos while we drew several bifurcation diagrams with different conditions, we analyze statistically the characteristics of intermittency observed on the route to chaos when the external-cavity laser is subject to moderate feedback strength at high injection current. This chapter is based on the publication:

- Daeyoung Choi, Michael J. Wishon, C. Y. Chang, D. S. Citrin, and A. Locquet. "Multistate intermittency on the route to chaos of a semiconductor laser subjected to optical feedback from a long external cavity", Chaos 28, 011102 (2018).

Intermittency in a dynamical system is characterized by the erratic alternation between regular (laminar) and irregular (turbulent) phases [34]. Intermittency has been widely observed in nonlinear systems as a parameter approaches a critical value corresponding to a bifurcation point or a crisis. Different types of intermittent behavior are associated with different dynamical instabilities. Pomeau and Manneville [121] introduced three intermittency mechanisms involving a fixed bifurcation point in the Poincaré map of a continuous-time system. They named three types of intermittency I, II, and III based on the nature of the bifurcation. Type I is associated with a saddle-node bifurcation, type II with a Hopf bifurcation, and III with a period-doubling (PD) bifurcation. Subsequently, other types of intermittency have been revealed and discussed. Crisis-induced intermittency originates

from a crisis in which chaotic attractors undergo sudden widening or merging [122]. Multistate intermittency switching between more than two dynamical states can occur due to the presence of external modulation or noise [36, 37, 123, 124]. Unlike previous types, on-off intermittency is characterized by a dynamic bifurcation point which induces laminar (steady) and bursting (turbulent) phases described as off and on states [125, 126, 127].

On-off intermittency has recently been reported in many physical systems [128, 129, 130, 131, 132, 133, 134, 135, 136, 137]. Interestingly, on-off intermittency has two universal statistical properties: the distribution of laminar phases shows a $-3/2$ power-law scaling for short laminar phases and the mean duration of laminar phases *versus* a control parameter has an exponential decay with slope -1 on a logarithmic scale near the onset of intermittency.

Intermittency has been observed and explored in various types of lasers including Nd-YAG [35], fiber [36, 37, 38, 39], optically pumped ring lasers [40, 41], and semiconductor lasers [42, 43, 44]. In particular, intermittency in semiconductor lasers subjected to optical feedback from an external mirror, or external-cavity lasers (ECSLs) has attracted considerable interest.

When an ECSL is biased slightly above the threshold current J_{th}, intermittency between continuous-wave operation and low-frequency fluctuations (LFFs) may be observed [44, 71, 119, 138, 139, 140]. Spontaneous-emission noise is believed to play a main role in causing the intermittency in this regime. The average time $\langle\tau\rangle$ between subsequent LFF periods versus injection current J follows a slope of -1 on a log-log scale, which was seemingly considered as type-II intermittency [72]; however, Sukow *et al.* showed numerically that this intermittency cannot be of type II because it is not consistent with type-II theory, which predicts $\langle\tau\rangle \to \infty$ when $J \to J_{th}$ [139]. Later, this intermittency was described in Ref. [44] as on-off intermittency based on power-law properties.

At higher injection current, a recent study by Karsaklian dal Bosco *et al.* [142] utilized a short external-cavity laser (ECSL), implemented by a photonic integrated circuit and

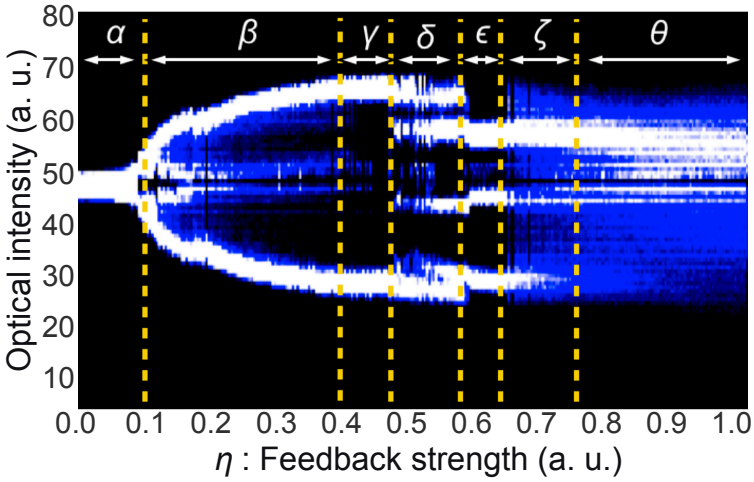

Figure 5.1: Example of an experimental bifurcation diagram of an external-cavity laser as a function of feedback strength [141]. We observe successively (δ) multistate intermittency and (ζ) intermittency between period-doubled and coherence collapse regimes.

found crisis-induced intermittency between PD dynamics and fully-developed coherence collapse (CC), which is interpreted as being caused by the switching between separated attractors born from different external-cavity modes (ECMs) in phase space. Later, it was shown that switching times between the regimes could be used as an entropy source for random number generation [143]. However, a bigger picture for intermittency of ECSLs operated at larger current levels that do not lead to LFF, in the long-cavity case, is still missing. In previous studies [141, 144], we drew experimental bifurcation diagrams (a typical bifurcation diagram is represented in Fig. 5.1 of an ECSL biased well-above J_{th} as a function of feedback level η, which display different dynamical regimes, including limit cycles (LC), quasiperiodicity (QP), subharmonics (SH), PD oscillations, as well as CC. We noted that intermittency is generally observed on the way to CC, regardless of the initial condition used to draw the bifurcation diagrams [141]. Here, we will demonstrate that two distinct intermittency regimes can be encountered by an ECSL on the way to CC: an intermittency between PD and CC regimes, similarly to what has been reported in the short-cavity case [142] but also multistate intermittency involving several different dynamical regimes.

Since the external-cavity length L plays an important role in determining the route to chaos [145], we study how the evolution of the various dynamical regimes observed during intermittency depends on both η and L.

Specifically, we investigate certain ranges of feedback level η where two regimes of intermittency are observed in the route to chaos as pointed out in Fig.5.1. First, multistate intermittency is observed in region δ of Fig.5.1. We statistically analyze the coexistence of various regimes, including, LC, QP, SH, and PD regimes. For cavities that are not too long ($L < 60$ cm), multistate intermittency gives way to a stable PD regime (ϵ in Fig. 5.1) after an increase in feedback. As feedback is increased even further, intermittency between PD and chaotic regimes (ζ in Fig. 5.1) is observed before finally leading to chaos. We find that the statistics of the latter intermittency is comparable to that of on-off intermittency.

Of note, the experimental setup is basically the same as conducted with the ECSL in the chapter 4, but higher current ($> 1.8J_{th}$) is used here.

5.2 Multistate intermittency

As the feedback level η ramps up, the ECSL exhibits a complex route to fully developed CC as shown in the bifurcation diagram of Fig. 5.1. In the beginning, the ECSL shows continuous-wave dynamics (α of Fig. 5.1), followed by QP (β of Fig. 5.1) and LC (γ of Fig. 5.1) oscillations. Before the ECSL enters the PD regime (ϵ of Fig. 5.1), the first intermittency region encountered (δ of Fig. 5.1) corresponds to a transitional region taking the laser from LC to PD oscillations. This is the intermittency alluded to Refs. [144, 141]. Contrary to what might be expected, we find that the intermittency does not only involve the LC observed in regime δ and PD observed in regime ϵ in Fig. 5.1, but also additional QP and SH regimes. The complex scenario described hereafter stems from the use of a long cavity, which leads to an highly multistable system in which numerous attractors and corresponding regimes can play a role in the dynamics. Figures 5.2(a) and (b) illustrate the switching between LC and QP, and SH and QP regimes, respectively. We tested different

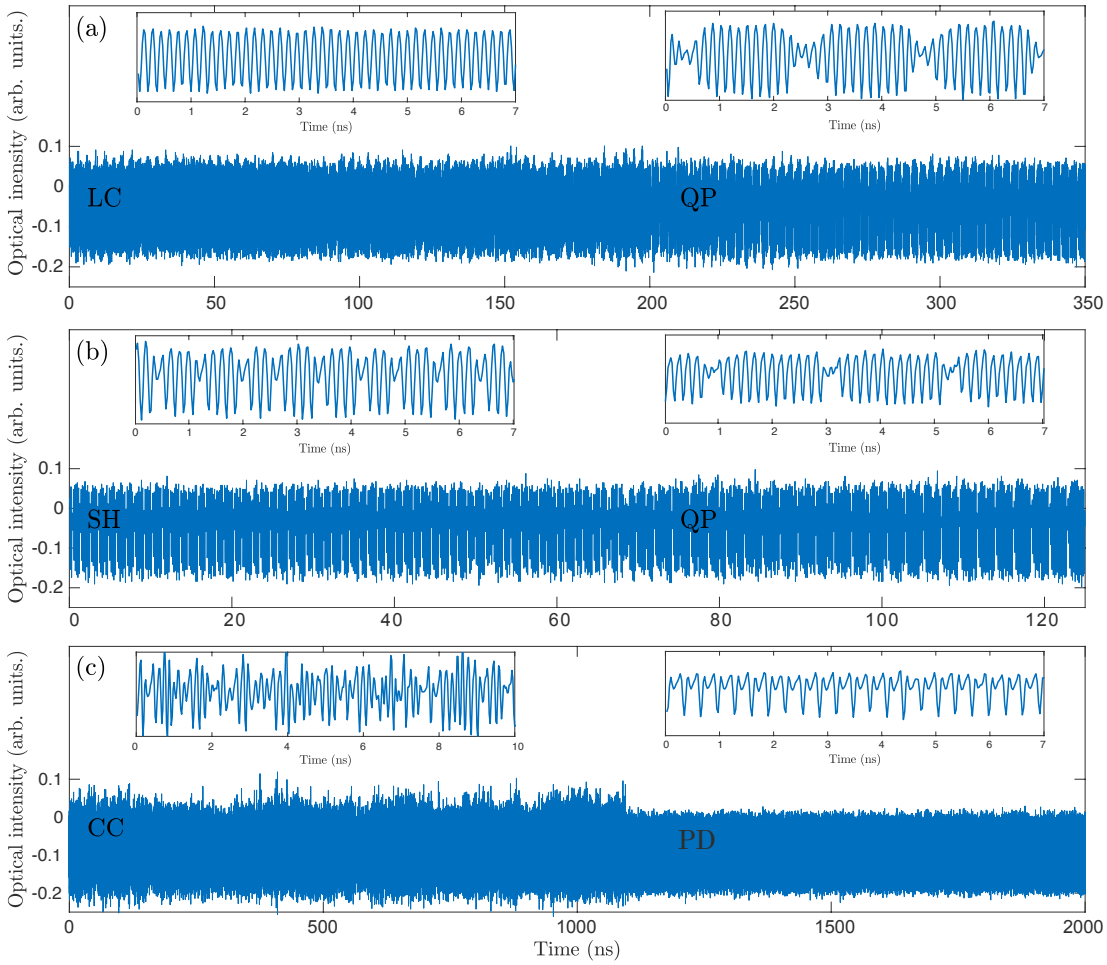

Figure 5.2: Snapshots of the time series of $I(t)$ when dynamical behavior change (a) from LC to QP, (b) from SH to QP, and (c) from CC to PD. Figures (a) and (b) correspond to region δ of Fig. 5.1 while (c) corresponds to region ζ. Insets are close-up of each dynamical behavior. $I(t)$ is sampled at 40 GS/s. $L = 30$ cm, $J = 21.15$ mA

ways of identifying the various regimes. As described by in Ref. [37], using amplitude threshold in time series may not be accurate for certain cases. The authors used wavelet spectrum energies to better distinguish several dynamical behaviors.

The amplitude method is also not applicable in our case since amplitude levels of different dynamics are very similar except for CC. Although we find that the results are substantially the same when using the wavelet spectrum method, due to the size of the oscilloscope's buffer and slow speed processing for a large amount of data, we identify the characteristics of a given phase based on the RF spectrum obtained by taking the Fourier

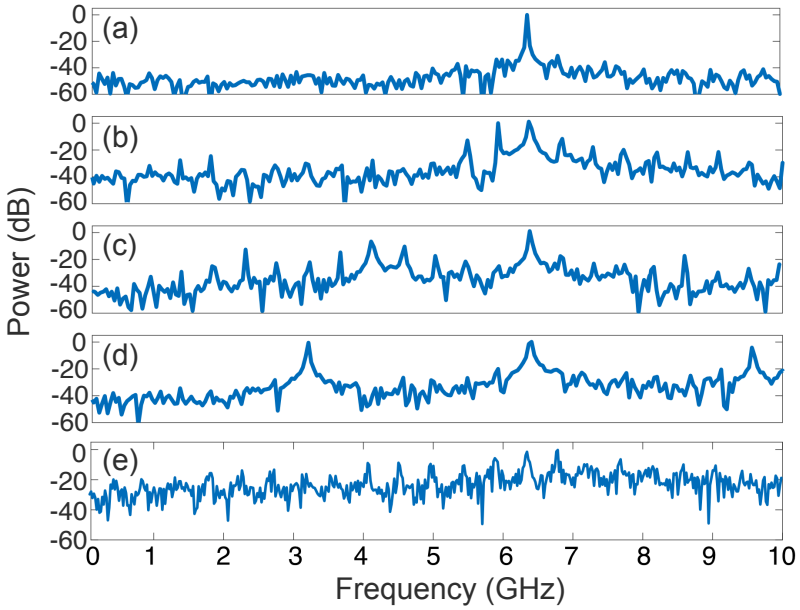

Figure 5.3: RF spectrum of dynamical behaviors observed in intermittency (a) LC, (b) QP, (c) SH, (d) PD, and (e) CC. $J = 21.15$ mA, $L = 30$ cm,

transform of the intensity time series $I(t)$ since the main peaks are clearly different in the RF spectra from one regime to another as shown in Fig. 5.3. The LC regime [Fig. 5.3(a)] is characterized by a main peak close to the relaxation-oscillation frequency f_{RO} while the QP regime [Fig. 5.3(b)] has, in addition to f_{RO}, RF sidebands separated by the external-cavity free-spectral range $f_L = c/(2L)$ where c is the speed of the light. The PD regime [Fig. 5.3(d)] is manifested by two main RF peaks f_{RO} and $f_{RO}/2$. The CC regime [Fig. 5.3(e)] exhibits rapid chaotic fluctuations and can be identified by its broad RF spectrum. The previous regimes and the associated spectral characteristics are extensively described in Refs. [144, 141]. An additional regime, named subharmonic (SH), is observed here, involving three main frequencies, f_1, f_2, and f_{RO} such that $f_{RO} = f_1 + f_2$. The frequencies f_1 and f_2 are subharmonic frequencies evident in the RF spectrum and are mainly located at the odd fractions of f_{RO}; $f_1/f_{RO} = (\frac{1}{3}, \frac{1}{5}, \text{or } \frac{2}{7})$, and thus, $f_2/f_{RO} = (\frac{2}{3}, \frac{4}{5}, \text{or } \frac{5}{7})$, respectively. Figure 5.3 (c) depicts one example of SH dynamics when $f_{RO} = 6.3$ GHz ($f_1 = 2.1$ GHz, $f_2 = 4.2$ GHz).

Specifically, we investigate the statistics of each phase for moderate η, from LC to CC,

spanning over regimes δ, ϵ, and ζ in Fig. 5.1. We record 1000 samples at each η at 40 GS/s from the oscilloscope (corresponding to 25 ns duration per sample, which is sufficient for classification) and classify the dynamic type based on its RF spectrum and obtain the probabilistic dominance of each phase. We estimate the accuracy of detecting each dynamics is $\sim 98\%$. Of note, we repeated the measurements presented in Fig. 5.4 multiple times and observed consistent results, allowing to exclude random thermal or mechanical fluctuations as being the origin of the observed phenomena. As shown in Fig. 5.4 for an external-cavity length $L = 30$ cm, we observe multistate intermittency involving 2 to 3 varying dynamical regimes. As η increases, the dominant phase progresses from LC, QP, SH, PD, to CC. LC dominates for small η, but its dominance decreases as first QP and then intermittent switching between LC, QP, and SH is prominently observed in a range around $\eta \sim 0.55$ [Fig. 5.4(a)]. SH occurs more frequently at moderate η after LC and QP become less dominant. Thus, we reveal that the transition from LC to PD, observed in [144, 141] and corresponding to region δ in Fig. 5.1, is in fact a complex regime of multistate intermittency. Two additional regimes, QP and SH, play a mediating role in the transition between the LC and PD regimes and highlight the multistability of the ECSL. As L increases, SH takes dominance over PD on the route to CC [Fig. 5.4(b)]. For $L > 60$ cm, we suspect that a variant of the route to chaos is achieved as PD is almost unobserved. The value of L is also related to the occurrence of intermittency between PD and CC, which is the subject of the following section. Similarly to what was done is Ref. [36], determining the critical exponents of the various coexisting dynamical regimes as the feedback level is increased would be of great interest. However, the regime of multistate intermittency involves the coexistence of short timescales (sub-ns oscillations) with significantly longer durations of the dynamical phases (up to ms). This leads to the experimental constraint of recording very long time series at very high sampling rates (in order to be able to distinguish between the regimes), vastly exceeding the memory depth of our oscilloscope. The determination of these characteristic exponents will be the subject of future research.

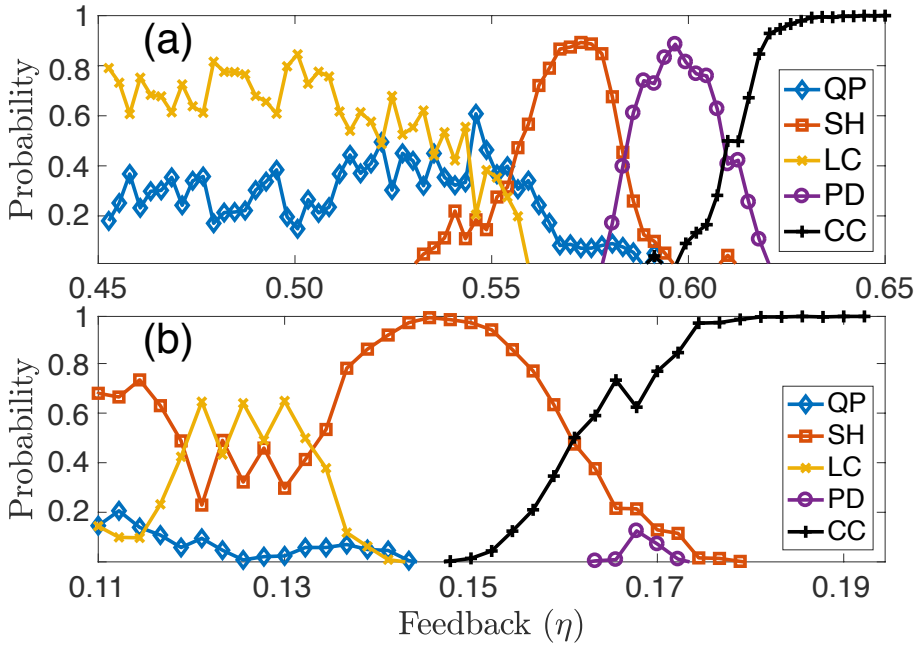

Figure 5.4: Probabilistic dominance of each dynamical type for (a) $L = 30$ cm, (b) $L = 55$ cm. $J = 21.15$ mA.

5.3 Intermittency between PD and CC regimes

When η is increased above the levels leading to multi-state intermittency, the PD regime becomes stable while QP and SH lose their dominance. This corresponds to region ϵ in Fig. 5.1. As η reaches the critical value η_c, we observe another intermittency corresponding to region ζ of Fig. 5.1 before entering fully-developed CC (θ in Fig. 5.1). This type of intermittency is qualitatively similar to what was observed in Ref. [142] for the short-cavity case but was not identified in our previous publications [144, 141] on the bifurcation diagrams of the long-cavity case. An example of such an intermittency between PD and CC is shown in Fig. 5.2(c).

We have studied the statistics of the transition from PD, which we consider as a laminar phase, to CC, which we name the turbulent phase since PD has periodic behavior and CC has higher amplitude pulsations. For this intermittency between PD and CC regimes, it is possible to measure the duration of laminar phases (τ) through a simple threshold method as amplitudes show distinct differences. The sampling rate of the oscilloscope is adjusted,

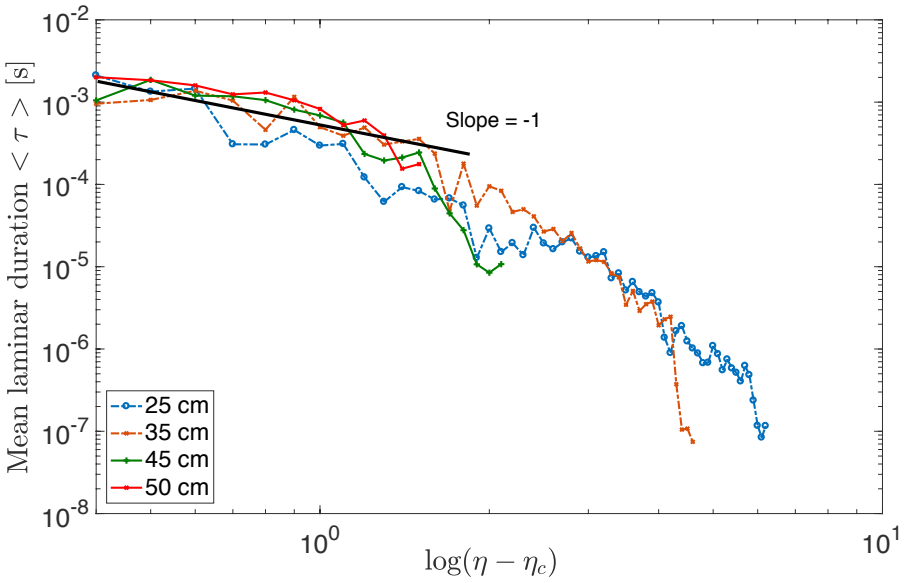

Figure 5.5: Mean duration $\langle\tau\rangle$ of the laminar phases (PD) as a function of η from the onset of intermittency (η_c) between PD and CC. The increment of η corresponds to a 0.1° change in the angle of the quarter-wave plate. The black line has a slope -1 and η_c varies with L. $J = 21.15$ mA

ranging from 20 MS/s to 40 GS/s as η increases. The oscilloscope can stream, in real time, 12×10^6 samples at rates (from 20 MS/s to 5 GS/s) and 2×10^6 samples at rates (from 10 GS/s to 40 GS/s). We are able to measure laminar phase length for a broad range of time scales (100 ns$< \tau <$0.6 s). The threshold is chosen empirically and the laminar phase is indicated by the absence of maxima above the threshold since the local maxima of the PD are lower than that of CC.

As η is increased, the duration τ of laminar phases tends to decrease until intermittency gives way to CC. Based on the collection, 1000 durations of laminar phase (PD), as η increased from η_c for various cavity lengths L (25, 35, 45, and 50 cm), the mean laminar length $\langle\tau\rangle$ versus η on a logarithmic scale is plotted as Fig. 5.5. Some of laminar phases right after the onset of the intermittency are longer than 0.6 s, which we cannot detect due to our experimental limitations and are thus ignored to avoid bad statistics. Even with the experimental limitation, we still have a large enough testing range to gather meaningful statistics on the intermittent regime. The average duration $\langle\tau\rangle$ of laminar phase over η is

consistent with a line of slope -1 on a logarithmic scale near the onset of intermittency [$0 < \log(\eta - \eta_c) < 1.6$]. In contrast, slopes ranging from 0.52 to 4.60, depending on operating parameters, were observed in Ref. [142] for the short-cavity case. It is seen that a deviation from a power-law relation at sufficiently large values of η from the onset in Fig. 5.5. We expect that the solutions of external cavity modes on the PD regime is more easily destabilized as feedback increases, resulting in shorter laminar phases. Experimental statistical results on the average laminar phases in various types of lasers show behavior to that we observe [44, 146]. In short, our tentative attribution of the exponential decay for a larger controlling parameter in the statistics of the laminar phase durations in Fig. 5.5 appears to be consistent with the assignment of this effect in other works. The range of fall-off tends to shorten with increasing L as the CC regime is entered for smaller η. It must be noted that the quality of the fit in Fig. 5.5 depends on what range of η close to the critical value is chosen because the ECSL enters CC at smaller η for longer L. For $L \gtrsim 60$ cm, the PD regime is hardly observed and SH takes over until the ECSL enters CC.

In Fig. 5.6, we study the probability distribution of the duration of the laminar phases near the onset of intermittency. It appears to be well-matched to a line of slope $-3/2$ on a logarithmic scale. Interestingly, these two power-law characteristics are usually observed in on-off intermittency [35, 43, 44, 127, 146, 147]. In our system, external noise is not applied; nonetheless, statistical properties similar to those of on-off intermittency are observed when the route to chaos is interrupted by PD dynamics (*i.e.*, when $L < 60$cm). As predicted by theory [126, 127], modulating a parameter or adding different amplitudes of noise to a system can change the crossover point in which exponential fall-off starts on a log-log plot while the power-law properties near the onset of intermittency are still the same. These features show similarities with our experimental results from varying L. Specifically, we observe the same critical exponent and probability distribution of periodic phases while the crossover point occurs with smaller η for longer L. This earlier fall-off effect with longer L indicates that intermittent behavior becomes less robust as the cavity

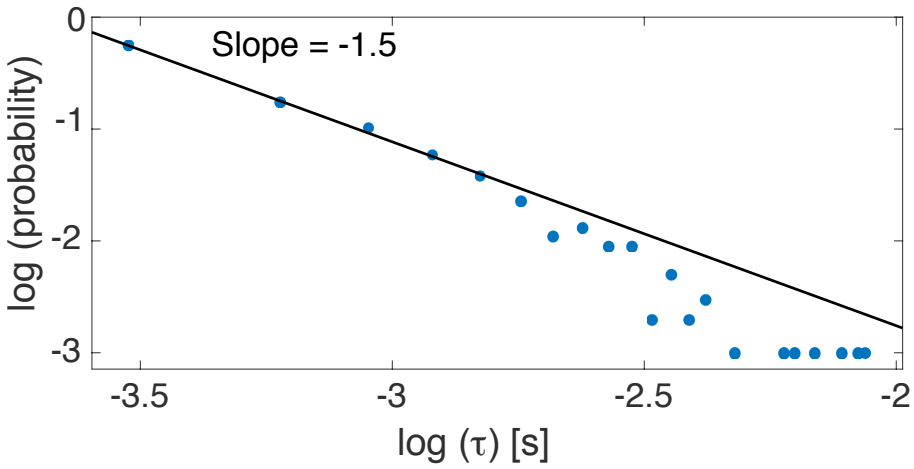

Figure 5.6: Probability distribution of the laminar phases near the onset of intermittency; The line indicates a power law fit with the slope -3/2. The shorter laminar phases are well fitted by the line. $\eta = 0.6$, $L = 30$ cm, $J = 21.15$ mA

length increases.

In Fig. 5.7, we compare the optical spectra in the PD and CC regimes for $L = 30$ cm. The main peak of the PD regime in the optical spectrum is positioned at a negative mode (ECM -11) [Fig. 5.7], which highlights the fact that the PD regime remains stable around what is probably the maximum gain mode [148]. As the ECSL enters CC, we observe from Fig. 5.7 that the dominant ECMs are close to those ECMs that are active in the PD regime. This proximity in phase space between attractors corroborates the interpretation that chaotic attractor of the CC regime is born through a crisis with a nearby PD attractor, similarly to what was suggested in Ref. [142] for the short-cavity case on the basis of the Lang and Kobayashi model. The crisis nature of the transition from the PD and CC regime is confirmed in a recent study from our group [149]. In this work, the study of the optical phase reveals that the PD attractor is suddenly destroyed and gives way to a chaotic behavior.

The influence of the external-cavity length L was studied by changing L in 10 cm increments from 20 cm. We find that intermittency between PD and CC is observed systematically when $L < 60$ cm. However, when $L \gtrsim 60$ cm, the second regime of intermittency between PD and CC is not observed. In this case, the regime of multistate intermittency

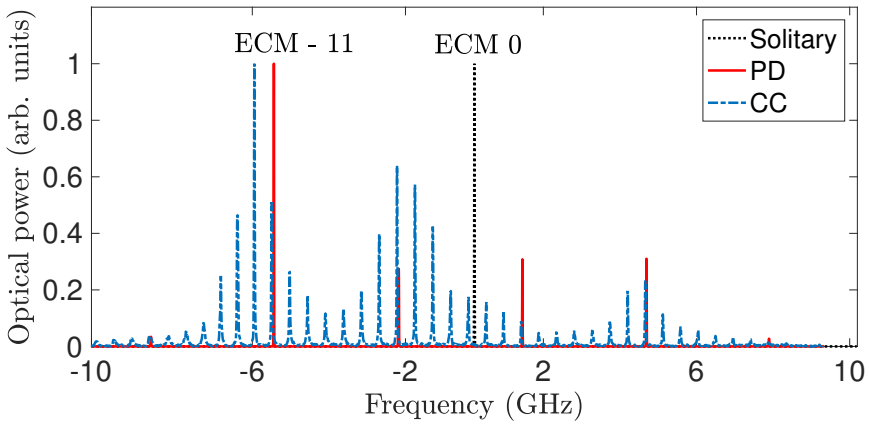

Figure 5.7: Optical spectrum at $L = 30$ cm, $J = 21.15$ mA. The main peak of the PD regime is located on a negative ECM before the onset of intermittency. In CC, the active ECMs appear to be around those that were active in PD. Optical power is normalized for better comparison. ECM 0 corresponds to the frequency of a solitary laser.

leads directly to CC through a final phase which is the intermittency between SH and CC regimes. Longer L leads to ECMs that are closer in phase space and more easily destabilized, possibly explaining the instability of the PD regime for large L.

5.4 Conclusion

We have shown experimentally that two regimes of intermittency can be observed on the route to chaos of a semiconductor laser subjected to optical feedback from a long external cavity, as the feedback level is increased. Multistate intermittency is experimentally observed first involving combinations of two or three of the following dynamics: limit cycle, quasiperiodic, subharmonic, and period-doubled. We find that the probabilisitic dominance of the dynamics varies with external cavity length and feedback level. A theoretical description for this phenomena, however, is not yet available. For larger feedback, we find that when the period-doubled regime is visited on the way to chaos, corresponding to an external-cavity length smaller than 60 cm, intermittency is seen between the two regimes, generalizing the results of Ref. [142] to the long-cavity case. In addition, we find that the latter intermittency has universal power-law properties which are comparable to

the statistical properties of on-off intermittency. For cavities longer than 60 cm, a stable period-doubled regime is not observed and longer L hinders the ECMs from staying in the maximum gain mode. Instead, intermittency between subharmonic and chaotic regimes is observed. These results highlight the complex nature of the intermittency phenomenon involved in the route to chaos, resulting from the high dimension and significant multistabiltiy of the dynamics of an external-cavity laser.

CHAPTER 6
THE DYNAMICS OF TERMINAL VOLTAGE OF EXTERNAL-CAVITY SEMICONDUCTOR LASERS

We have discussed the unstable dynamics, *i.e.*, intermittency in an ECSL under various conditions in the previous chapters 4 and 5. Based on the detailed analysis on the instability of SLs including BDs, we have seen that the laser output can exhibit periodic oscillation, quasi-periodic oscillation, subharmonics, LFFs or fully-developed CC when moderate and strong feedback is applied. On the other hand, we can observe continuous wave (CW) operation from ECSLs with low optical feedback. Under conditions of stable operation, an SL biased by constant current usually emits laser with a constant intensity (continuous wave). In particular, when an ECSL is operated with single mode in the optical spectrum, self-mixing interference (SMI) is used for remote sensing and instrumentations for the metrological quantities. To begin with, it is essential to first understand the dynamics of terminal voltage across the laser junction, which will be discussed based on the following publication:

- A. A. Sahai, Byungchil Kim, Daeyoung Choi, A. Locquet, and D. S. Citrin. "Mapping the nonlinear dynamics of a laser diode via its terminal voltage", Optics Letters, Vol. 39, No. 19, Oct (2014).

We show that the bifurcations between dynamical regimes of an ECSL can be detected via its terminal voltage V_{LD} of a laser diode (LD). V_{LD} conveys information on the change in the dynamical-state variable N and tracks the optical intensity based BDs as well.

The dynamics of ECSLs are significantly affected by external cavity length, feedback level, and feedback phase. It is theoretically and experimentally proven that the longer external cavity and stronger feedback level lead an ECSL to be unstable. However, for the

variations of feedback phase, only a few experimental studies have been done because it is difficult to experimentally change the phase delay of an ECSL. In this chapter, we utilze a linear motor stage to change the position of a reflecting mirror on nanometric scales and observe the effects of phase delay on the stability of ECSLs. Finally, we will introduce how V_{LD} can be utilized for SMI applications instead of relying on photodiodes.

6.1 Theoretical framework

6.1.1 The dynamics of an ECSL via its terminal voltage

The dynamics of an external-cavity semiconductor laser (ECSL) is studied for various applications [17] by sampling the photo-detected optical output. Compared to the optical output, the terminal voltage of an laser diode (V_{LD}) can be preferred for compact and simple applications since a laser system does not necessitate photo-detectors. Only few applications of terminal voltage V_{LD} across a LD [45, 46] have been discussed in the weak feedback regime where the linear behavior of the ECSL occurs. In order to properly understand dynamics of the terminal voltage when feedback is applied to an ECSL, abrupt transitions of the dynamical state between different regions of the phase-space should be fully investigated. It is shown that in the nonlinear regime, for a negligible instantaneous change in optical feedback, the carrier density N changes significantly at the bifurcations corresponding to jumps of phase-space trajectory across several external cavity spatial modes (ECMs). The quasi-Fermi level difference across the *p-i-n* active-medium changes proportional to change in N.

We show here that the dynamical regimes as well as bifurcations are indeed evidenced in the dc component V_{dc} of V_{LD} along with the photo-detected optical output. These fluctuations of V_{LD} are shown to be directly related to the active-region carrier density, $N(t)$. Thus, we will directly access a key dynamical variable in the system, namely the carrier density N, and thus the inversion, which will be compared to the more conventionally used optical intensity since we have observed various types of bifurcation diagrams (BDs) from

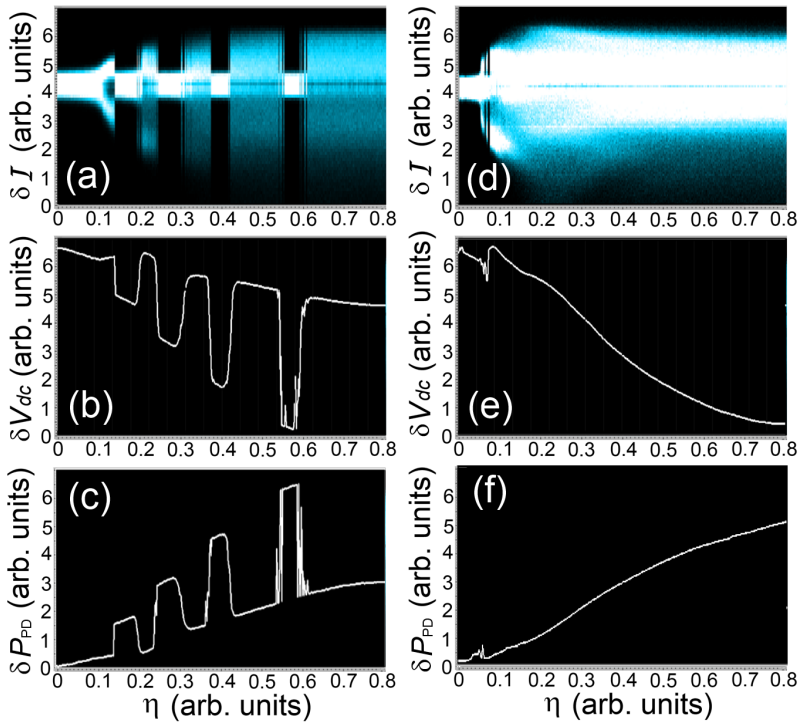

Figure 6.1: Experimental BD based on optical I, corresponding δV_{dc} and $\mathcal{I}$ from P_{PD} the back-facet optical leakage sensed by the internal photodiode (a), (b), (c) for $I = 11.42$ mA and $L = 15$ cm. (d), (e), (f) for $I = 11.42$ mA and $L = 65$ cm.

the optical intensity of a LD with different conditions. Here, we explain the dynamics of the terminal voltage and optical intensity based on the Lang and Kobayashi (LK) model and see experimentally if the terminal voltage and the optically detected signal are in agreement with the LK model. Note that the experimental setup is basically the same as we have introduce in chapter 3. The only difference is that we added probes to detect $V_{\rm LD}$ across the laser junction through a multimeter.

We present the experimental results in Fig. 6.1 where the optical BD, corresponding dc terminal voltage change from no feedback, $\delta\ V_{dc} = V_{dc} - V_{dc}\ (\eta = 0)$ and LD internal photodiode signal change δP_{PD} (from no feedback) equivalent to the average intensity $\mathcal{I}$ from the optical leakage sensed at the back-facet of the optical cavity, are shown as functions of the feedback strength η for a given L and injection current J. The BD in Figs. 6.1(a),(d) is obtained by detecting the time-series of $I(t)$ envelope fluctuations; plotted by the histogram of local extremal values of $\mathcal{I}$ for a given η. As we have seen from BDs at

low injection current, bifurcation cascades between apparently stable and unstable regions are observed in Figs. 6.1(a), (d) as changes in δI with varying η. The stable thinner regions of δI do not necessarily correspond to stable CW behavior but also contain regimes in which phase-space trajectories have small excursions within an island of stability resulting in low-amplitude instabilities that have developed around a single ECM attractor [90].

The differences between Fig. 6.1(a), (c) and Fig. 6.1(d), (f) are largely attributed to the separation between ECMs in phase space. When L is long (65 cm), the spectral separation between ECMs is reduced (for $L = 15$ cm, the external-cavity free spectral range is 1 GHz, for $L = 65$ cm, 233 MHz) in the optical spectrum. Each participating mode being close in phase space, large-amplitude itinerancy between several modes is easily observed. Indeed, numerical simulations of the trajectories on the ellipse in phase space projected on the N *vs. phase* plane show that the proximity of the ECMs prevents independent attractors from developing, and therefore the existence of a bifurcation cascade is suppressed. Conversely, increased distance between the ECMs for shorter L means that larger δI is needed before attractor merging occurs, thus explaining the longer stable regions. The wider regions in δI, referred to as unstable regions, typically correspond to regimes in which phase-space trajectories wander around several and occasionally non- adjacent ECMs and are thus above the system noise. In Figs. 6.1(c), (f) also shows the bifurcations in δI, it has an overall rising trend for increasing τ due to a rising stimulated emissions rate.

In Figs. 6.1(b) and (e) is plotted $V_{\rm dc}$ as η is varied. We note an overall decrease in $\delta V_{\rm dc}$ with increasing η; these correspond to the optical-BDs in Figs. 6.1(a),(d), respectively. Various bifurcations that occur in $\delta I(t)$ in Figs. 6.1(a), (d) at specific values of η are clearly reflected at the same η in the terminal voltage $\delta\ V_{dc}$ in Figs. 6.1(b), (e). This is a clear trend in δV_{dc} opposite to $\mathcal{I}$ illustrates the ability to reliably tap into additional dimensions of phase space without a photodetector.

Figure 6.2 shows the theoretical (a) BD (having subtracted off the time-averaged intensity) and (b) the time-averaged carrier density $N_{\rm dc}$ as a function of κ. Note that the BDs

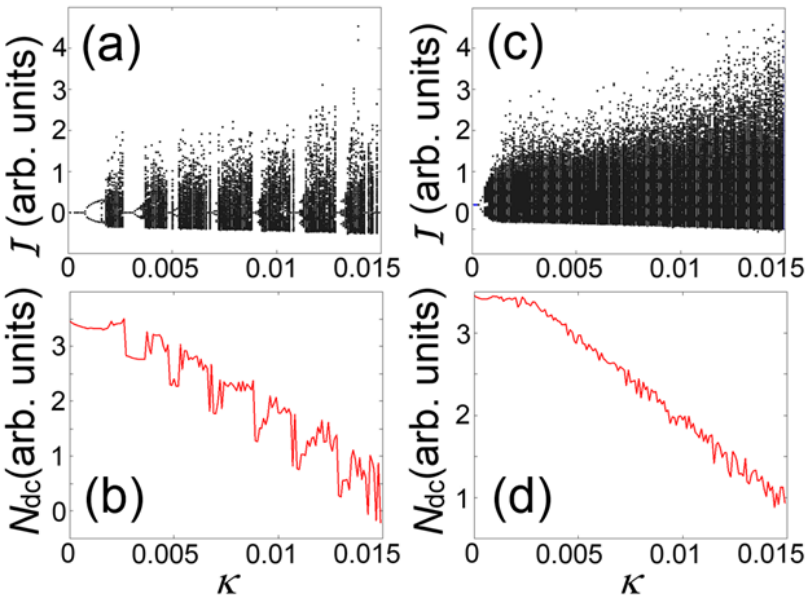

Figure 6.2: (a) Theoretical BD and (b) corresponding $N_{\rm dc}$ ($\propto V_{\rm dc}$) for $p = 1.3$ and L = 15 cm. (c) Theoretical BD and (d) $N_{\rm dc}$ for $p = 1.3$ and L = 65 cm.

bear a close resemblance to those of Figs. 6.1(a) and (d). As we explain below, $N_{\rm dc}$ is directly connected to $V_{\rm dc}$ as measured experimentally.

The voltage across a p-i-n structure of the LD, $V_{\rm LD}$ is the difference Φ(t) between the quasi-Fermi levels $\mathcal{E}_F^j$ on the $j = p$ and n side. Thus, assuming flat bands in the quasi-neutral regions,

$$\begin{aligned} V(t) &= -e\Phi(t) \\ &= \mathcal{E}_F^n(t) - \mathcal{E}_F^h(t) = \left[\ln\left(\frac{N_e(t)}{N_e^i(T)}\right) - \ln\left(\frac{N_h(t)}{N_h^i(T)}\right)\right] k_B T, \end{aligned} \tag{6.1}$$

where N_e, N_h, $N^i(T)$ are the electron, hole (in the n and p-type regions, respectively), and intrinsic concentrations [45]. We assume that I and T are constant, and the ECSL is fluctuating around a basin of attraction (ECM). The change in the carrier concentration is assumed to be small compared with the carrier concentration $N_{\rm ECM}$ in the quasi-neutral intrinsic region (gain medium), giving $N(t) = N_e(t) = N_h(t) = N_{\rm ECM}$. By measuring Φ as N changes, we can determine the voltage change in $V_{\rm LD}$ in response to the the change

in N due to the optical-feedback induced dynamical state. It should be noted that when the ECSL undergoes a bifurcation, N undergoes a discontinuity; however, the expression is related to the change in $V_{\rm dc}$ due to the variations in the dc value of N starting with Eq. (6.1) is

$$\delta V_{\rm dc} = e\delta\Phi_{\rm dc} = \frac{e}{N_{\rm ECM}}\left(\frac{\partial\mathcal{E}_F^e}{\partial\ln N_e} - \frac{\partial\mathcal{E}_F^h}{\partial\ln N_h}\right)\delta N_{\rm dc} \tag{6.2}$$

holds where $\delta N_{\rm dc} = N - N_i$ in the gain medium within a given dynamical regime. Since $\partial\mathcal{E}_F^e/\partial\ln N_e > 0$ and $\partial\mathcal{E}_F^h/\partial\ln N_h < 0$, $\delta V_{\rm dc}$ is proportional and of the same sign as $\delta N_{\rm dc}$.

Since the logarithmic derivatives in Eq. (6.2) depend relatively weakly on T, the voltage fluctuation $\delta\Phi_{\rm dc}$ (and hence $\delta V_{\rm dc}$) is proportional to $\delta N_{\rm dc}$. Optical feedback induces an increase in the photon number $\propto |E|^2$ in the active region, which results in reduction of $N_{\rm dc}$. Externally feeding light back into the gain region in turn increases the rate of stimulated emission. This thereby reduces the population inversion. Consequently, the overall reduction in $N_{\rm dc}$ in the active region leads to a reduction in $\Phi_{\rm dc}$ and therefore in $V_{\rm dc}$. While the dc analysis provides rich insight into the physics at a level comparable to the BD associated with $\mathcal{I}$, we have also conducted ac analysis including BDs and confirmed that V_{ac} provides the similar dynamical behaviors with $\mathcal{I}$ on sub-nano timescales. [16]. Clearly, signatures of the various bifurcations are observed both in the experiment [Fig. 6.1(b) and (d)] as well as in the theory [Fig. 6.2(b) and (d)], the latter is computed by means of the LK equations [Eq. (6.1)] in the dc limit, we see that these latter curves are proportional to $V_{\rm dc}$. Namely, the overall downward trend in $V_{\rm dc}$ with increasing feedback (experiment κ; theory η) is interrupted by abrupt jumps at bifurcations, as can be seen by comparing with the corresponding BDs [Fig. 6.1(a) and (c); Fig. 6.2(a) and (c)]. For the case of $L = 65$ cm, the ECSL enters a chaotic regime at fairly low κ.

The ECSL, for comparison with the LK model, is described by three dynamical variables, *viz.* the electric-field amplitude $|E(t)|$ (or $\mathcal{I}(t) = |E(t)|^2$), the optical phase $\varphi(t) = \arg E(t)$, and the carrier density $N(t)$. $\mathcal{I}(t)$ is the quantity probed in the vast majority of published work. We provide information on the carrier density N, though only the dc value

N_{dc} here. Such information is indeed valuable and provides insight in the the system on a level comparable to the BD constructed from the optical intensity $\mathcal{I}$. The steady-state solutions of the LK equations are the stable ECMs and unstable antimodes. Plotted in the N - *vs.*-ϕ plane (Fig. 2.4), these are points lying on an ellipse. Thus, measuring $V_{\rm dc}$ provides information on those ECMs that dominate the phase-space trajectory. Such measurements can be directly coupled with measurements of the optical spectrum from the optical output power [90]. While the dc measurement here does not directly reveal the underlying detailed dynamics, it is clear that when the system undergoes a bifurcation, the relevant ECMs can be identified by measuring $V_{\rm dc}$.

A different phase ($\varphi - \varphi_0$) is controlled by sub-wavelength adjustment of L. While changing φ_0 is known to affect the ECSL dynamics including its stability; it shifts the value of feedback where specific bifurcations occur although it has minor impact on the global dynamics in terms of the sequence of bifurcations [70].

From this work, we have observed that the detected voltage change is necessarily related to N. Thus, the dynamics of the voltage could give information on the dynamics of N. Indeed, we can consider the current work in the broader context in which a photodetector could be replaced with terminal voltage. Based on this result, we will explore laser applications such as displacement sensors using optical feedback effects in a stable CW regime.

6.2 Effects of phase change in the dynamics of an ECSL with optical feedback

Nanodisplacement (or position sensors) have been demonstrated based on a wide variety of physical effects and have been developed for various applications [150, 151]. The sensor we demonstrate here is a noncontact sensor based on effects of phase change in the ECSL dynamics. As for noncontact nanodisplacement sensors, there are a number of approaches, including those based on capacitance, eddy currents, and atomic-force microscopy (see [152, 153]). These approaches, while in some cases sensitive to atomic-scale displace-

ments, however, can be complex and sensitive to quite small displacement ranges.

We experimentally measure the emission frequency and terminal junction voltage of an external-cavity semiconductor laser under low optical feedback when the location of a remote target varies on the sub-wavelength scale. We investigate the self-mixing effect in an external-cavity semiconductor laser and find the optimal working conditions for nano-displacement sensing.

6.2.1 Self mixing interferometry

SMI, widely observed in various types of lasers, is based on light, reflected back into the active region of a laser, which in turn affects the laser operation in a fashion dependent on the optical phase of the reflected light [154, 155]. SMI itself provides sensitivity at least on the scale of the emission wavelength λ, though below we show that indeed the minimum detectible displacement (MDD) can be far less than λ. Semiconductor-laser-diode-based approaches to SMI are certainly of most direct relevance to many practical sensing applications. The MDD of conventional interferometric sensors is set overall by the λ employed. For example, in a reflective sensor based solely on detecting the interference between a reference beam and a split-off portion reflected from a target, as the optical-path distance varies over λ, the phase difference between the beams varies over 2π. The intensity of the interference pattern changes sinusoidally with one period for each distance change λ. As this variation is sinusoidal, conventional interferometry enables to measure displacements over many λ but small sub-λ changes in the optical-path difference may be difficult to detect.

Heuristically, SMI as a sensing mechanism works as follows. When the target distance L is varied by ΔL, the properties of an ECSL (laser emission frequency ν, linewidth, and threshold gain) undergo periodic variation, which is broadly understood on the basis of the Lang and Kobayashi (LK) equations [3]. In fact, the emission-frequency variation with L is a manifestation of mode frequency pulling, and has been described in ECSL's using a three-

mirror model [154]. The idea is that as the various external-cavity modes move across the gain spectrum of the active region, the emission frequency is dragged along until a mode stable external-cavity mode (ECM) is reached, at which point the emission frequency ν undergoes a discontinuous jump we call mode hopping. The result is that ν as well as the optical output power P_{PD} and the LD terminal voltage V_{LD} exhibit sawtooth behavior as functions of L with a period of $\lambda/2$. Due to the expense of measuring ν, SMI signals obtained from P_{PD} or V_{LD} are typically preferred to monitor ΔL. However, use of P_{PD} and V_{LD} each has its own pros and cons. P_{PD} requires a PD either internal to the LD package or an external PD, adding complication, and expense. Also, there is a possibility that stray light might be lost on the back-facet internal PD without reaching the active region [93]. On the other hand, V_{LD} is used to circumvent this unnecessary optical-to-electrical conversion, but it is known that the SMI signals from V_{LD} tend to exhibit lower signal-to-noise ratio (SNR) than those of P_{PD} from the internal PD [156, 157].

We demonstrate SMI sensors operated in a regime enabling unprecedentedly high sensitivity providing a pronounced sawtooth dependence on L of the sensing parameter. We concentrate here on V_{LD} as the sensing parameter and find a highly linear dependence of V_{LD} on ΔL between discontinuities exhibiting a period $\lambda/2$ (since the reflected light undergoes a change in round-trip travel of λ). The physical mechanism underlying this sawtooth behavior is mode frequency pulling (the continuous portions of the sawtooth) together with mode hopping (the discontinuities of the sawtooth) [154, 158], which makes ν highly L dependent. This in turn affects V_{LD} in a highly linear fashion during the continuous parts of the sawtooth, which is the sensing signal employed. While other SMI sensors have been demonstrated by a moving target such as a harmonic piezo-actuator or a loudspeaker that sweeps several micrometers, combined with high sampling speed to measure fringes of SMI signals. Their MDDs were from hundreds of nm to a few nm based on methods of interferometry; a microchip feedback-shifted laser (1 nm) [159], multiple self-mixing ($\lambda/4$) [160], frequency tuning (10-60 nm) [161], laser feedback grating (< 10 nm) [162],

Fourier transform ($\lambda/50$) [163], phase shifting ($\lambda/12$) [164], linear interpolation ($\lambda/12$) [165], and phase unwrapping (40 nm) [166]. In contrast to the works just cited, our approach is quasi-static as the sensing mechanism is independent of the time over which the displacement occurs (so long as it is greater than relevant timescales in the ECSL). We tentatively attribute the superior performance of our SMI sensor to two sources. First, as a quasi-static sensor, the ECSL can settle upon the stable ECM for a given value of L. In the other works, where the target oscillates at acoustic frequencies, the ECSL might not have time during the acoustic oscillations to settle consistently on the stable ECM each cycle; hopping between ECM's, based on our work on intermittency in ECSLs [167] may take more than milliseconds. Moreover, there may be uncharacterized cycle-to-cycle variation in the displacement of the speaker cone measured in these works. The second reason is that we employ a narrow linewidth ($\ll 40$ MHz) distributed Bragg reflector (DBR) LD which is expected based on frequency-mode-pulling theory [158] to provide sharp sawtooth behavior at relatively low feedback strengths compared with the broader linewidth Fabry-Perot LD's used in other studies.

SMI indeed has been exploited in the past for various applications: imaging [47, 49, 168], biomedical sensing [169] and measuring absolute distance [51, 52, 53], displacement [56, 57, 62, 170], reflective index [171], velocity [60, 61], and flow [172, 173]. Recently, Keeley *et al.* [174] investigated the emission spectrum of a THz QCL by measuring ν and V_{LD} as functions of ΔL and showed that a method of SMI can achieve a similar spectral resolution as Fourier transform infrared spectroscopy. Certainly, the approach is broadly applicably employing a wide range of LD's.

The novelty in our work is the combination of record values of MDD for a quasi-static sensor, low-cost, and simplicity. We demonstrate a SMI sensor with a MDD of $\lambda/130$. Indeed, as we argue below, the MDD of this class of sensor might actually be significantly less than this value. The SMI sensor we demonstrate here has the advantages of interferometric sensors in general of being able to count fringes for high-accuracy sensing over

ΔL of many λ, but also provides a sensing mechanism that is highly linear in the displacement, and thus permits precision measurements *well below* λ for total displacements either sub-λ or of many λ. The essential difference between SMI sensors and conventional interferometric sensors is that the interference affects the operation of the ECSL itself through the nonlinear optical properties of the active region. In our work presented here, the laser diode (LD) emits at $\lambda \approx 1550$ nm, which is an inexpensive, readily available telecom laser. Indeed, higher performance with this sensor might be possible; the quoted MDD is actually limited by the stability of the piezoelectric displacement stage (~ 10 nm) used for its characterization and the resolution limit of multimeter upon which the measurements are made to monitor the LD terminal voltage V_{LD}. Specifically, target displacement near the MDD of 12 nm results in variations in V_{LD} on the order of μVs, which is measured with a 5-1/2-digit-resolution multimeter. Therefore, this scheme could be further improved with a higher resolution multimeter in highly sensitive applications where MDD < 10 nm is needed. Moreover, by choosing shorter-λ lasers, smaller MDDs are expected to be possible.

We start with a brief review of some important theoretical points that describe the variation in ν (and consequently in V_{LD}) with L. We measure ν and V_{LD} of an ECSL in single-mode operation under the influence of optical feedback. We use this information to characterize the MDD of the nanodisplacement sensor. Next, we focus on practical sensors exploiting V_{LD} as the SMI signal under controllable working parameters (injection current J, external cavity length L, and feedback level κ) leading to the smallest MDD. We then conclude.

To specifically point out different part of experimental setup from the chapter 3, we use a single-longitudinal-mode multi-quantum well InGaAsP DFB laser. The LD emits at 1550 nm with a free-running threshold current $J_{th} = 29.8$ mA. The LD used is *unpackaged* such that we can directly measure V_{LD} across the LD junction without using an internal photodiode (PD). In this particular experiment, the remote mirror (RM) is placed on the

linear motor stage (Newport RMS50) whose position is adjusted by the driver (Newport XPS-RL2) with 40 nm/step (with error ± 10 nm). Thus, we can control the distance between the reflecting mirror (RM) and the LD that determines the cavity length L on nanometric scales.

6.2.2 The excess phase equation from the LK model

The theoretical understanding of SMI has already been discussed by numerous authors [154, 175]. To briefly review the excess-phase equation derived from the LK model,

$$\Delta\varphi = 2\pi\tau_{ext}(\nu - \nu_0) + C\sin(2\pi\nu\tau_{ext} + \arctan\alpha) \tag{6.3}$$

where κ is the optical feedback strength coupled back into the laser cavity and α is the linewidth enhancement factor. One defines the feedback parameter

$$C = \frac{\kappa}{\tau_{in}}\tau_{ext}\sqrt{1+\alpha^2}$$

where τ_{in} and τ_{ext} are the optical round-trip times within the internal LD cavity and in the external cavity, respectively. C determines the fundamental dynamics of an ECSL combined with external phase φ such that it is conventionally used to qualitatively classify the regimes from various SMI systems [69]. Thus, an ECSL emission frequency ν with respect to ν_0 (the emission frequency in the absence of feedback) is relative to round-trip phase $\Delta\varphi$ (relative because we are unable to make an absolute phase determination), described as

$$\nu = \nu_0 - \frac{C}{2\pi\tau_{ext}}\sin(2\pi\nu\tau_{ext} + \arctan\alpha) \tag{6.4}$$

As shown in Fig. 6.3, the variation of ν from ν_0 when the target can be $\nu(\varphi) = \nu_0[1 + mF(\varphi)]$ where m is the optical-feedback modulation index which defines the signal slope with respect to L, L is the remote target displacement from the LD, $F(\varphi)$ is a periodic

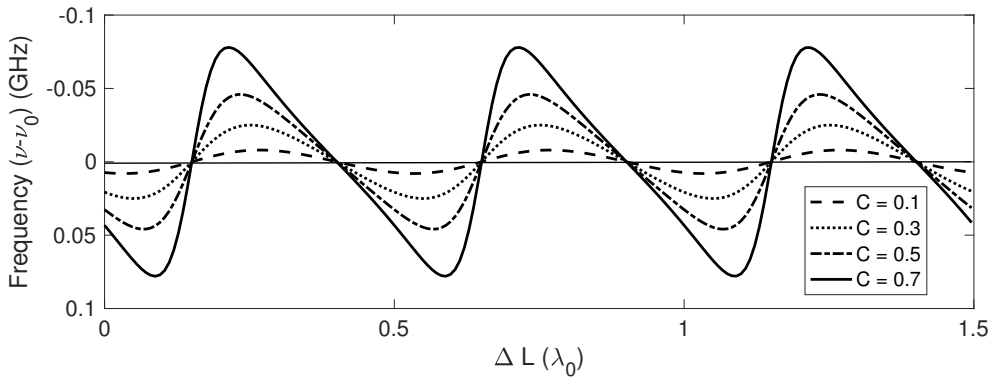

Figure 6.3: Theoretical laser frequency shift $\nu - \nu_0$ versus target displacement based on Eq. 6.4. The central line ($\nu - \nu_0 = 0$) is when no feedback is applied. The displacements are in the units of the laser wavelength.

function $\varphi = 2kL$ with period 2π, and $k = 2\pi/\lambda$ is the wavenumber in the external cavity. The SMI shape of $\nu(\varphi)$ depends on C when the target displacement ΔL is made. The SMI shape is rather sinusoidal when $0.1 < C \ll 1$. As C is increased, the SMI signal gradually becomes a sawtooth wave at moderate feedback level ($1 < C < 4.6$) with discontinuity (*i.e.*, abrupt mode hopping to a neighboring lasing mode) at every integer multiple of $\lambda/2$, *i.e.,* 2π external-cavity round-trip phase shift. Also, increasing C results in greater amplitudes of $\nu(\varphi)$ (Fig. 6.3).

6.3 Experimental results

We present our experimental results pertaining to nano-displacement sensing. $\Delta\varphi$ is related to small variations ΔL in the external-cavity length L. Working in the vicinity of $L = 30$ cm, we adjust $\Delta\varphi$ by changing L in 40 nm steps using a linear motor stage (LMS). As mentioned above, our ability to measure small displacements can most directly be related to the L dependence of ν even though we focus on $V_{\rm LD}$ as the SMI signal. We therefore set aside detailed discussion of $V_{\rm LD}$, and return to it later once we understand the physical basis for the sensor operation.

Figure 6.4 shows the experimental values of $\nu - \nu_0$ ($\nu = \nu_0$ when $\kappa = 0$) and $V_{\rm LD}$ versus ΔL beginning at very weak feedback. For $\kappa = 0.0005$, $\nu - \nu_0$ exhibits a noisy

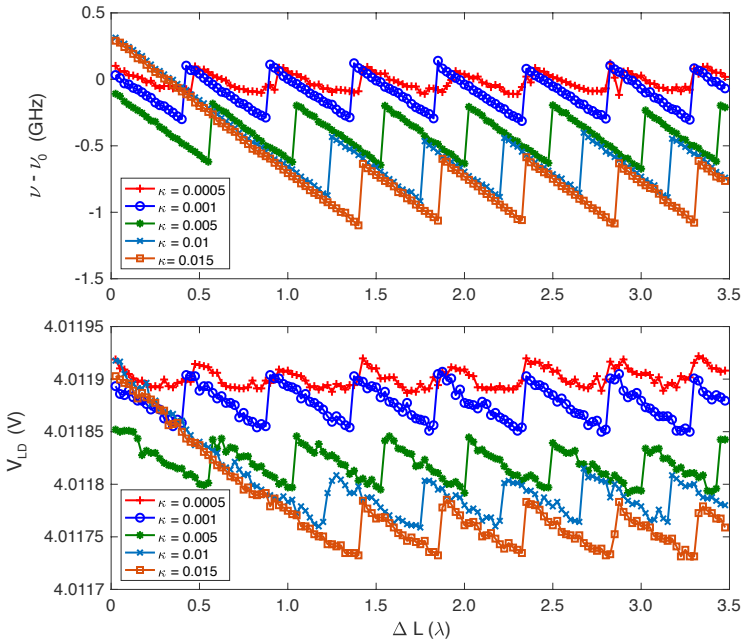

Figure 6.4: Laser frequency shift $\nu - \nu_0$ and $V_{\rm LD}$ versus target displacement (in the units of λ) obtained from the experiment. The small displacement is characterized by movement away from the LD (40 nm/step). The base external-cavity length $L = 30$ cm, $J = 69$ mA, and $\nu_0 \simeq 193281.8$ GHz.

skewed sine-like behavior. As κ is increased, the dominant optical peak at ν is shifted downward in frequency with respect to ν_0 and displays increasingly pronounced sawtooth behavior with discontinuity periods at every $\lambda/2$. When $\kappa \geq 0.01$ (Fig. 6.4), equivalent to moderate feedback ($C > 1$), the initial sawtooth periods for small ΔL are lost. This is because the single-mode laser dwells on one of several external-cavity modes (ECM) before finally jumping discontinuously to another ECM [176]. We tentatively infer that the narrow linewidth of a DFB laser contributes to the pronounced sawtooth behavior in our experiments. From the observation of emission spectrum before mode hoping occurs, linewidth of single longitudinal mode extends over the external-cavity free-spectral range $f_{ext} = \tau_{ext}^{-1} \simeq 460$ MHz at very weak feedback level (*i.e.*, $\kappa = 0.0005$ in Fig. 6.4), which renders rather smooth transition to a neighboring ECM. As κ is increased, the linewidth of the lasing mode is significantly narrowed ($\ll 40$ MHz), thereby inducing a abrupt discontinuity. Since the results in Fig. 6.4 are obtained by moving the target away from the LD,

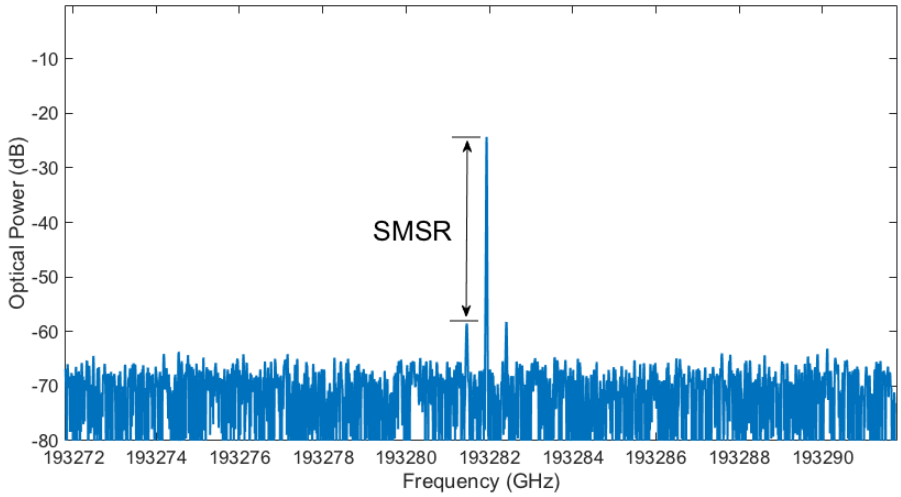

Figure 6.5: Side mode suppression ratio (SMSR). The relation of power between dominant (center) longitudinal mode and the nearest higher order mode.

the slopes of the linear variations in $\nu - \nu_0$ are negative. Conversely, the slopes are positive when the target moves closer to the LD (not presented here).

As expected from the theory, we observe sawtooth behavior in $\nu - \nu_0$ as well as V_{LD} with periodic discontinuities separated by $\lambda/2$ in ΔL. Of note, the sawtooth behavior in $\nu - \nu_0$ is *not* around 0 (*i.e.*, the value in the absence of feedback) because ν is shifted as soon as κ is applied. Larger κ leads the ECSL to be shifted further away from ν_0. This trend has been reproduced numerically [5] and is also found in the experimental route to chaos [141, 177]. The sawtooth behavior appears as long as the ECSL shows continuous-wave (CW) operation. The ECSL is destabilized by complicated dynamics with undamped relaxation oscillations at which point the sawtooth behavior is suppressed.

In addition, we find it useful to map the experimental feedback strength κ onto the feedback parameter C via the side-mode suppression ratio (see Fig. 6.5), which is the ratio between the central longitudinal mode and the largest side mode in the optical spectrum [69, 178]. We can therefore track the transition from single-mode behavior to one where several ECMs are active around ν by considering the SMSR. Clearly, the participation of more than one ECM will lead to more complicated dynamics, and consequently ruin SMI signals. We increase κ from the weakest possible value in our setup and monitor the crossover from

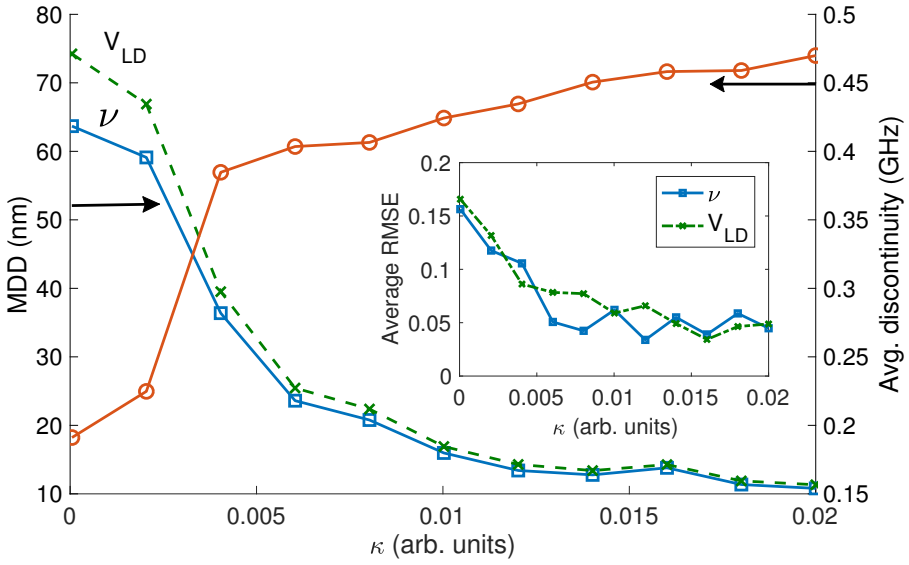

Figure 6.6: The minimum detectible displacement (MDD) by ν and V_{LD}, and average discontinuity in $\nu - \nu_0$ as a function of κ. The average RMSE (inset) displays the deviation of the differences between the best linear fit and measured values. The average values are obtained from a range of 16π phase shift. $\kappa > 0.01$ corresponds to $C > 1$. $J = 69$ mA, $L = 30$ cm.

weak to moderate feedback. In the weak-feedback regime ($C < 1$), the ECSL emits on only one ECM, which corresponds to CW operation, and the SMSR exceeds 35 dB. For moderate feedback ($1 < C < 4.6$), we define (25 dB<SMSR<35 dB) as side modes start to appear while the ECSL still operates in CW. The SMI signals in the moderate feedback regime show clear sawtooth behavior, but some of the first few periods are lost (hysteresis effect [176]) as shown in Fig. 6.4 when $\kappa \leq 0.01$. As κ is further increased ($C > 4.6$, strong feedback), several ECMs participate in the emission after the SMSR is degraded below 25 dB. As a result, the sawtooth behavior is no longer observed in ν as the ECSL exhibits frequent mode-hopping among several ECMs. Thus, we can identify the angle range of the QWP to limit κ so that the ECSL exhibits only CW operation.

6.4 Self-mixing sensors based on terminal voltage

We have hitherto concentrated attention on the behavior of $\nu - \nu_0$ as L is varied. In passing, ν and the carrier density are mutually interrelated since the effective refractive index and

the threshold gain vary along with optical feedback [56]. Correspondingly, the variation of carrier density is manifested in V_{LD} [93].

We explore the MDD attainable using our approach. Our method will be to consider variations of $\nu - \nu_0$ ($\Delta\nu$) since the key point is to find a feedback condition where $\Delta\nu$ is highly correlated with variations of V_{LD} (ΔV_{LD}). We measure the discontinuities of $\Delta\nu$ for various values of κ. As shown in Fig. 6.6, Increasing κ from weak to moderate feedback, the average discontinuity is increased, and then stays around at $f_{ext} \simeq 460$ MHz in which we observe clear sawtooth periods of $\Delta\nu$, implying that the discontinuity is locked to two neighboring ECMs.

In the following, we consider the MDD. Let G be the signal being measured (*e.g.*, ν, P_{PD}, or V_{LD}). The ideal sensitivity is $dG/dL = m$ where m is the signal slope with respect to L (neglecting the discontinuities in G). It is therefore advantageous, all else equal, to choose parameters to maximize $|m|$. Due, however, to unavoidable sensitivity error, the MDD (ΔL_{min}) also depends on the error variations $n(L)$ in G. To find ΔL_{min}, we begin with G including $n(L)$,

$$G = mL + n(L). \tag{6.5}$$

A displacement ΔL will produce a change ΔG in F given by

$$\Delta G = \frac{dG}{dL}\Delta L \approx m\Delta L + [n(L + \Delta L) - n(L)]. \tag{6.6}$$

This can be clearly detected provided

$$\Delta L \gg \frac{1}{m}[n(L + \Delta L) - n(L)]. \tag{6.7}$$

This quantity on average is independent of L though it does depend on ΔL. We can simply identify the quantity in brackets on the right-hand side of Eq. (6.8) as a characteristic noise amplitude n_{avg}. Namely, suppose it is adequate to identify n_{avg} with the root-mean square error (RMSE) between experimental G and its best linear fit. We therefore approximate values for the MDD as

$$\Delta L_{min} = \frac{1}{m} n_{avg}. \tag{6.8}$$

This analysis is expected to be valid so long as the correlation length of $n(L)$ is less than the MDD. We find that when the discontinuity in ν is locked at $\sim f_{ext}$, the linewidth of the ν gets narrower and highly linearized $\Delta\nu$ between the discontinuity periods, resulting in significantly reduced RMSE of ν (inset of Fig. 6.6) which we attribute to narrowing of an oscillation mode as κ increases. We can therefore interpolate $\Delta\nu$ made by $\Delta\varphi$ of LMS. As shown in Fig. 6.6 ($0.015 < \kappa < 0.02$), the MDD obtained by ν is as small as 12 nm, which is very close to the experimentally limited resolution (10 nm) of the LMS, strongly suggesting that the LMS we employ is itself a major noise source in the measurement.

Note that monitoring $\Delta\nu$ with high precision is an expensive task for practical SMI sensors. Instead, we need to exploit either $P_{\rm PD}$ or $V_{\rm LD}$ to gauge $\Delta\nu$. In order to obtain MDD below $\lambda/2$ without using ν, the highly linear nature of G is preferred so as to correlate $\Delta\nu$ to $\Delta V_{\rm LD}$. $\Delta V_{\rm LD}$ is also linearly changed as a function of $\Delta\varphi$ thereby leading to reduced RMSE (inset of Fig. 6.6) when the discontinuity remains at $\sim f_{ext}$, which allows us to safely predict $\Delta\nu$ by scaling $\Delta V_{\rm LD}$.

We have further verified that the changes in ν and in $V_{\rm LD}$ are highly correlated by programing the LMS to change its position randomly within the range 40-500 nm. We find that a correlation coefficient reaches to ~ 0.96 when the discontinuity stays at $\sim f_{ext}$ ($0.01 < \kappa < 0.02$ in Fig. 6.6). When unclear sawtooth (or nonlinear) of $\Delta\nu$ is observed at very weak κ (*i.e.*, $\kappa < 0.0005$ in Fig. 6.6), a correlation coefficient between $\Delta\nu$ and $\Delta V_{\rm LD}$ is reduced to ~ 0.88. The lower correlation at weaker κ, we suspect, is because ν and $V_{\rm LD}$

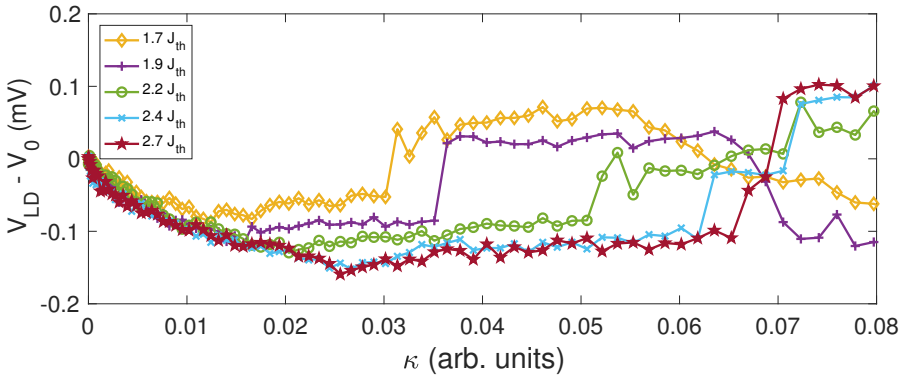

Figure 6.7: $V_{\mathrm{LD}} - V_0$ as a function of κ ($V_{\mathrm{LD}} = V_0$ when $\kappa = 0$). A certain range of $V_{\mathrm{LD}} - V_0 < 0$ is observed before jumping back to 0 for larger values of κ. Higher J leads to longer intervals of κ where $V_{\mathrm{LD}} - V_0 < 0$. $L = 30$ cm, and $J_{th} = 29.8$ mA.

tend to be susceptible to systematical noise including phase noise while sampling for them are independent of the time.

To check the validity of V_{LD} for MDD, as an example at $L = 30$, when ν and V_{LD} vary with ΔL, the slope dG/dL (*i.e.*, $d\nu/dL,\ dV_{\mathrm{LD}}/dL$) gives values of 1.2 MHz/nm and 0.25 μV/nm, respectively, which can be converted in $dV_{\mathrm{LD}}/d\nu \approx 0.2$ μV/MHz. After adding correlation coefficients earned at different κ to RMSE for ΔL_{min} in Eq. (6.8), we can derive the MDD by V_{LD}, enhanced close to MDD by ν when the discontinuity sticks around at $\sim f_{ext}$. This observation indicates that V_{LD} can be used to detect displacement on a par with ν at a certain range of κ. It is then necessary to see if there is a method to calibrate the optimal range of κ that can render enhanced MDD by V_{LD}. We can therefore only use V_{LD} for practical purposes.

Interestingly, we find that V_{LD} can also be utilized to search the optimal range κ. As shown in Fig. 6.7, when κ is increased (ΔL is not changed here), V_{LD} gradually decreases less than its value V_0 with $\kappa = 0$, and then V_{LD} remains less than V_0 before it exceeds V_0 for larger values of κ. This negatively shifted flat range of κ corresponds to where the discontinuity stays at $\sim f_{ext}$; For $1.7J_{th}$, $0.011 < \kappa < 0.03$, $1.9J_{th}$: $0.015 < \kappa < 0.035$, $2.2J_{th}$: $0.02 < \kappa < 0.05$, $2.4J_{th}$: $0.025 < \kappa < 0.062$, $2.7J_{th}$: $0.026 < \kappa < 0.066$, respectively, which renders the optimal resolution for nano-displacement sensing. Within

those optimal intervals of κ, the more initial periods of sawtooth are lost with the stronger κ. This plateau in V_{LD} tends to broaden with increasing J because stronger κ is required to render an ECSL unstable for the case of larger J [179]. When V_{LD} moves back to vicinity of V_0, the SMSR is significantly degraded to less than 25 dB, which indicates that several ECMs are actively involved in the ECSL dynamics . Therefore, it is difficult to maintain a periodic sawtooth behavior used for SMI.

What about the optimal external-cavity length L? In part, this will be determined by the displacements to be measured, but assuming that the displacements will be at most a few λ, what is critical is that f_{ext} does not become so small that more than one ECM contributes to the emission at feedback strengths required to keep the discontinuity of ν at $\sim f_{ext}$. Once more than one ECM begins to participate, the ECSL becomes more susceptible to noise and begins to exhibit complex dynamics related to undamped relaxation oscillations f_{RO}. To understand the role of this phenomenon on sensor performance, we vary L by 10 cm increments and find that when $L \geq 60$ cm, the ECSL tends to lose stability for SMI even with a very low κ, in turn resulting in low SMSR < 25 dB and frequent mode hopping among several ECMs. Therefore, combined with the observation that larger J enables sawtooth behavior for a broader range of κ, we suggest that sawtooth behavior in ν, and in turn in V_{LD}, for practical SMI sensors can be maintained when $J > 1.5J_{th}$ and $L < 60$ cm; however, the details will also depend on λ and other parameters of the LD.

Based on current understanding of ECSLs, we expect that there is more room to maintain stable operation for longer L and moderate κ when f_{RO}/f_{ext} is an integer for which the undamping f_{RO} is suppressed (*i.e.*, maintaining high SMSR) regardless of $\Delta\varphi$ [180, 181].

The question naturally arises: are the results presented above fortuitous, or can they be reproduced in SMI nanodisplacement sensors based on other LDs? We therefore conducted experiments using an ECSL based on a *packaged* DFB laser to monitor P_{PD} using the internal PD. The SMI signals were found to have no significant difference between P_{PD}

measured by the internal PD and V_{LD} due to our experimental limitation on the multimeter. Other authors have concluded that signals obtained by internal PDs have slightly better SNR than those from V_{LD} [56, 156, 157]. However, we do not observe the negative shifted behavior of P_{PD} with increasing κ unlike V_{LD} as shown in Fig. 6.7. Under conditions where P_{PD} and V_{LD} are affected by independent noise sources (multimeter noise, PD Shottky noise, and amplifier noise), V_{LD} can be used to calibrate optimal κ for SMI sensing when it is negatively shifted from V_0. Therefore, it seems reasonable to use V_{LD} when an internal PD is not available because V_{LD} provides a direct measurement and eliminates systematic noise due to optical-to-electrical conversion for P_{PD}.

6.5 Conclusion

We have experimentally investigated the dynamics of a single-mode semiconductor laser with weak and moderate optical feedback and found that the terminal voltage V_{LD} is well-suited to track nanoscale displacements when the laser frequency exhibits a saw-tooth behavior as a function of excess phase and frequency discontinuities as L with a period given by $\lambda/2$. Interestingly, we have found that the average frequency discontinuity is saturates at the external-cavity free-spectral range f_{ext} in the moderate feedback regime where the lowest MDD is found. Given the LD wavelength of 1550 nm, our quasi-static nanodisplacement sensor achieved the resolution of 12 nm, representing a MMD of $\lambda/130$. MDD far less than $\lambda/2$ distinguish SMI displacement sensors from conventional interferometric sensors and these impressive results are enabled by exploiting the nonlinear properties of ECSLs. Indeed, this MMD of 12 nm is likely due to limitations of our piezo-actuator (with a precision of 10 nm) and the multimeter used to make voltage measurements. We have also discovered that V_{LD} can be used to calibrate a proper feedback level for optical SMI sensing by setting V_{LD} negatively shifted from V_0, which is, however, not observed from I. Using V_{LD}, rather than ν or I, results in a simple and low-cost sensor with record values of MMD for an SMI nanodisplacement sensor. Given SMSR that helps to examine the stable

boundary for single mode operation of the ECSL, the external cavity should be within the range of few tens of centimeters.

CHAPTER 7
CONCLUSION

7.1 Summary of results

In this thesis, we presented experimental and numerical studies of the nonlinear dynamics of ECSLs subject to delayed feedback and especially focused on understanding of chaotic dynamics including intermittency of an ECSL. Furthermore, we explored optical feedback interferometry that uses the stability of an ECSL for imaging and measuring distance, displacement and velocity of a remote target.

The first part of thesis was to understand the nonlinear dynamics of SLs with time-delayed feedback. Despite the numerous studies of ECSLs, the detailed dynamics for ECSLs remain still as an open question. In order to analyze in detail, we applied state-of-the-art measurement methods to obtain information on nonlinear dynamics. We investigated several aspects of fundamental importance for dynamics of an ECSL using a tool from bifurcation theory. We mapped detailed BDs of ECSLs as function of a feedback strength η for various J and L, covering a significant portion of phase space. This offers perspectives for an ECSL with various operating parameters.

When an ECSL is operated at low injection current and subjected to feedback from a distant reflectors, we observe bifurcation cascades resulting from the destabilization of external-cavity modes (ECMs) that appear successively when the feedback is increased, and explain, with the LK model, how the cascades are influenced by various laser operating parameters. We experimentally observed a decrease in the number of stable regions with increasing J, which is consistent with the LK model. Indeed, at low J, the unstable regions correspond to the LFF regime, involving a drift toward the maximum gain mode (MGM), while at larger J, fully-developed CC occurs, with no drift toward the MGM.

On the other hand, when an ECSL is biased at relatively high injection current, we see a quasiperiodic route to chaos interrupted by several windows of periodicity when feedback strength is increased. Those windows of periodicity correspond to the transition between two limit cycles either on the same or neighboring ECMs. For larger feedback, the laser operates in a chaotic regime around numerous negatively shifted external-cavity modes. These experimental observations detail the bifurcations leading to fully developed CC in the ECSLs, and further provide detailed insight on the standard theoretical framework applied to these lasers.

When an ECSL is biased at relatively high injection current, we proposed a procedure that allows one to select experimentally different modes of the external cavity as different initial states. We use this procedure to reveal experimentally generalized multistability in an ECL through the demonstration that different routes to chaos exist in an ECL, depending on the initial state selected. In particular, we show that the well-known quasiperiodic route to chaos is only observed for specific choices of initial conditions.

We studied the LFF and fully developed CC regimes on the basis of extreme events (EEs). We found that while a significant number of EEs are observed when LFF is stable or intermittent, no EEs can be observed in fully developed CC. This difference is attributed to the specific dynamical behavior in the ECSL. In the LFF regime, the ECSL involves an abrupt dropout followed by irregular multi-ps pulses and some of which can be qualified as EEs. Indeed, according to the LK model, only a portion of the trajectories of an ECSL approaches the MGM that ends up being rejected along an unstable manifold, leading to a dropout and successively to EEs.

We observed the two types of intermittency on the route to CC. The first intermittent regime encountered corresponds to multistate intermittency involving two or three states composed of several combinations of periodic, quasiperiodic, and subharmonic dynamics. This multistate intermittent regime plays a mediating role in the transition between the periodic and period-doubled (PD) regimes. As L increases, subharmonics takes dominance

over PD, we suspect that a different route to chaos is achieved as PD is almost unobserved. Instead, intermittency between subharmonic and CC regimes is observed.

The second regime is observed for larger feedback levels and involves intermittency between PD and CC regimes. This type of intermittency displays statistical properties similar to those of on-off intermittency. Interestingly, on-off intermittency has two universal statistical properties. The distribution of laminar phases (stable PD) shows a 3/2 power-law scaling for short laminar phases and the mean duration of laminar phases versus a control parameter has an exponential decay with slope -1 on a logarithmic scale near the onset of intermittency. Investigation on the two types of intermittency highlights the complex nature of the intermittency phenomenon involved in the route to chaos, resulting from the high dimension and significant multistabiltiy of the dynamics of an external-cavity laser.

Also, we showed that the bifurcations between dynamical states in the nonlinear dynamics of an ECSL can be detected by its terminal voltage V_{LD}. Based on numerical results from the LK model, V_{LD} is associated with population-inversion carrier density N and provides information on the changes in the dynamical-state when the feedback level is varied, which is comparable with the more conventionally used optical output intensity. Hence, measuring the laser terminal voltage is another simple way to measure the feedback level in an ECSL instead of optical intensity.

Our work not only highlighted complexity of chaotic dynamics of ECSLs, but also demonstrated the high potential for applications when an ECSL is operated at a stable regime with a single-mode operation. We experimentally investigated the dynamics of a single-mode semiconductor laser with weak and moderate optical feedback and found that V_{LD} is well-suited to track excess phase and correspondingly variations of laser emission frequency. We directly measured the modulation of the laser emission frequency when the excess phase changes, which is in a good agreement with the LK model. We investigated the self-mixing effect in an external-cavity semiconductor laser and find the optimal working conditions for nano-displacement sensing. The variations of the emission frequency

and phase change are highly correlated at a certain range of feedback level, which leads to high resolution for displacement sensing such that we achieved 10 nm resolution for displacement sensing. We also show that terminal voltage of a laser not only can indicate the optimal feedback range but also can be an alternative to a photodiode for ultracompact and economical optical-feedback interferometry. High reliability for nano-displacement sensing is achieved when the external-cavity length is shorter than 60 cm with high injection current as stability of an external-cavity laser can be maintained with moderate optical feedback level.

7.2 Perspectives

We grounded our discussion in extensive theoretical studies based on the LK model and provided physical insights into the experimentally observed ECSL dynamics, which is a very important process in order to make ECSLs applicable for various scientific fields and industries. There are several perspectives for future work based on the results in thesis. Firstly, we observed several intermittencies on the route to CC and statistically analyzed them. Hence, it would be an interesting topic to search methods to control such intermittent behaviors in an ECSL and to predict intermittency before it occurs. Intermittency is one of chaotic behaviors and is slower than CC. With adjusting feedback strength, it would be possible to control the speed of those chaotic dynamics that can be used for random number generations. In addition, interest has grown recently in developing realizations of neural network systems in various fields, which allows one to develop algorithms that can be utilized for modeling complex patterns and prediction problems. Given the fact that nonlinearity in ECSL can be exploited in neural network systems, ECSLs have high potentials for a high-speed reservoir computing. Last but not least, LiDAR (Light Detection and Ranging [14]) has been widely investigated for state-of-the-art applications such as ranging finders for driverless cars and imaging sensors for 3D geographic mapping thanks to its high ranging and special resolutions. In general, LiDAR systems analyze the information

exhibited by the phase variations of a laser. Thus, understanding how phase shift of lasers affects characteristics of lasers is of great interest. As we discussed in chapter 6, V_{LD} can remove the necessity of extracting optical intensity from photodiodes. In the stable mode operations at a certain range of feedback level, V_{LD} is highly correlated with the variations of the emission frequency of a laser when feedback phase is varied. This correlation phenomenon observed in ECSLs allows easily converting measured information between V_{LD} and phase shift without using high computational power for post-processing. Hence, figuring out methods to maintain the optimal feedback range with V_{LD} remains promising for commercial self-mixing displacement sensors. Also, those displacement sensors would be compact and relatively cheaper to build and offer wide displacement sensing range from centi- to nano-meters without losing high precision.

REFERENCES

[1] H Haken, "Analogy between higher instabilities in fluids and lasers," *Phys. Lett. A*, vol. 53, no. 1, pp. 77 –78, 1975.

[2] N. M. Lawandy, "Instabilities in laser-pumped gas lasers: Experimental oscillation line shapes," *J. Opt. Soc. Am. B*, vol. 2, no. 1, pp. 108–111, 1985.

[3] R. Lang and K. Kobayashi, "External optical feedback effects on semiconductor injection laser properties," *IEEE Journal of Quantum Electronics*, vol. 16, no. 3, pp. 347–355, 1980.

[4] D. Brunner, X. Porte, M. C. Soriano, and I. Fischer, "Real-time frequency dynamics and high-resolution spectra of a semiconductor laser with delayed feedback," *Scientific reports*, vol. 2, 732 EP, 2012.

[5] C. Masoller and N. B. Abraham, "Stability and dynamical properties of the coexisting attractors of an external-cavity semiconductor laser," *Phys. Rev. A*, vol. 57, pp. 1313–1322, 2 1998.

[6] J. Mørk, J. Mark, and B. Tromborg, "Route to chaos and competition between relaxation oscillations for a semiconductor laser with optical feedback," *Phys. Rev. Lett.*, vol. 65, pp. 1999–2002, 16 1990.

[7] J. Ohtsubo, "Feedback induced instability and chaos in semiconductor lasers and their applications," *Optical Review*, vol. 6, no. 1, pp. 1–15, 1999.

[8] S. Wieczorek, B. Krauskopf, and D. Lenstra, "A unifying view of bifurcations in a semiconductor laser subject to optical injection," *Optics. Commun.*, vol. 172, no. 1, pp. 279 –295, 1999.

[9] H. F. Liu and W. F. Ngai, "Nonlinear dynamics of a directly modulated 1.55 um ingaasp distributed feedback semiconductor laser," *IEEE Journal of Quantum Electronics*, vol. 29, no. 6, pp. 1668–1675, 1993.

[10] W. E. E. Tilmann Heil Ingo Fischer, "Dynamics of dfb lasers subject to optical feedback: Stability properties of the stable modes," *Proc.SPIE*, vol. 3944, pp. 3944 –3944 –11, 2000.

[11] D. Rontani, M. Sciamanna, A. Locquet, and D. S. Citrin, "Multiplexed encryption using chaotic systems with multiple stochastic-delayed feedbacks," *Phys. Rev. E*, vol. 80, p. 066 209, 6 2009.

[12] A. Argyris, D. Syvridis, L. Larger, V. Annovazzi-Lodi, P. Colet, I. Fischer, J. García-Ojalvo, C. R. Mirasso, L. Pesquera, and K. A. Shore, "Chaos-based communications at high bit rates using commercial fibre-optic links," *Nature*, vol. 438, 343 EP, 2005.

[13] W. L. Zhang, W. Pan, B. Luo, X. H. Zou, M. Y. Wang, and Z. Zhou, "Chaos synchronization communication using extremely unsymmetrical bidirectional injections," *Opt. Lett.*, vol. 33, no. 3, pp. 237–239, 2008.

[14] F.-Y. Lin and J.-M. Liu, "Chaotic lidar," *IEEE J. Sel. Top. Quantum*, vol. 10, no. 5, pp. 991–997, 2004.

[15] C. Y. Chang, M. J. Wishon, D. Choi, J. Dong, K. Merghem, A. Ramdane, F. Lelarge, A. Martinez, A. Locquet, and D. S. Citrin, "Tunable x-band optoelectronic oscillators based on external-cavity semiconductor lasers," *IEEE Journal of Quantum Electronics*, vol. 53, no. 3, pp. 1–6, 2017.

[16] C. Y. Chang, D. Choi, A Locquet, M. J. Wishon, K Merghem, A. Ramdane, F. Lelarge, A Martinez, and D. S. Citrin, "A multi-ghz chaotic optoelectronic oscillator based on laser terminal voltage," *Appl. Phys. Lett.*, vol. 108, no. 19, pp. 191 109–5, 2016.

[17] M. C. Soriano, J. García-Ojalvo, C. R. Mirasso, and I. Fischer, "Complex photonics: Dynamics and applications of delay-coupled semiconductors lasers," *Rev. Mod. Phys.*, vol. 85, pp. 421–470, 1 2013.

[18] A. Uchida, K. Amano, M. Inoue, K. Hirano, S. Naito, H. Someya, I. Oowada, T. Kurashige, M. Shiki, S. Yoshimori, K. Yoshimura, and P. Davis, "Fast physical random bit generation with chaotic semiconductor lasers," *Nature Photon.*, vol. 2, 728 EP, 2008.

[19] D Rontani, D Choi, C. Y. Chang, A Locquet, and D. S. Citrin, "Compressive sensing with optical chaos," *Sci. Rep.*, vol. 6, pp. 1–7, Nov. 2016.

[20] Y Paquot, F Duport, A Smerieri, J Dambre, B Schrauwen, M Haelterman, and S Massar, "Optoelectronic reservoir computing," *Sci. Rep.*, vol. 2, 287 EP, Feb. 2012.

[21] L Appeltant, M. C. Soriano, G Van der Sande, J Danckaert, S Massar, J Dambre, B Schrauwen, C. R. Mirasso, and I Fischer, "Information processing using a single dynamical node as complex system," *Nature commun.*, vol. 2, 468 EP, 2011.

[22] T.-Y. Li and J. A. Yorke, "Period three implies chaos," *The American Mathematical Monthly*, vol. 82, no. 10, pp. 985–992, 1975.

[23] E. N. Lorenz, "Deterministic nonperiodic flow," *J. Atmos. Sci*, vol. 20, no. 2, pp. 130–141, 1963.

[24] H. Poincaré and R. Magini, "Les méthodes nouvelles de la mécanique céleste," *Il Nuovo Cimento (1895-1900)*, vol. 10, no. 1, pp. 128–130, 1899.

[25] D. Ruelle and F. Takens, "On the nature of turbulence," *Commun. Math. Phys.*, vol. 20, no. 3, pp. 167–192, 1971.

[26] M. J. Feigenbaum, "Quantitative universality for a class of nonlinear transformations," *J. Stat. Phys.*, vol. 19, no. 1, pp. 25–52, 1978.

[27] U. Frisch, P.-L. Sulem, and M. Nelkin, "A simple dynamical model of intermittent fully developed turbulence," *J. Fluid Mech.*, vol. 87, no. 04, pp. 719–736, 1978.

[28] R. Reategui, A. Kirỳanov, A. Pisarchik, Y. O. Barmenkov, and N. Ilìchev, "Experimental study and modeling of coexisting attractors and bifurcations in an erbium-doped fiber laser with diode-pump modulation," *Laser Phys*, vol. 14, no. 10, pp. 1277–1281, 2004.

[29] H. Poincaré, "Sur l'équilibre d'une masse fluide animée d'un mouvement de rotation," *Acta Math.*, vol. 7, no. 1, pp. 259–380, 1885.

[30] B. Krauskopf and D. Lenstra, "Fundamental issues of nonlinear laser dynamics.," in *AIP conference proceedings*, vol. 548, 2000.

[31] C. Bonatto, M. Feyereisen, S. Barland, M. Giudici, C. Masoller, J. R. R. Leite, and J. R. Tredicce, "Deterministic optical rogue waves," *Phys. Rev. Lett.*, vol. 107, no. 5, p. 053 901, 2011.

[32] S. Perrone, R. Vilaseca, J. Zamora-Munt, and C. Masoller, "Controlling the likelihood of rogue waves in an optically injected semiconductor laser via direct current modulation," *Phys. Rev. A*, vol. 89, p. 033 804, 3 2014.

[33] J. Zamora-Munt, B. Garbin, S. Barland, M. Giudici, J. R. R. Leite, C. Masoller, and J. R. Tredicce, "Rogue waves in optically injected lasers: Origin, predictability, and suppression," *Phys. Rev. A*, vol. 87, no. 3, p. 035 802, 2013.

[34] H. G. Schuster and W. Just, *Deterministic Chaos*, ser. An Introduction. John Wiley & Sons, Mar. 2006.

[35] S.-H. Gong and C.-M. Kim, "On-off intermittency in the threshold of a continuous-wave nd:yag laser," *J. Opt. Soc. Am. B*, vol. 18, no. 9, pp. 1285–1287, Sep. 2001.

[36] G. Huerta-Cuellar, A. N. Pisarchik, and Y. O. Barmenkov, "Experimental characterization of hopping dynamics in a multistable fiber laser," *Phys. Rev. E*, vol. 78, no. 3, p. 035 202, Sep. 2008.

[37] A. E. Hramov, A. A. Koronovskii, O. I. Moskalenko, M. O. Zhuravlev, R. Jaimes-Reategui, and A. N. Pisarchik, "Separation of coexisting dynamical regimes in multistate intermittency based on wavelet spectrum energies in an erbium-doped fiber laser," *Phys. Rev. E*, vol. 93, no. 5, pp. 052 218–8, May 2016.

[38] A. N. Pisarchik, R. Jaimes-Reátegui, R. Sevilla-Escoboza, G. Huerta-Cuellar, and M. Taki, "Rogue waves in a multistable system," *Phys. Rev. Lett.*, vol. 107, p. 274 101, 27 2011.

[39] A. N. Pisarchik, R. Jaimes-Reátegui, R. Sevilla-Escoboza, and G. Huerta-Cuellar, "Multistate intermittency and extreme pulses in a fiber laser," *Phys. Rev. E*, vol. 86, p. 056 219, 5 2012.

[40] D. Y. Tang, J Pujol, and C. O. Weiss, "Type-III intermittency of a laser," *Phys. Rev. A*, vol. 44, no. 1, R35–R38, Jul. 1991.

[41] D. Y. Tang, M. Y. Li, and C. O. Weiss, "Laser dynamics of type-I intermittency," *Phys. Rev. A*, vol. 46, no. 1, pp. 676–678, Jul. 1992.

[42] A. N. Pisarchik and V. J. Pinto-Robledo, "Experimental observation of two-state on-off intermittency.," *Phys. Rev. E*, vol. 66, no. 2 Pt 2, p. 027 203, Aug. 2002.

[43] S Osborne, A Amann, D Bitauld, and S O'Brien, "On-off intermittency in an optically injected semiconductor laser," *Phys. Rev. E*, vol. 85, no. 5, p. 056 204, May 2012.

[44] A. Campos-Mejía, A. N. Pisarchik, and D. A. Arroyo-Almanza, "Noise-induced on-off intermittency in mutually coupled semiconductor lasers," *Chaos Solitons Fract*, vol. 54, pp. 96–100, 2013.

[45] R. Kazarinov and R. Suris, "Heterodyne reception of light by an injection laser," *Sov. Phys. JETP*, vol. 66, pp. 1067–1078, 1974.

[46] Y. Mitsuhashi, J. Shimada, and S. Mitsutsuka, "Voltage change across the self-coupled semiconductor laser," *IEEE Journal of Quantum Electronics*, vol. 17, no. 7, pp. 1216–1225, 1981.

[47] E. Gagnon and J. F. Rivest, "Laser range imaging using the self-mixing effect in a laser diode," *IEEE Trans. Instrum. Meas.*, vol. 48, no. 3, pp. 693–699, 1999.

[48] E. Lacot, R. Day, J. Pinel, and F. Stoeckel, "Laser relaxation-oscillation frequency imaging," *Opt. Lett.*, vol. 26, no. 19, pp. 1483–1485, 2001.

[49] Y. L. Lim, M. Nikolic, K. Bertling, R. Kliese, and A. D. Rakić, "Self-mixing imaging sensor using a monolithic vcsel array with parallel readout," *Opt. Express*, vol. 17, no. 7, pp. 5517–5525, 2009.

[50] M. Norgia, G. Giuliani, and S. Donati, "New absolute distance measurement technique by self-mixing interferometry in closed loop," *Proc. 21st IEEE Instrum. Meas. Technol. Conf.*, vol. 1, pp. 216–221, 2004.

[51] L. Kervevan, H. Gilles, S. Girard, M. Laroche, and Y. Monfort, "Absolute distance measurement with heterodyne optical feedback on a yb:er glass laser," *Appl. Opt.*, vol. 45, no. 17, pp. 4084–4091, 2006.

[52] D. Guo and M. Wang, "Self-mixing interferometry based on a double-modulation technique for absolute distance measurement," *Appl. Opt.*, vol. 46, no. 9, pp. 1486–1491, 2007.

[53] Z. Duan, Y. Yu, B. Gao, and C. Jiang, "Absolute distance measurement based on multiple self-mixing interferometry," *Opt. Commun.*, vol. 389, pp. 270 –274, 2017.

[54] M. Norgia, G. Giuliani, and S. Donati, "Absolute distance measurement with improved accuracy using laser diode self-mixing interferometry in a closed loop," *IEEE Trans. Instrum. Meas.*, vol. 56, no. 5, pp. 1894–1900, 2007.

[55] D. Guo and M. Wang, "Self-mixing interferometer based on temporal-carrier phase-shifting technique for micro-displacement reconstruction," *Opt. Commun.*, vol. 263, no. 1, pp. 91 –97, 2006.

[56] Y. L. Lim, K Bertling, P. Rio, J. R. Tucker, and A. D. Rakic, "Displacement and distance measurement using the change in junction voltage across a laser diode due to the self-mixing effect," *Proc. SPIE*, vol. 6038, 60381O, 2006.

[57] U. Zabit, F. Bony, T. Bosch, and A. D. Rakic, "A self-mixing displacement sensor with fringe-loss compensation for harmonic vibrations," *IEEE Photon. Technol. Lett.*, vol. 22, no. 6, pp. 410–412, 2010.

[58] A. L. Arriaga, F. Bony, and T. Bosch, "Real-time algorithm for versatile displacement sensors based on self-mixing interferometry," *IEEE Sens. J*, vol. 16, no. 1, pp. 195–202, 2016.

[59] A. N. Lukashkin, M. E. Bashtanov, and I. J. Russell, "A self-mixing laser-diode interferometer for measuring basilar membrane vibrations without opening the cochlea," *J. Neurosci. Methods*, vol. 148, no. 2, pp. 122 –129, 2005.

[60] L. Scalise, Y. Yu, G. Giuliani, G. Plantier, and T. Bosch, "Self-mixing laser diode velocimetry: Application to vibration and velocity measurement," *IEEE Trans. Instrum. Meas.*, vol. 53, no. 1, pp. 223–232, 2004.

[61] L. Lv, H. Gui, T. Zhao, J. Xu, D. He, A. Wang, X. Chen, F. Li, H. Ming, and J. Xie, "Theoretical and numerical analysis of polarization properties used as doppler velocimetry in vertical-cavity surface-emitting lasers," *Proc. SPIE*, vol. 5644, 2005.

[62] B. Liu, Y. Yu, J. Xi, Q. Guo, J. Tong, and R. A. Lewis, "Displacement sensing using the relaxation oscillation frequency of a laser diode with optical feedback," *Appl. Opt.*, vol. 56, no. 24, pp. 6962–6966, 2017.

[63] J.-m. Liu, *Photonic devices*. Cambridge: Cambridge Univ. Press, 2005.

[64] F. Arecchi, G. Lippi, G. Puccioni, and J. Tredicce, "Deterministic chaos in laser with injected signal," *Opt. Commun*, vol. 51, no. 5, pp. 308 –314, 1984.

[65] E. Ott, *Chaos in dynamical systems*. Cambridge university press, 2002.

[66] G Agrawal, "Line narrowing in a single-mode injection laser due to external optical feedback," *IEEE J. Quantum Electron*, vol. 20, no. 5, pp. 468–471, 1984.

[67] T Heil, I Fischer, and W Elsäßer, "Stabilization of feedback-induced instabilities in semiconductor lasers," *J Opt B Quantum Semiclassical Opt.*, vol. 2, no. 3, p. 413, 2000.

[68] T. Paoli and J. Ripper, "Frequency stabilization and narrowing of optical pulses from cw gaas injection lasers," *IEEE J. Quantum Electron*, vol. 6, no. 6, pp. 335–339, 1970.

[69] R. Tkach and A. Chraplyvy, "Regimes of feedback effects in 1.5 um distributed feedback lasers," *J. Lightwave Technol.*, vol. 4, no. 11, pp. 1655–1661, 1986.

[70] B. Kim, A. Locquet, N. Li, D. Choi, and D. Citrin, "Bifurcation-cascade diagrams of an external-cavity semiconductor laser: Experiment and theory," *IEEE J. Quant. Electron.*, vol. 50, no. 12, pp. 965–972, 2014.

[71] T Heil, I Fischer, and W Elsäßer, "Coexistence of low-frequency fluctuations and stable emission on a single high-gain mode in semiconductor lasers with external optical feedback," *Phys. Rev. A*, vol. 58, no. 4, R2672–R2675, Oct. 1998.

[72] J. Sacher, W. Elsäßer, and E. O. Göbel, "Intermittency in the coherence collapse of a semiconductor laser with external feedback," *Phys. Rev. Lett.*, vol. 63, no. 20, p. 2224, 1989.

[73] B Tromborg and J Mork, "Stability analysis and the route to chaos for laser diodes with optical feedback," *IEEE Photon. Technol. Lett.*, vol. 2, no. 8, pp. 549–552, 1990.

[74] J. Ohtsubo, *Semiconductor Lasers: Stability, Instability and Chaos; 2nd ed.* Ser. Springer Series in Optical Sciences. Berlin: Springer, 2008.

[75] D. M. Kane and K. A. Shore, *Unlocking Dynamical Diversity: Optical Feedback Effects on Semiconductor Lasers*. Chichester: Wiley, 2005.

[76] A. Hohl and A. Gavrielides, "Bifurcation cascade in a semiconductor laser subject to optical feedback," *Phys. Rev. Lett.*, vol. 82, pp. 1148–1151, 6 1999.

[77] D. Brunner, X. Porte, M. C. Soriano, and I. Fischer, "Real-time frequency dynamics and high-resolution spectra of a semiconductor laser with delayed feedback," *Scientific reports*, vol. 2, no. 1, p. 1198, 2012.

[78] S. Wieczorek and W. W. Chow, "Bifurcations and chaos in a semiconductor laser with coherent or noisy optical injection," *Opt. Commun.*, vol. 282, no. 12, pp. 2367 –2379, 2009.

[79] K. Green, B. Krauskopf, F. Marten, and D. Lenstra, "Bifurcation analysis of a spatially extended laser with optical feedback," *SIAM J. Appl. Dyn. Syst.*, vol. 8, no. 1, pp. 222–252, 2009.

[80] I. V. Ermakov, G. V. der Sande, and J. Danckaert, "Semiconductor ring laser subject to delayed optical feedback: Bifurcations and stability," *Commun. Nonlinear Sci. Numer. Simul.*, vol. 17, no. 12, pp. 4767 –4779, 2012.

[81] J. Mork, B. Tromborg, and J. Mark, "Chaos in semiconductor lasers with optical feedback: Theory and experiment," *IEEE Journal of Quantum Electronics*, vol. 28, no. 1, pp. 93–108, 1992.

[82] J. Ye, H. Li, and J. G. McInerney, "Period-doubling route to chaos in a semiconductor laser with weak optical feedback," *Phys. Rev. A*, vol. 47, pp. 2249–2252, 3 1993.

[83] A. N. Pisarchik, Y. O. Barmenkov, and A. V. Kir'yanov, "Experimental characterization of the bifurcation structure in an erbium-doped fiber laser with pump modulation," *IEEE Journal of Quantum Electronics*, vol. 39, no. 12, pp. 1567–1571, 2003.

[84] D. Arroyo-Almanza, A. Pisarchik, I. Fischer, C. Mirasso, and M. Soriano, "Spectral properties and synchronization scenarios of two mutually delay-coupled semiconductor lasers," *Optics Communications*, vol. 301-302, pp. 67 –73, 2013.

[85] S. Valling, B. Krauskopf, T. Fordell, and . Lindberg, "Experimental bifurcation diagram of a solid state laser with optical injection," *Opt. Commun.*, vol. 271, no. 2, pp. 532 –542, 2007.

[86] F. T. Arecchi, R. Meucci, G. Puccioni, and J. Tredicce, "Experimental evidence of subharmonic bifurcations, multistability, and turbulence in a q-switched gas laser," *Phys. Rev. Lett.*, vol. 49, pp. 1217–1220, 17 1982.

[87] T. Midavaine, D. Dangoisse, and P. Glorieux, "Observation of chaos in a frequency-modulated CO_2 laser," *Phys. Rev. Lett.*, vol. 55, pp. 1989–1992, 19 1985.

[88] S. Wieczorek, B. Krauskopf, T. Simpson, and D. Lenstra, "The dynamical complexity of optically injected semiconductor lasers," *Phys. Rep.*, vol. 416, no. 1, pp. 1 – 128, 2005.

[89] T. Simpson, "Mapping the nonlinear dynamics of a distributed feedback semiconductor laser subject to external optical injection," *Opt. Commun.*, vol. 215, no. 1, pp. 135 –151, 2003.

[90] B. Kim, N. Li, A Locquet, and D. Citrin, "Experimental bifurcation-cascade diagram of an external-cavity semiconductor laser," *Opt. Express*, vol. 22, no. 3, pp. 2348–2357, 2014.

[91] F. R. Ruiz-Oliveras and A. N. Pisarchik, "Phase-locking phenomenon in a semiconductor laser with external cavities," *Opt. Express*, vol. 14, no. 26, pp. 12 859–12 867, 2006.

[92] W. Ray, W.-S. Lam, P. N. Guzdar, and R. Roy, "Observation of chaotic itinerancy in the light and carrier dynamics of a semiconductor laser with optical feedback," *Phys. Rev. E*, vol. 73, p. 026 219, 2 2006.

[93] A. A. Sahai, B. Kim, D. Choi, A. Locquet, and D. S. Citrin, "Mapping the nonlinear dynamics of a laser diode via its terminal voltage," *Opt. Lett.*, vol. 39, no. 19, pp. 5630–5633, 2014.

[94] A. Ritter and H. Haug, "Theory of the bistable limit cycle behavior of laser diodes induced by weak optical feedback," *IEEE Journal of Quantum Electronics*, vol. 29, no. 4, pp. 1064–1070, 1993.

[95] D. Pieroux, T. Erneux, T. Luzyanina, and K. Engelborghs, "Interacting pairs of periodic solutions lead to tori in lasers subject to delayed feedback," *Phys. Rev. E*, vol. 63, p. 036 211, 3 2001.

[96] A. Prasad, Y.-C. Lai, A. Gavrielides, and V. Kovanis, "Complicated basins in external-cavity semiconductor lasers," *Phys. Lett. A*, vol. 314, no. 1, pp. 44 –50, 2003.

[97] D. Brunner, M. C. Soriano, X. Porte, and I. Fischer, "Experimental phase-space tomography of semiconductor laser dynamics," *Phys. Rev. Lett.*, vol. 115, p. 053 901, 5 2015.

[98] E. Eschenazi, H. G. Solari, and R. Gilmore, "Basins of attraction in driven dynamical systems," *Phys. Rev. A*, vol. 39, pp. 2609–2627, 5 1989.

[99] J. M. Saucedo-Solorio, A. N. Pisarchik, A. V. Kir'yanov, and V. Aboites, "Generalized multistability in a fiber laser with modulated losses," *J. Opt. Soc. Am. B*, vol. 20, no. 3, pp. 490–496, 2003.

[100] F. T. Arecchi, G. Giacomelli, A. Lapucci, and R. Meucci, "Dynamics of a CO_2 laser with delayed feedback: The short-delay regime," *Phys. Rev. A*, vol. 43, pp. 4997–5004, 9 1991.

[101] A. P. A. Fischer, O. K. Andersen, M. Yousefi, S. Stolte, and D. Lenstra, "Experimental and theoretical study of filtered optical feedback in a semiconductor laser," *IEEE Journal of Quantum Electronics*, vol. 36, no. 3, pp. 375–384, 2000.

[102] C. Masoller, "Coexistence of attractors in a laser diode with optical feedback from a large external cavity," *Phys. Rev. A*, vol. 50, pp. 2569–2578, 3 1994.

[103] E. Pelinovsky and C. Kharif, *Extreme ocean waves*. Springer Science & Business Media, 2008.

[104] K. Dysthe, H. E. Krogstad, and P. Müller, "Oceanic rogue waves," *Annu. Rev. Fluid Mech.*, vol. 40, pp. 287–310, 2008.

[105] D. Sornette, *Why stock markets crash: Critical events in complex financial systems*. Princeton University Press, 2009.

[106] M. Beniston and D. B. Stephenson, "Extreme climatic events and their evolution under changing climatic conditions," *Glob. Planet. Change*, vol. 44, no. 1-4, pp. 1–9, 2004.

[107] A. Ganshin, V. Efimov, G. Kolmakov, L. Mezhov-Deglin, and P. V. McClintock, "Observation of an inverse energy cascade in developed acoustic turbulence in superfluid helium," *Phys. Rev. Lett.*, vol. 101, no. 6, p. 065 303, 2008.

[108] M. G. Kovalsky, A. A. Hnilo, and J. R. Tredicce, "Extreme events in the ti: Sapphire laser," *Opt. Lett.*, vol. 36, no. 22, pp. 4449–4451, 2011.

[109] A. Karsaklian Dal Bosco, D. Wolfersberger, and M. Sciamanna, "Extreme events in time-delayed nonlinear optics," *Opt. Lett.*, vol. 38, no. 5, pp. 703–705, 2013.

[110] J. A. Reinoso, J. Zamora-Munt, and C. Masoller, "Extreme intensity pulses in a semiconductor laser with a short external cavity," *Phys. Rev. E*, vol. 87, no. 6, p. 062 913, 2013.

[111] D. V. Churkin, O. A. Gorbunov, and S. V. Smirnov, "Extreme value statistics in raman fiber lasers," *Opt. Lett.*, vol. 36, no. 18, pp. 3617–3619, 2011.

[112] A Montina, U Bortolozzo, S Residori, and F. Arecchi, "Non-gaussian statistics and extreme waves in a nonlinear optical cavity," *Phys. Rev. Lett.*, vol. 103, no. 17, p. 173 901, 2009.

[113] D. Solli, C Ropers, P Koonath, and B Jalali, "Optical rogue waves," *Nature*, vol. 450, no. 7172, pp. 1054–1057, 2007.

[114] É. Mercier, A. Even, E. Mirisola, D. Wolfersberger, and M. Sciamanna, "Numerical study of extreme events in a laser diode with phase-conjugate optical feedback," *Phys. Rev. E*, vol. 91, no. 4, p. 042 914, 2015.

[115] S. Randoux and P. Suret, "Experimental evidence of extreme value statistics in raman fiber lasers," *Opt. Lett.*, vol. 37, no. 4, pp. 500–502, 2012.

[116] T. Heil, I. Fischer, W. Elsäßer, B. Krauskopf, K. Green, and A. Gavrielides, "Delay dynamics of semiconductor lasers with short external cavities: Bifurcation scenarios and mechanisms," *Phys. Rev. E*, vol. 67, p. 066 214, 6 2003.

[117] I. Fischer, G. H. M. van Tartwijk, A. M. Levine, W. Elsässer, E. Göbel, and D. Lenstra, "Fast pulsing and chaotic itinerancy with a drift in the coherence collapse of semiconductor lasers," *Phys. Rev. Lett.*, vol. 76, pp. 220–223, 2 1996.

[118] G. Van Tartwijk, A. Levine, and D. Lenstra, "Sisyphus effect in semiconductor lasers with optical feedback," *IEEE J. Sel. Top. Quantum*, vol. 1, no. 2, pp. 466–472, 1995.

[119] A Hohl, H. J. van der Linden, and R Roy, "Determinism and stochasticity of power-dropout events in semiconductor lasers with optical feedback.," *Opt. Lett*, vol. 20, no. 23, p. 2396, Dec. 1995.

[120] S. Residori, U. Bortolozzo, A. Montina, F. Lenzini, and F. T. Arecchi, "Rogue waves in spatially extended optical systems," *Fluct. Noise Lett.*, vol. 11, no. 01, p. 1 240 014, 2012.

[121] Y. Pomeau and P. Manneville, "Intermittent transition to turbulence in dissipative dynamical systems," *Commun. Math. Phys.*, vol. 74, no. 2, pp. 189–197, 1980.

[122] C Grebogi, E Ott, F Romeiras, and J. A. Yorke, "Critical exponents for crisis-induced intermittency," *Phys. Rev. A*, vol. 36, no. 11, pp. 5365–5380, 1987.

[123] B. K. Goswami, "Control of multistate hopping intermittency," *Phys. Rev. E*, vol. 78, p. 066 208, 6 2008.

[124] S. Kraut and U. Feudel, "Multistability, noise, and attractor hopping: the crucial role of chaotic saddles," *Phys. Rev. E*, vol. 66, no. 1, pp. 015 207–4, Jul. 2002.

[125] N Platt, E. A. Spiegel, and C Tresser, "On-off intermittency: a mechanism for bursting," *Phys. Rev. Lett.*, vol. 70, no. 3, pp. 279–282, Jan. 1993.

[126] J. F. Heagy, N. Platt, and S. M. Hammel, "Characterization of on-off intermittency," *Phys. Rev. E*, vol. 49, pp. 1140–1150, 2 1994.

[127] N. Platt, S. M. Hammel, and J. F. Heagy, "Effects of additive noise on on-off intermittency," *Phys. Rev. Lett.*, vol. 72, no. 22, pp. 3498–3501, 1994.

[128] P. W. Hammer, N. Platt, S. M. Hammel, J. F. Heagy, and B. D. Lee, "Experimental observation of on-off intermittency," *Phys. Rev. Lett.*, vol. 73, no. 8, pp. 1095–1098, Aug. 1994.

[129] D. L. Feng, C. X. Yu, J. L. Xie, and W. X. Ding, "On-off intermittencies in gas discharge plasma," *Phys. Rev. E*, vol. 58, pp. 3678–3685, 3 1998.

[130] A. Vella, A. Setaro, B. Piccirillo, and E. Santamato, "On-off intermittency in chaotic rotation induced in liquid crystals by competition between spin and orbital angular momentum of light," *Phys. Rev. E*, vol. 67, p. 051 704, 5 2003.

[131] F. Rödelsperger, A. Čenys, and H. Benner, "On-off intermittency in spin-wave instabilities," *Phys. Rev. Lett.*, vol. 75, pp. 2594–2597, 13 1995.

[132] R. Delage, Y. Takayama, and T. Biwa, "On–off intermittency in coupled chaotic thermoacoustic oscillations," *Chaos*, vol. 27, no. 4, p. 043 111, 2017.

[133] M. Bottiglieri and C. Godano, "On-off intermittency in earthquake occurrence," *Phys. Rev. E*, vol. 75, p. 026 101, 2 2007.

[134] A. Hramov, A. A. Koronovskii, I. S. Midzyanovskaya, E. Sitnikova, and C. M. van Rijn, "On-off intermittency in time series of spontaneous paroxysmal activity in rats with genetic absence epilepsy," *Chaos*, vol. 16, no. 4, p. 043 111, 2006.

[135] A. A. Koronovskii, A. E. Hramov, V. V. Grubov, O. I. Moskalenko, E. Sitnikova, and A. N. Pavlov, "Coexistence of intermittencies in the neuronal network of the epileptic brain," *Phys. Rev. E*, vol. 93, p. 032 220, Mar. 2016.

[136] J. L. Cabrera and J. G. Milton, "On-off intermittency in a human balancing task," *Phys. Rev. Lett.*, vol. 89, p. 158 702, 15 2002.

[137] E. Sitnikova, A. E. Hramov, V. V. Grubov, A. A. Ovchinnkov, and A. A. Koronovsky, "On-off intermittency of thalamo-cortical oscillations in the electroencephalogram of rats with genetic predisposition to absence epilepsy," *Brain Res.*, vol. 1436, no. Supplement C, pp. 147 –156, 2012.

[138] T. Heil, I. Fischer, W. Elsäßer, J. Mulet, and C. R. Mirasso, "Statistical properties of low-frequency fluctuations during single-mode operation in distributed-feedback lasers: Experiments and modeling," *Opt. Lett.*, vol. 24, no. 18, pp. 1275–1277, 1999.

[139] D. W. Sukow, J. R. Gardner, and D. J. Gauthier, "Statistics of power-dropout events in semiconductor lasers with time-delayed optical feedback," *Phys. Rev. A*, vol. 56, no. 5, R3370–R3373, Nov. 1997.

[140] D. Choi, M. J. Wishon, J Barnoud, C. Y. Chang, Y Bouazizi, A Locquet, and D. S. Citrin, "Low-frequency fluctuations in an external-cavity laser leading to extreme events," *Phys. Rev. E*, vol. 93, no. 4, p. 042 216, Apr. 2016.

[141] A. Locquet, B. Kim, D. Choi, N. Li, and D. S. Citrin, "Initial-state dependence of the route to chaos of an external-cavity laser," *Phys. Rev. A*, vol. 95, p. 023 801, 2 2017.

[142] A. K. D. Bosco, Y. Akizawa, K. Kanno, A. Uchida, T. Harayama, and K. Yoshimura, "Photonic integrated circuits unveil crisis-induced intermittency," *Opt. Express*, vol. 24, no. 19, pp. 22 198–22 209, 2016.

[143] A. K. D. Bosco, N. Sato, Y. Terashima, S. Ohara, A. Uchida, T. Harayama, and M. Inubushi, "Random number generation from intermittent optical chaos," *IEEE J. Sel. Top. Quantum Electron.*, vol. 23, no. 6, pp. 1–8, 2017.

[144] B. Kim, A. Locquet, D. Choi, and D. S. Citrin, "Experimental route to chaos of an external-cavity semiconductor laser," *Phys. Rev. A*, vol. 91, p. 061 802, 6 2015.

[145] Y. H. Kao, N. M. Wang, and H. M. Chen, "Mode description of routes to chaos in external-cavity coupled semiconductor lasers," *IEEE J. Quant. Electron*, vol. 30, no. 8, pp. 1732–1739, 1994.

[146] G.-S. Yim, Y.-J. Park, C.-M. Kim, and Y.-S. Kim, "Transition from laser-off to laser-on through on–off intermittency in a gain-modulated CO_2 laser," *J. Opt. Soc. Am. B*, vol. 21, no. 12, pp. 2112–2116, 2004.

[147] P. W. Hammer, N. Platt, S. M. Hammel, J. F. Heagy, and B. D. Lee, "Experimental observation of on-off intermittency," *Phys. Rev. Lett.*, vol. 73, no. 8, pp. 1095–1098, Aug. 1994.

[148] A. M. Levine, G. H. M. van Tartwijk, D. Lenstra, and T. Erneux, "Diode lasers with optical feedback: Stability of the maximum gain mode," *Phys. Rev. A*, vol. 52, R3436–R3439, 5 1995.

[149] M. J. Wishon, A. Locquet, C. Y. Chang, D. Choi, and D. S. Citrin, "Crisis route to chaos in semiconductor lasers subjected to external optical feedback," *Phys. Rev. A*, vol. 97, p. 033 849, 3 2018.

[150] H. Hansen, K. Carneiro, H. Haitjema, and L. D. Chiffre, "Dimensional micro and nano metrology," *CIRP Annals*, vol. 55, no. 2, pp. 721 –743, 2006.

[151] A. J. Fleming, "A review of nanometer resolution position sensors: Operation and performance," *Sensors and Actuators A: Physical*, vol. 190, pp. 106 –126, 2013.

[152] D. J. Bell, T. J. Lu, N. A. Fleck, and S. M. Spearing, "Mems actuators and sensors: Observations on their performance and selection for purpose," *Journal of Micromechanics and Microengineering*, vol. 15, no. 7, S153, 2005.

[153] M. A. Haque and M. T. A. Saif, "A review of mems-based microscale and nanoscale tensile and bending testing," *Experimental Mechanics*, vol. 43, no. 3, pp. 248–255, 2003.

[154] K. Petermann, *Laser diode modulation and noise*. Springer Science & Business Media, 2012, vol. 3.

[155] G. Giuliani, M. Norgia, S. Donati, and T. Bosch, "Laser diode self-mixing technique for sensing applications," *J. Opt*, vol. 4, no. 6, S283, 2002.

[156] J. Perchoux, H. E. Dougan, F. Bony, and A. D. Rakic, "Photodiode-free doppler velocimeter based on self-mixing effect in commercial vcsels," *2008 IEEE Sensors*, pp. 290–293, 2008.

[157] S. Donati, "Responsivity and noise of self-mixing photodetection schemes," *IEEE J. Quantum Electron.*, vol. 47, no. 11, pp. 1428–1433, 2011.

[158] L. Goldberg, H. F. Taylor, A. Dandridge, J. F. Weller, and R. O. Miles, "Spectral characteristics of semiconductor lasers with optical feedback," *IEEE Transactions on Microwave Theory and Techniques*, vol. 30, no. 4, pp. 401–410, 1982.

[159] S. Zhang, Y. Tan, Z. Ren, Y. Zhang, and S. Zhang, "A microchip laser feedback interferometer with nanometer resolution and increased measurement speed based on phase meter," *Appl. Phys. B*, vol. 116, no. 3, pp. 609–616, 2014.

[160] R. C. Addy, A. W. Palmer, K. Thomas, and V. Grattan, "Effects of external reflector alignment in sensing applications of optical feedback in laser diodes," *J. Light. Technol.*, vol. 14, no. 12, pp. 2672–2676, 1996.

[161] T. Yoshino, M. Nara, S. Mnatzakanian, B. S. Lee, and T. C. Strand, "Laser diode feedback interferometer for stabilization and displacement measurements," *Appl. Opt.*, vol. 26, no. 5, pp. 892–897, 1987.

[162] D. Guo, M. Wang, and H. Hao, "Displacement measurement using a laser feedback grating interferometer," *Appl. Opt.*, vol. 54, no. 31, pp. 9320–9325, 2015.

[163] M. Wang and G. Lai, "Displacement measurement based on fourier transform method with external laser cavity modulation," *Rev. Sci. Instrum.*, vol. 72, no. 8, pp. 3440–3445, 2001.

[164] N. Servagent, T. Bosch, and M. Lescure, "Design of a phase-shifting optical feedback interferometer using an electrooptic modulator," *IEEE J. Sel. Top. Quantum*, vol. 6, no. 5, pp. 798–802, 2000.

[165] N. Servagent, F. Gouaux, and T. Bosch, "Measurements of displacement using the self-mixing interference in a laser diode," *J. Opt.*, vol. 29, no. 3, p. 168, 1998.

[166] C. Bes, G. Plantier, and T. Bosch, "Displacement measurements using a self-mixing laser diode under moderate feedback," *IEEE Trans Instrum Meas*, vol. 55, no. 4, pp. 1101–1105, 2006.

[167] D. Choi, M. J. Wishon, C. Y. Chang, D. S. Citrin, and A. Locquet, "Multistate intermittency on the route to chaos of a semiconductor laser subjected to optical feedback from a long external cavity," *Chaos*, vol. 28, no. 1, p. 011 102, 2018.

[168] P. Dean, Y. L. Lim, A. Valavanis, R. Kliese, M. Nikolić, S. P. Khanna, M. Lachab, D. Indjin, Z. Ikonić, P. Harrison, A. D. Rakić, E. H. Linfield, and A. G. Davies, "Terahertz imaging through self-mixing in a quantum cascade laser," *Opt. Lett.*, vol. 36, no. 13, pp. 2587–2589, 2011.

[169] S. Donati and M. Norgia, "Self-mixing interferometry for biomedical signals sensing," *IEEE J. Sel. Top. Quantum Electron.*, vol. 20, no. 2, pp. 104–111, 2014.

[170] S. Donati, G. Giuliani, and S. Merlo, "Laser diode feedback interferometer for measurement of displacements without ambiguity," *IEEE J. Quantum Electron.*, vol. 31, no. 1, pp. 113–119, 1995.

[171] L. Xu, S. Zhang, Y. Tan, and L. Sun, "Simultaneous measurement of refractive-index and thickness for optical materials by laser feedback interferometry," *Rev. Sci. Instrum.*, vol. 85, no. 8, p. 083 111, 2014.

[172] M Norgia, A Pesatori, and L Rovati, "Self-mixing laser doppler spectra of extra-corporeal blood flow: a theoretical and experimental study," *IEEE Sens. J*, vol. 12, no. 3, pp. 552–557, Jan. 2012.

[173] M. H. Koelink, F. F. M. de Mul, A. L. Weijers, J. Greve, R. Graaff, A. C. M. Dassel, and J. G. Aarnoudse, "Fiber-coupled self-mixing diode-laser doppler velocimeter: Technical aspects and flow velocity profile disturbances in water and blood flows," *Appl. Opt.*, vol. 33, no. 24, pp. 5628–5641, 1994.

[174] J. Keeley, J. Freeman, K. Bertling, Y. L. Lim, R. A. Mohandas, T. Taimre, L. H. Li, A. D. R. Indjin Dragan and, E. H. Linfield, A. G. Davies, and P. Dean, "Measurement of the emission spectrum of a semiconductor laser using laser-feedback interferometry," *Sci. Rep.*, pp. 1–9, Jul. 2017.

[175] W. M. Wang, K. T. V. Grattan, A. W. Palmer, and W. J. O. Boyle, "Self-mixing interference inside a single-mode diode laser for optical sensing applications," *Journal of Lightwave Technology*, vol. 12, no. 9, pp. 1577–1587, 1994.

[176] R. Kliese, T. Taimre, A. A. A. Bakar, Y. L. Lim, K. Bertling, M. Nikolić, J. Perchoux, T. Bosch, and A. D. Rakić, "Solving self-mixing equations for arbitrary feedback levels: A concise algorithm," *Appl. Opt.*, vol. 53, no. 17, pp. 3723–3736, 2014.

[177] B. Kim, A. Locquet, D. Choi, and D. S. Citrin, "Experimental route to chaos of an external-cavity semiconductor laser," *Phys. Rev. A*, vol. 91, p. 061 802, 6 2015.

[178] D. Lenstra, M. V. Vaalen, and B. Jaskorzyska, "On the theory of a single-mode laser with weak optical feedback," *Physica B+C*, vol. 125, no. 2, pp. 255 –264, 1984.

[179] Y. Fan, Y. Yu, J. Xi, and Q. Guo, "Stability limit of a semiconductor laser with optical feedback," *IEEE J. Quantum Electron.*, vol. 51, no. 2, pp. 1–9, 2015.

[180] D. Lenstra, "Relaxation oscillation dynamics in semiconductor diode lasers with optical feedback," *IEEE Photon. Technol. Lett.*, vol. 25, no. 6, pp. 591–593, 2013.

[181] D D'Agostino, H. P. M. M. Ambrosius, M. K. Smit, and D Lenstra, "Integrated laser with optical feedback shows suppressed relaxation-oscillation dynamics," *IEEE Photon. Technol. Lett.*, vol. 27, no. 21, pp. 2292–2295, 2015.

VITA: Daeyoung Choi

CONTACT INFORMATION
Georgia Tech Lorraine
Rue 2 Marconi, Metz, France 57070
(+33) 6 87 87 21 68
daeyoung@gatech.edu

EDUCATION

Georgia Institute of Technology, Atlanta, GA

Ph.D. in Electrical & Computer Engineering,

- Research interests: Nonlinear laser dynamics, intermittency, laser-feedback interferometry.
- Expected graduation: Summer 2018

Chonbuk National University (CBNU), Jeonju, South Korea

B.S. in Electrical Engineering, 02/2011

RESEARCH EXPERIENCE

Graduate Research Assistant 01/2014 to present

Georgia Institute of Technology

• Build experimental setups for highly-stabilized free-space/fiber laser systems.
• Study nonlinear dynamics of laser diodes (time-series analysis, bifurcation, intermittency, chaos complexity.
• Apply external-cavity lasers for applications (ranging detection, interferometry, random number generation, reservoir computing.

PUBLICATIONS

1. Michael J. Wishon, A. Locquet, C. Y. Chang, **Daeyoung Choi**, and D. S. Citrin. "Crisis route to chaos in semiconductor lasers subjected to external optical feedback", Physical Review A 97, 033849 (2018).

2. **Daeyoung Choi**, Michael J. Wishon, C. Y. Chang, D. S. Citrin, and A. Locquet. "Multistate intermittency on the route to chaos of a semiconductor laser subjected to optical feedback from a long external cavity", Chaos 28, 011102 (2018).

3. Chien-Yuan Chang, Michael J. Wishon, **Daeyoung Choi**, Junliang Dong, Kamel Merghem, Abderrahim Ramdane, Franois Lelarge, Anthony Martinez, Alexandre Locquet, and D. S. Citrin. "Tunable X Band Optoelectronic Oscill-ators Based on External-Cavity Semiconductor Lasers", IEEE Journal of Quan-tum Electronics, Vol 53, Issue 3, June (2017).

4. Michael J. Wishon, A. Locquet, Guillaume Mourozeau, **Daeyoung Choi**, Sreejith K.R., Aakash Sahai, and David Citrin. "Reading bits on a CD-ROM without a photodiode", IET Optoelectronics, Vol 11, Issue 5, October (2017).

5. A. Locquet, Byungchil Kim, **Daeyoung Choi**, Nianqiang Li, and D. S. Citrin. "Initial-state dependence of the route to chaos of an external-cavity laser", Physical Review A 95, 023801 (2017).

6. D. Rontani, **Daeyoung Choi**, C. Y. Chang, A. Locquet and D. S. Citrin. "Compressive Sensing with Optical Chaos", Scientific Reports,Vol 6, 35206 (2016).

7. **Daeyoung Choi**, Michael J. Wishon, J. Barnoud, C. Y. Chang, Y. Bouazizi, A. Locquet, and D. S. Citrin."Low-frequency fluctuations in an external-cavity laser leading to extreme events", Physical Review E 93, 042216 (2016).

8. C. Y. Chang, **Daeyoung Choi**, A. Locquet, Michael J. Wishon, K. Merghem, Abderrahim Ramdane, Franois Lelarge, A. Martinez, and D. S. Citrin. "A multi-GHz chaotic optoelectronic oscillator based on laser terminal voltage", Applied Physics Letters 108, 191109 (2016).

9. Byungchil Kim, A. Locquet, **Daeyoung Choi**, and D. S. Citrin. "Experimental route to chaos of an external-cavity semiconductor laser" Physical Review A 91, 061802 (2015).

10. Nianqiang Li, Zunino, A. Locquet, Byungchil Kim, **Daeyoung Choi**, Wei Pan, and D. S. Citrin. "Multiscale Ordinal Symbolic Analysis of the Lang Kobayashi Model for External-Cavity Semiconductor Lasers: A Test of Theory", IEEE Journal of Quantum Electronics, Vol. 51, Issue. 8 (2015).

11. Byungchil Kim, A. Locquet, Nianqiang Li, **Daeyoung Choi**, and D. S. Citrin, "Bifurcation-Cascade Diagrams of an External-Cavity Semiconductor Laser: Experiment and Theory", IEEE Journal of Quantum Electronics, Vol. 50, No. 12, Dec (2014).

12. A. A. Sahai, Byungchil Kim, **Daeyoung Choi**, A. Locquet, and D. S. Citrin. "Mapping the nonlinear dynamics of a laser diode via its terminal voltage", Optics Letters, Vol. 39, No. 19, Oct (2014).

13. Nianqiang Li, Byungchil Kim, A. Locquet, **Daeyoung Choi**, Wei Pan, and D. S. Citrin. "Statistics of the optical intensity of a chaotic external-cavity DFB laser", Optics Letters, Vol. 39, No. 20 Oct (2014).

14. Nianqiang Li, Byungchil Kim, **Daeyoung Choi**, V. N. Chizhevsky, A. Locquet, M. Bloch, D. S. Citrin, and Wei Pan "Fast random bit generation with a single chaotic laser subjected to optical feedback", Proc. SPIE 9134, Semiconductor Lasers and Laser Dynamics VI, 913427, May (2014).

Conference presentations

1. Daeyoung Choi, M. Wishon, A. Locquet, and D. S. Citrin. "Intermittency on the route to chaos of an external cavity semiconductor laser", International Symposium on Physics and Applications of Laser Dynamics (Paris, France, 15 Nov, 2017).

2. Daeyoung Choi, M. Wishon, D. S. Citrin, and A. Locquet. "Intermittency in the Dynamics of an External-Cavity Semiconductor Laser", European Semi-conductor Laser Workshop 2016 (Darmstadt, Germany, 23 Sep, 2016).

3. Daeyoung Choi, A. Locquet, J. Barnoud, C-Y. Chang, M. Wishon, D. S. Citrin. "Extreme events in external-cavity lasers: from low frequency fluctuations to coherence collapse", International Symposium on Physics and Applications of Laser Dynamics (Metz, France, 4 Nov, 2015).

4. Daeyoung Choi, J. Barnoud, C-Y Chang, M. Wishon, Y. Bouazizi, A. Locquet, D. S. Citrin. "Extreme events in the chaotic dynamics of external-cavity semiconductor lasers", Dynamics Days Europe (University of Exeter, U.K., 6 Sep, 2015).

References

David S. Citrin
Professor (advisor) e-mail: david.citrin@ece.gatech.edu
School of Electrical & Computer Engineering
Georgia Institute of Technology

Alexandre Locquet
Professor (co-advisor) e-mail: alexandre@gatech.edu
School of Electrical & Computer Engineering
Georgia Tech-Lorraine